Jing Xu

Transport phenomena in a temperature gradient studied by NEMD. A chemical reaction and a phase transition

Thesis for the degree of Philosophiae Doctor

Trondheim, October 2009

Norwegian University of Science and Technology
Faculty of Natural Sciences and Technology
Department of Chemistry

NTNU
Norwegian University of
Science and Technology

NTNU
Norwegian University of Science and Technology

Thesis for the degree of Philosophiae Doctor

Faculty of Natural Sciences and Technology
Department of Chemistry

ISBN 978-82-471-1784-2 (printed ver.)
ISBN 978-82-471-1785-9 (electronic ver.)
ISSN 1503-8181

Doctoral theses at NTNU, 2009:193

Printed by NTNU-trykk

All difficult things have their origin in that which is easy, and great things in that which is small.

Laozi

Acknowledgements

The research work presented on this thesis was carried out in 2003-2007 at the Department of Chemistry, Norwegian University of Science and Technology (NTNU), Trondheim, Norway. This Ph.D project was granted by the Norwegian research council (NFR).

First of all, I owe my deepest gratitude to Professor Signe Kjelstrup. As my primary supervisor, she has been extremely helpful during these years, supporting my work in many ways with invaluable discussions, suggestions, and encouragements. I also appreciate her for leading me to the field of non-equilibrium thermodynamics and guiding me to the art of scientific research.

I would like to thank my co-supervisor Professor Dick Bedeaux for invaluable help during my doctoral research. I really appreciate his support with the theory and equations. I was fortunate to work with him on the Onsager project (transport properties in a phase transition) in the early stages of my research. Without his help, comments, and questions, that paper would not ever exist!

I am grateful to Dr. Jean Marc Simon who has made available his support in valuable discussions and advices of my research. I really enjoyed working with him on the chemical reaction project.

I am pleased to acknowledge the Department of Chemistry of NTNU, for creating welcoming and pleasant working atmosphere. I would like to thank all of my colleagues at the department. Special thanks to Terje Bruvoll for helping me on many practical problems. Einar Ryeng and Dr. Audun Røsjorde, are acknowledged for providing the computer support. Most of all, I wish to appreciate my friend Dr. Live Rekvik, who has been a doctoral student during the first two years of my Ph.D. She generously shared her knowledge and experiences on Fortran programming with me, especially on molecular modelling, and helped me on many other practical things. I also appreciate her help on using Linux and Latex.

I would like to thank my dear parents, Liuzhu Xu and Cuiping Tang, for their unconditional love, support and encouragement. They have been a source of motivation and strength throughout my life.

Last but not least, I would like to thank my family: Qubo, Leon, and Jessica for their support and understanding, which have been crucial for me to accomplish my research.

Finally, I cannot forget my second father, Xianzhou Tao, who taught me lot about life and encouraged me not giving up my education in the difficult times. His kindness and support will be memorised for ever. This thesis is dedicated to him!

Summary

In this thesis we used non-equilibrium molecular dynamics (NEMD) to study non-equilibrium behaviors of two irreversible systems, both exposed to large temperature gradients. As modeling systems, we have chosen a simple chemical reaction, $2F \rightleftarrows F_2$, and a liquid-vapor interface of a Lenard-Jones spline fluid. The primary goal of this thesis is to investigate the nature of coupled transfer of heat and mass, and to obtain insight into the underlying molecular mechanisms, dynamic structure and properties of the non-equilibrium systems.

Heat and mass transports are central in mechanical as well as in chemical engineering. In order to predict transport properties of such systems, we need to confirm that there is a sound basis for the relevant transport equations. For the purpose, NEMD simulations have been used to study both equilibrium and dynamical behavior of the systems. To model the chemical reaction, Stillinger and Weber's two- and three-body potentials were used. In addition to the two-body potential, the three-body potential is needed in order to sufficiently represent the main features of the reaction. Suitable NEMD techniques with the efficient reaction model were developed to study the fluorine reaction, in both stationary equilibrium and non-equilibrium states. Large temperature gradients were imposed through the boundaries in the NEMD box. With the NEMD simulations, the usefulness and validity of the theory of non-equilibrium thermodynamics (NET) have been investigated. The validity of the assumption of 'local equilibrium' was tested for the chemical reaction in various temperature gradients. Furthermore, the quantitative definitions for the local 'chemical' equilibrium were presented using the results from NEMD. The dynamic properties of the system are governed by the system's entropy production. We gave the expression for the entropy production from NET to define the fluxes and forces in the system. Proper transport equations were presented for determination of the transport coefficients of the reacting system. Origins of transport properties, i.e. thermal diffusion coefficients (or Soret coefficient), heats of transfer, and Onsager coefficients, were discussed in a microscopic level. A dissipative or dynamic structure of the chemical reaction was displayed.

In addition we studied a phase transition, i.e. coupled heat and mass transfer across a liquid-vapor interface of a one-component system. The NEMD simulations with a Lenard-Johns spline potential were performed in different thermodynamic environments, e.g. with temperature gradients or/and concentration gradients. In the first place of this work, we proofed the validity of the assumption of local equilibrium at the surface where heat and mass transfer simultaneously. We then developed new algorithms to independently determine all four interfacial transfer coefficients for the surface. In the framework of

NET, two sets of force- flux equations were defined by using the measurable heat flux on the vapor side as well as on the liquid side. The aim of this work is to find the interfacial coupling (Onsager) coefficients along the liquid-vapor coexistence curve and to add a proof of the Onsager's reciprocal relations (ORR). To the best of our knowledge, this is the first time to test the validity of Onsager relations for a surface using NEMD.

Nomenclature

Here follows an overview of notation used in chapters 1 to 6.

Abbreviations

MC	Monte Carlo
MD	molecular dynamics
NEMD	non-equilibrium molecular dynamics
BD-NEMD	boundary-driven non-equilibrium molecular dynamics
NVE	constant number of particles, volume, and energy
NVT	constant number of particles, volume, and temperature

Latin letters

c	molar density, mol m^{-3}
$c_{k,eq}$	Molar density of component k in equilibrium, mol m^{-3}
c_k^0	Standard molar density of component k, mol m^{-3}
D	Interdiffusion coefficient in the reacting mixture, m^2 s^{-1}
E	energy, J
$\mathbf{F}$	force
$\mathbf{F}_i$	force on particle i
$\mathbf{F}_{ij}$	force on particle i exerted by particle j
f	fugacity, bar
f_k^0	Maxwell-Boltzmann velocity distribution of component k
f_k	Maxwell-Boltzmann velocity distribution of component k, in a temperature gradient
G	Gibbs free energy, J mol^{-1}
$\Delta_r G^{\ominus}$	standard reaction Gibbs energy, J mol^{-1}
$\Delta_r G$	reaction Gibbs energy, J mol^{-1}
H	molar enthalpy, J mol^{-1}
$\Delta_r H$	reaction enthalpy, J mol^{-1}
J	molar flux, mol m^{-2} s^{-1}

J_q	total heat flux or energy flux, J m^{-2} s^{-1}
J'_q	measurable heat flux, J m^{-2} s^{-1}
K_p	equilibrium constant
K_{eq}	thermodynamic equilibrium constant
k_B	Boltzmann's constant, 1.381×10^{-23} J K^{-1}
k_f	Forward reaction rate constant, m^3 mol^{-1} s^{-1}
L_{ij}	conductivity coefficient
L_α	length of the MD box in $\alpha-$coordinate, m
M	Maxwell velocity distribution
m	mass, kg
m_0	atomic mass, 10^{-26} kg
N	number of particles
N_A	Avogadro's number
P	probability distribution
p	pressure, bar
$p^\ominus$	standard pressure, 1 bar
Q	reaction quotient
q^*	heat of transfer, J mol^{-1}
R_{ij}	Resistivity coefficient
r	net reaction rate, mol m^{-3} s^{-1}
r_b	backward reaction rate, mol m^{-3} s^{-1}
r_c	cutoff distance for bonded fluorine molecule, $1.7\sigma_0$ m
r_f	forward reaction rate, mol m^{-3}s
r_{ij}	distance between particle i and particle j, m
r_{list}	cutoff distance for neighbour list, m
S_k	Entropy of component k, J mol^{-1} K^{-1}
$\Delta_r S$	Reaction entropy, J mol^{-1} K^{-1}
T	temperature, K
T_t	temperature at the triple point, K
t	time, s
u	potential, J
V	volume, m^3
$\mathbf{v}_k$	velocity of component k, m s^{-1}
w	weight function
y_k	molar fraction of component k, mol m^{-3}

Greek letters

β	k_BT
Δ	increment, difference
λ	conductivity
Φ	the total potential energy, J
ϕ_k	Pertubation factor for Maxwell distribution of component k
μ	chemical potential, J mol^{-1}

$\Delta_r \mu_{eq}$	Reaction chemical potential in equilibrium, J mol^{-1}
σ	entropy production rate, W K^{-1} m^{-3}
ρ	density (N/V)
ρ_t	density at the triple point
γ	surface tension
γ_k	activity coeffcient of component k
γ_p	activity coeffcient ratio

Subscripts and superscripts

α	direction (x, y or z)
k	component
i, j, k	particle numbers
2	2-body contribution
3	3-body contribution

Contents

Chapter 1

Introduction

1.1 Main objective and motivation

For more than 150 years, heat and mass transfer has been studied and received much attention, because of its universal existence in many branches of science and engineering. The most common systems existing in nature and in industry are normally far from global equilibrium. They occur normally not only in the presence of concentration gradients, but also in the presence of temperature and pressure gradients. As a consequence of these exposed gradients, heat and mass transfer occur simultaneously in many processes, for instance, evaporation at the surface of a water drop, wood drying, and cooling processes, etc. In this thesis, we shall employ non-equilibrium dynamics (NEMD) simulations to study the coupled heat and mass transport in two systems, a chemical reaction and a surface, both in a large temperature gradient. The main aim of this thesis is to obtain molecular insight into the nature of such transport processes, and to contribute to the understanding of the coupling effects between heat and mass transfer.

1.1.1 A chemical reaction

Combined heat and mass transports especially in conjunction with chemical reactions are of great importance in many processes of plants. Chemical reactions occurring in flame, chemical reactor, combustors, turbines, in micro-porous or turbulent flow fields, are normally out of global equilibrium. For instance, the temperature gradient in flames is as high as about 10^8 K m^{-1}. The theory of non-equilibrium thermodynamics (NET) provides a sound non-equilibrium description of the coupled transport processes in systems driven out of global equilibrium [1–3]. The hypothesis of local equilibrium is fundamental in NET. It says that, although the total system is not in equilibrium, there exists within a small volume element a state of '*local equilibrium*', for which all normal thermodynamic relations hold. Knowledge of conditions for local equilibrium will offer a sound basis for relevant transport equations in non-equilibrium systems where heat and mass transport. In the modeling of chemical and mechanical processes in typical engineering problems,

it is normally taken as granted that this assumption of local equilibrium is valid and all normal thermodynamic relations can be applied in any volume element of the system [3].

The assumption of local equilibrium have been validated earlier, in a homogeneous two-component mixture [4] and at surfaces [5,6]. Non-equilibrium dynamics (NEMD) simulations were employed to successfully characterize these non-equilibrium systems on the molecular scale, all exposed to large thermal gradients. Hafskjold and Ratkje [4] verified the assumption of local equilibrium holds in the homogeneous non-reactive two-component system, in a temperature gradient up to 10^8 K m^{-1}. They gave four different criteria to analyze the concept of local equilibrium in the homogeneous mixture with transport of heat and mass. To our knowledge, chemical reactions have not been investigated before from this perspective. One may wonder how good the assumption of local equilibrium is in a chemical reacting system in a large temperature gradient, for instance, in flame.

According to the original formulation of Prigogine, the Gibbs equation remains valid for a large class of irreversible processes, provided that the Maxwell distributions of molecular velocities are perturbed only slightly. The class includes also chemical reactions slow enough not to disturb the equilibrium form of the distribution to an appreciable extent. In this thesis, it is therefore interesting to examine weather our reacting system is Maxwellian in its component velocity distributions or not? Related questions are arisen: are their shifts related to the temperature gradient, and how far the reaction is from *local chemical* equilibrium? Local *chemical* equilibrium as a subclass of local thermodynamic equilibrium, has thus to be introduced and means that in addition, the reaction Gibbs energy is equal to zero in the volume element of the system [3].

Transport properties are of primary importance as they reflect not only what happens at equilibrium but the rate at which equilibrium is attained. The state of thermodynamic equilibrium is well defined, being that state for which the total entropy of the system and its surroundings is a maximum [7]. With a sound statistical basis for use of nonequilibrium thermodynamics theory, NEMD simulations have also been used to predict transport properties for pure components and mixtures [6, 8, 9]. Computations showed that separations of the components and mole fraction gradients are displayed in a fluid mixture in a thermal gradient [4], which is well known as the Soret effect (or the thermal effect). For more sophisticated mixtures, in the presence of a chemical reaction, it shall be a challenge to learn the specific transport coefficients and how they vary with a temperature gradient. These coefficients, especially coupling coefficients, shall sled light on their practical use in non-equilibrium transport processes; for instance in chemical reactor engineering, or in flame modeling.

1.1.2 A surface

Phase transitions are common phenomena in industrial as well as in living systems. It involves simultaneous transfer of heat and mass across a surface. Evaporation or condensation is one such central example of heat and mass transport. In spite of the technical importance of vapor-liquid phase transitions, little systematic information is known about

the interface resistivity to transport. From a literature review [10], most of the thermodynamic modeling of these transitions assumes equilibrium between the phases at the phase boundary, i.e., continuity in the chemical potential and the temperature. It means that the resistivites of the surface to heat and mass transfer is negligible, like in most engineering description of phase transitions. However, experimental [11–13], numerical [14] and computational [6, 8, 9] evidence have been accumulated to show that this assumption is not generally true. One aim of this thesis is thus to question this assumption for a liquid-vapor phase transition in a large temperature gradient.

In the description of the transfer coefficients, we use nonequilibrium thermodynamics theory for surfaces. In NET theory, the famous Onsager's reciprocal relations express the equality of certain relations between fluxes and forces in thermodynamic systems out of equilibrium, but where a notion of local equilibrium holds [15]. The importance of the Onsager's relations is that it can reduce the number of phenomenological coefficients which are essential in processes. More practically to say, it simplifies transport problems. In homogeneous system the Onsager relations have been verified both experimentally [1] and by NEMD simulations [4]. However, for this respective such verification has not yet been given for the interface. A few years ago, Røsjorde et al. computed a liquid-vapor phase transition in a one-component system by NEMD. They showed the validity of local thermodynamic equilibrium at the interfacial film [5]. They also obtained interfacial transfer (coupling or Onsager) coefficients and resistivities for the interface, but by assuming a validity of the Onsager reciprocal relations [9]. In this thesis, our aim is to find the interfacial coupling coefficients independently and to add a proof of the Onsager's reciprocal relations (ORR). Here the same system shall be use by NEMD studies to investigate the coupled transport phenomena of heat and mass as used by Røsjorde at al. for a surface. To our knowledge, this is the first verification of ORR for a liquid-vapor interface tested by NEMD.

1.2 Non-equilibrium thermodynamics as a necessary tool

Non-equilibrium thermodynamics provides theoretical prediction of transport properties of irreversible systems that are out of global equilibrium. This theory was first established in 1931 by Onsager [15], to describe transport processes in homogeneous systems. Later large efforts [16–18] have been devoted to extend it for transports in heterogeneous systems. Until recently, a systematic NET description has been given by Kjelstrup and Bedeaux [3] for transports in heterogeneous systems and in particular to surface transport phenomena.

According to the second law of thermodynamics, the primary quantity of a non-equilibrium system is the entropy production. This quantity governs the equations of transport. In NET, the second law of thermodynamics is reformulated in terms of the local entropy production rate, σ, by assuming its local validity. By filling the energy balance, mass balance, charge conservation, second law of thermodynamics, into the Gibbs equation, the local entropy production rate is given by the product sum of so-called conjugate

fluxes, J_i and driving forces, X_i, in the system. The second law becomes

$$\sigma = \sum_i J_i X_i \geq 0 \tag{1.1}$$

Onsager prescribed that each flux is connected to its conjugate forces via the phenomenological coefficients [15]. A linear relation between each flux and all forces exist and it is

$$J_i = \sum_{j=1}^{n} L_{ij} X_j \qquad (i = 1, 2, \cdots, n) \tag{1.2}$$

Alternatively, each force is a linear combination of all forces:

$$X_i = \sum_{j=1}^{n} R_{ij} J_j \qquad (i = 1, 2, \cdots, n) \tag{1.3}$$

The phenomenological coefficients L_{ij} in Eq. 1.2 are conductivities, while the ones in Eq. 1.3 are resistivities. Onsager assumed the regression of microscopic thermal fluctuations at equilibrium follows the macroscopic law of relaxation of small non-equilibrium disturbances, known as the Onsager's regressionhypothesis. Using also the principle of microscopic reversibility, Onsager proved the equality of the coupling coefficients for independent forces and fluxes (Onsager's reciprocal relations) [15]:

$$L_{ij} = L_{ji} \quad \text{and} \quad R_{ij} = R_{ji} \qquad (i, j = 1, 2, \cdots, n) \tag{1.4}$$

In the Onsager symmetric matrix, the coupling coefficient L_{ij} or R_{ij} is only a function of the state variables (e.g. the local pressure and temperature), but not of the force X_j or the flux J_j. By introducing the complete set of extensive, independent thermodynamic variables, A_i, the conjugate fluxes and forces are defined as

$$J_i = dA_i/dt \quad \text{and} \quad X_i = \partial S/\partial A_i \tag{1.5}$$

The usefulness of non-equilibrium thermodynamics has been generalized in four ways [3]. First of all, the theory gives an accurate description of coupled transport processes. In complex systems, for instance, mass transports take place not only in the presence of the concentration gradient, but also in the presence of the temperature gradient or the electric potential gradient. The simple flux equations of heat, mass and charge transport given by Fourier, Fick and Ohm's laws are not enough to describe the coupled transport phenomena. The coupling among fluxes can be captured in NET by the so-called coupling coefficients. Secondly, a framework can be obtained for the definition of experiments. Non-equilibrium thermodynamics is instrumental for design of experiments that aim to find transport properties. Thirdly, the theory quantifies not only the entropy that is produced during transport, but also the work that is done and the lost work. Non-equilibrium thermodynamics is probably the only method that can be used to assess how energy resources are exploited within a system. According to NET, processes with small losses in exergy (In thermodynamics, the exergy of a system is the maximum work possible during a process that brings the system into equilibrium with a heat reservoir.), have a high second law efficiency. Finally, The NET theory allows us to check that the thermodynamics equations that have been used to model the system are in agreement with the second law. The entropy balance of the system and the expression for the entropy production can be used to control the internal consistency of the thermodynamic description.

1.3 Outline of the thesis

The outline of this thesis is as follows. Chapter 2 serves as an introduction to molecular dynamics. In Chapter 2, we present background information on molecular simulation techniques, especially on boundary driven NEMD methods. We then present our NEMD studies in two modeling systems in Chapters 3-5, which have been published in the journals.

In Chapters 3 and 4, we study a simple chemical reaction, $2F \rightleftarrows F_2$, in a temperature gradient, using NEMD simulations. In Chapter 3 we aim to find conditions for *local* equilibrium in the reaction. We first set up a reaction model to be used with NEMD. Suitable NEMD algorithms with the Stillinger and Weber's 2- and 3-body potential are developed for the chemical reaction A. The reliability of our new NEMD program is tested, by comparing the results from Stillinger and Weber in equilibrium MD (EMD) simulations. We present some important thermodynamic properties of the reacting mixture in EMD and NEMD simulations. Local chemical equilibrium as a subclass of local thermodynamic equilibrium is investigated under six NEMD cases. Our results show *local* equilibrium holds in the chemical reaction where heat and mass transport in a temperature gradient up to 10^{12} K m^{-1}.

In Chapter 4 we continue the study of the chemical reaction that is in stationary non-equilibrium state. We find further supports to define local equilibrium in the reaction. We investigate transport behaviors of the chemical reaction. Analysis is made for the NEMD cases at their stationary states, both in *local chemical equilibrium* and near *local chemical equilibrium* (close, but not at chemical equilibrium). A dissipative (dynamic) picture of the reaction in a temperature gradient is drawn according to minimum entropy production of the reaction itself. Transport coefficients, such as the thermal conductivity and the inter-diffusion coefficient, are determined from our analytical solutions of the relevant transport equations. Impacts of the chemical reaction with a thermal driving force on these coefficients are discussed.

In Chapter 5 we investigate transfers of heat and mass into, across and out of a surface which is a flat thin film between liquid and vapor phases of a one-component system. In this heterogeneous system, a temperature gradient or/and a concentration gradient are applied. The surface is described by Gibbs excess properties and is regarded as an autonomous system with its own temperature and chemical potential. In this work, we firstly test the validity of the assumption of local equilibrium as this assumption is crucial for the proof of the Onsager relations [1–3]. All four interfacial coefficients are determined independently from 48 NEMD simulations. The cross (coupling) coefficients are shown as equal within the calculation accuracy. This gives a first verification of the Onsager's reciprocal relations for transport through a surface by molecular simulations. Furthermore, appropriate expressions for the interface film resistivities are proposed with kinetic theory (as only a function of the temperature of the surface). They can be well compared with NEMD values.

Finally, in Chapter 6 we give some concluding remarks and outlook for future studies. The implementation of 2- and 3-body potential in NEMD for fluorine reaction is presented

in Appendix A.

Chapter 2

Molecular simulations

2.1 Introduction

In recent years, molecular simulations have been widely used to supply valuable insight into molecular systems and to understand and achieve research goals. The developments were progressed not only with the rapid growth of high performance computing, but also with the development of much of the methodology of simulation techniques. Molecular simulations based on model systems constitute a link between experiment and theory. Simulations benefit from avoiding costly and dangerous experiments. On the other side, molecular simulations can be used as a test of the validity of a theory or a theoretical conjecture. Comparing the simulation results to those of real experiments, one can check if the model is a good one and provide useful information to both theory and experiment. Moreover, simulations provide a direct route between the microscopic and the macroscopic world. For example, given microscopic details of a system (such as atomic mass, interactions between particles, molecular structure, etc.) one can use molecular simulations to obtain macroscopic properties of the system, i.e. thermodynamic quantities, transport coefficients, equations of state, etc..

In molecular simulations, any physical system (gas, liquid, or solid) is treated as a collection of particles. Molecular simulation techniques require the adoption of an intermolecular potential to represent interactions between the particles of the physical system. The computer generates either the motion or different states of the particles and the values of the physical quantities of interest can be calculated. Two general classes of molecular simulations are Monte Carlo (MC) and molecular dynamics (MD) simulations.

2.1.1 Monte Carlo

The MC method, which has its origin in the Metropolis algorithm [19], is based on a stochastic approach. It seeks to efficiently calculate ensemble averages of a model system based on the underlying distribution known from statistical mechanics. The basic

Metropolis Monte Carlo is achived by the following three steps: (1) Assign an initial position of a randomly selected particle i, and calculate its energy $u\left(\mathbf{r}^N\right)$. (2) Give the particle a random displacement, $r' = r + \Delta$, and calculate its new energy $u\left(\mathbf{r}'^N\right)$. (3) Accept the move from $\mathbf{r}^N$ to $\mathbf{r}'^N$ with probability, $\min\left[1, \exp\left\{-\beta\left[u\left(\mathbf{r}'^N\right) - u\left(\mathbf{r}^N\right)\right]\right\}\right]$, in which $\beta = 1/k_BT$ and k_B is the Boltzmann constant and $\mathbf{r}^N \equiv \mathbf{r}_1, \mathbf{r}_2, \cdots, \mathbf{r}_N.$, or reject it otherwise.

The Metropolis MC and the other numerous methods based on it are suitable to study equilibrium properties of physical systems. A conventional MC simulation probes a canonical ensemble with constant number of particles (N), volume (V) and temperature (T). To relate the simulation to experiments one can implement MC in various ensembles. Some important kinds of MC methods are the constant NPT Monte Carlo, the grand canonical Monte Carlo (GCMC) (i.e. constant μVT), and the microcanonical Monte Carlo (i.e. constant NVT) [20].

Other advanced Monte Carlo methods, for example, the reaction ensemble Monte Carlo (RxMC) is developed to predict equilibrium properties of chemically reacting mixtures. RxMC simulations have been applied to reactions at high temperature and/or high pressure, at phase interfaces and highly non-ideal environments [21]. The RxMC method was published by two different groups in 1994 [22, 23]. The RxMC simulation method uses Monte Carlo (MC) sampling to directly simulate pre-defined forward and reverse reaction events in a simulation, yielding the equilibrium composition of the reacting mixture. In these simulations, completed forward and reverse reaction events are sampled, so that the energetics of bond breaking and bond formation are unnecessary. Another important feature of the RxMC is that this approach can be performed in any number of basic ensembles. For example, the RxMC method can be combined with the Gibbs ensemble Monte Carlo (GEMC) technique to simulate combined reaction and phase equilibria (i.e. vapor-liquid coexistence) [24, 25].

2.1.2 Molecular dynamics

Molecular dynamics (MD) is a specialized discipline of molecular simulation giving insight into molecular motion on an atomic scale. In addition to study static properties of many-body systems, molecular dynamics simulations also provide information about their dynamical behavior, including time correlation functions, diffusion, and other transport properties. The molecular dynamics (MD) technique follows a dynamic approach, which implies a numerical solution of the Newtonian equations of motion for all atoms in the classical many-body system. Hence, the molecular trajectories are the time related positions of individual particles, which can be viewed in a classical dynamical motion picture. The basics of the MD method [26–30] relies on classical mechanics, determining the trajectory in the phase space of the system and taking time averages of the observables of interest along this trajectory. At each step of the MD simulation, the microscopic coordinates and momentum of all the particles are calculated according to equations of classical mechanics where forces are computed from some predefined expressions, called the force field. With a classical inter-particle potential, the particle (i) motion in a N-body system can be given

by the Newton's second law (force equals mass times acceleration):

$$m_i \frac{d^2 \mathbf{r}_i}{dt^2} = -\frac{\partial U(\mathbf{r}^N)}{\partial \mathbf{r}_i} \tag{2.1}$$

where m_i is the mass of particle i, $\mathbf{r}_i$ the position of particle i and U the interaction potential.

Basic MD produces a NVE ensemble (microcanonical, with constant number of particles N, volume V, and total energy E). Similar to MC, MD can also be implemented with other ensembles, for example, at constant pressure, at constant temperature (canonical MD), and at constant chemical potential (grand canonical MD). The main justification of the MD method is that statistical ensemble averages are equal to time averages of the system, known as the ergodic hypothesis. To implement a MD simulation, special attentions have to be put on the integration scheme and a proper time step that does not violate the energy conservation implicit in the Newton's equations. The time step is usually chosen of the order of femtoseconds (10^{-15} s) and a typical MD simulation covers a time interval of $10^{-8} - 10^{-10}$ seconds. In MD, the (velocity) Verlet algorithm is the most common and usually the best numerical scheme to integrate the equations of motion Eq. 2.1 [20].

Molecular dynamics has two basic classes: equilibrium molecular dynamics (EMD) and non-equilibrium molecular dynamics (NEMD). Both the EMD and the NEMD can be used to compute the equilibrium and transport properties of the many body system. In EMD simulations, transport properties can be determined by Einstein or Green-Kubo [31] integrals. The appealing property of NEMD is that this method can be used to study the properties of the many body systems, in both global equilibrium and out of global equilibrium [32]. One can therefore first find the equation of state and other equilibrium properties (in equilibrium systems), and then the transport properties (in non-equilibrium systems).

For chemical reactions, the reaction ensemble molecular dynamics (RxMD) [33] was developed to study the equilibrium transport properties of chemically reacting mixtures. RxMD combines the RxMC method with constant-temperature MD [20]. In the RxMD simulation box, a molecular dynamics simulation cell (dynamic cell) is placed in the center of two reaction mixture simulation cells (control cells). In the control cells, the RxMC method is applied to forward and reverse reaction steps. Constant-temperature molecular dynamics simulations are performed in both the dynamic cell and the control cells. At chemical equilibrium, thermodynamic and equilibrium transport properties such as the velocity autocorrelation functions and the self-diffusion coefficients are calculated in the dynamic cell. This method can be applied to both homogenous and inhomogeneous systems, while the control cells must remain at identical thermodynamic conditions via the RxMC method. However, in the dual control cell reaction ensemble molecular dynamics method (DCC-RxMD), the control cells can be maintained at different thermodynamic conditions via the RxMC and GCMC methods, respectively. The DCC-RxMD method allows calculation of both equilibrium properties and non-equilibrium transport properties in nanoporous materials such as diffusion coefficients, permeability and mass flux [34]. Similiar to the RxMD simulation cells, a membrane is placed at the centre of the DCC-RxMD simulation box and two control cells (one for reactions and another for transport)

are sitted at two sides of the membrane. The trajectories of the fluid particles within the entire DCC-RxMD simulation box are generated by the MD simulation method, while the reaction equilibrium is controlled in the reaction control cell by the RxMC method. To maintain a flux of particles through the membrane, a pressure gradient has to be imposed by performing GCMC particle insertion and deletion steps in the transport control cell. Algorithms and application of these methods have been described in the literatures [21] and references therein.

2.2 Boundary-driven NEMD simulations

Non-equilibrium molecular dynamics (NEMD) is a powerful computing technique that is designed to investigate particle behavior in systems with gradients in intensive variables. Algorithms of boundary-driven NEMD (simply called NEMD in this thesis) were developed by Hafskjold and coworkers [35]. The basic idea of the NEMD method is that one can apply external forces through the boundaries of a system as in a real experiment [4–6, 32, 35–46]. The external force must be congruous with the boundary conditions, like introducing some types of walls into the system. At the boundaries, one can impose a temperature gradient or a chemical potential gradient (concentration gradient), or the walls can be interactive [36] as in a porous system. Another known non-equilibrium molecular dynamics method is called synthetic NEMD where the external thermodynamic force is built into the equation of motion for the system [32].

2.2.1 The interaction potential

On a microscopic level, any system is composed by particles ($i = 1, \cdots, N$). It is important to find a proper potential which describes interactions between particles in the system. Often, one can approximate the atomic interactions with a classical potential. A general form of the interaction potential $\mathrm{U}(\mathbf{r}^N)$ is the sum of grouped terms dependent on two-body, three-body, etc. contributions:

$$U(\mathbf{r}^N) = \sum_{i,j}^{i<j} u_2(\mathbf{r}_i, \mathbf{r}_j) + \sum_{i,j,k}^{i<j<k} u_3(\mathbf{r}_i, \mathbf{r}_j, \mathbf{r}_k) + \cdots \tag{2.2}$$

where the subscripts i, j and k indicate different atoms, u_2 is a two-atom potential and u_3 is a three-atom potential.

In addition to the intermolecular potentials, intramolecular potentials are also important in the simulation of the molecular and crystal behaviors [6, 46]. The intramolecular potentials describe the bond-stretching, bending and torsion vibration of each particle. In the present work, these potentials are not of interest.

Pair potential

Often, the molecular properties are assumed to be 'pair-additive' and interactions between pairs of particles make the overwhelming contribution to the overall intermolecular interaction. The interaction potential is thus usually taken from a classical pair-wise interaction potential, which is a function of the atom-atom distance r_{ij} ($r_{ij} \equiv |\mathbf{r}_i - \mathbf{r}_j|$). A most common pair potential for particle interaction in fluids is the Lennard-Jones potential:

$$u(r_{ij}) = 4\epsilon \left[\left(\frac{\sigma}{r_{ij}} \right)^{12} - \left(\frac{\sigma}{r_{ij}} \right)^{6} \right] \tag{2.3}$$

where σ is the collision diameter, which is the separation of the particle at which $u(r_{ij}) = 0$, and ϵ is the depth of the potential well at the minimum in $u(r_{ij})$. The Lennard-Jones (LJ) potential provides an adequate description of the interaction between pairs of inert gas atoms and also of some molecules. In molecular dynamics, several truncated LJ potentials can be applied to save computation time. A simple truncated LJ potential uses a cut-off r_c, called as the cut-off LJ potential. When the distance is beyond the cut-off distance, $r \geq r_c$, this potential is taken to be equal to zero. In order to obtain a consistent description of equilibrium and non-equilibrium properties, it is necessary to use a shifted cut-off LJ potential [47].

Another alternative pair-wise interaction potential is the Lennar-Jones spline potential, which was used in our NEMD simulations of this thesis to study behaviors of a liquid-vapor interface. The potential is expressed in terms of the inter-particle distance r_{ij} between any pair of particles i and j:

$$U(r_{ij}) = \begin{cases} 4\epsilon[(\sigma/r_{ij})^{12} - (\sigma/r_{ij})^{6}] & \text{for} \quad 0 < r_{ij} < r_c \\ a(r_{ij} - r_s)^2 - b(r_{ij} + r_s)^3 & \text{for} \quad r_c < r_{ij} < r_s \\ 0 & \text{for} \quad r_s < r_{ij} \end{cases} \tag{2.4}$$

where the shifted distance r_s follows $r_s = (48/67)r_c$. Detailed expressions of the constants a_{ij} and b_{ij} can be found in Chapter 5. In this thesis, we used the cut-off distant $r_c \cong 1.7371\sigma$ rather short range compared to the truncated cut-off distance implemented in the other works by Ge et al. [48]. They chosen $r_c = 2.5\sigma$ and $r_s = (48/67)r_c \cong 1.7910$. With this long range LJ spline potential, Ge et al. performed NEMD simulations for the same heterogeneous system under the same experimental conditions as we investigated. They reported different NEMD results in the equilibrium as well as the non-equilibrium behaviors of the system. These significant changes have been discussed and considered as the influence of the different choices of the truncated distances, i.e. short-range and long range LJ splines [3, 48].

The two- and three-body potential

Recently researches have been done to seek more 'virtual' potentials for effective presentation of the dynamics of chemical reactions. Stillinger and Weber pointed out that the traditional additive pair-wise interaction (i.e. LJ spline) can not suffice to represent the

main features of chemical bonding in a chemical reactive system. The interactions of the triple particles can make a significant contribution to the total interactions [49–54]. Stillinger and Weber constructed a linear combination of two-body and three-body potentials to give a energy surface in a chemical reaction, $2\mathrm{A} \rightleftarrows \mathrm{A}_2$ where A represents a highly chemical reacting substance, such as fluorine and sulfur [50–53]. The general form for the potential surfaces was given:

$$\Phi(\mathbf{r}_1, \cdots, \mathbf{r}_N) = \sum_{\text{pairs } i,j} u_2(r_{ij}) + \sum_{\text{triplets } i,j,k} u_3(r_{ij}, r_{ik}, r_{jk}). \tag{2.5}$$

where u_2 is a function of the atom-atom distance, and u_3 is a function of the three atom-atom distances r_{ij}, r_{ik} and r_{jk}.

In this thesis we shall study the chemical reaction:

$$2\mathrm{F} \rightleftarrows \mathrm{F}_2 \tag{2.6}$$

The two- and three-body potential surface for the fluorine reaction was given by Stillinger and Weber. Detailed functions of u_2 and u_3 are expressed in Chapters 3. Stillinger and Weber provided this combined potential based on the acceptable approximation to the ground electronic state potential surface for the collection of atoms. The pair potential u_2 was selected to give a good representation of the isolated diatomic fluorine molecule. The triple potential u_3 was fitted to the atomic behavior by a scaling from the well-known potential surface of $\mathrm{H}+\mathrm{H}_2$ [52]. The combined u_2 and u_3 are required to produce weak van der Waals attractions between neighboring diatomic molecules. A major role of the three-body potential is to prevent formation of more than one covalent bond to each fluorine atom. With the two- and three-body potential, Stillinger and Weber modeled the reaction (Eq. 2.6) by performing equilibrium MD simulations in a cubic MD box with 1000 fluorine particles. They computed the time correlation functions of fluorine monomers and other equilibrium properties of the reaction under various thermodynamic environments. Compared with the experimental at the same conditions, their results have shown that the two- and three-body potential model can sufficiently represent the main features of the chemical binding in Eq. 2.6 [52].

In NEMD and other molecular simulations, it is common to apply periodic boundary conditions. This is a very effective way to overcome the obstacle of surface effects and thus efficiently compute a larger and more representative system. Figure 2.1 shows such a system at the periodic boundary condition in two-dimensions. The simulation box is indicated by the black lines and its periodic images are indicated by the grey lines. When a particle moves out of the simulation box, one of its images enters the box through the opposite face. There are no walls at the boundary of the simulation box, and there are no surface particles. In order to effectively compute the interactions between particles, it is also necessary to use an approximation called the 'minimum image convention'. Taking particle i as a center, one can construct a box (grey dashed lines) with the same size and shape of the original simulation box. By using a cutoff radius r_c , one can further reduce the number of particles need to be considered in the interactions with particle i. Clearly, r_c must be less than half of the box length to avoid the interaction of particles with their own periodic images.

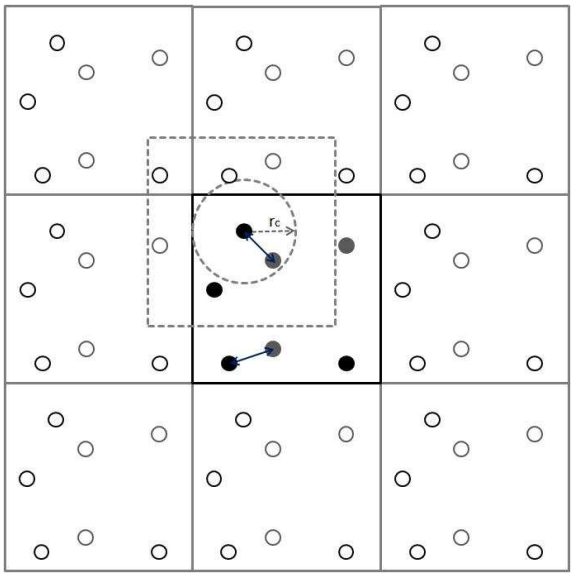

Figure 2.1: Periodic boundary conditions, minimum image convention and cutoff. The arrows indicate pair-wise forces. The original simulation box is in black boundaries. The periodic images are in grey boundaries. The minimum image box is in dashed boundaries. r_c is a cutoff radius.

In molecular dynamics simulations, the most computational and time costly part is the force calculation. At every time step, potential energy and forces are calculated for the N particles in the system. To save CPU and increase the efficiency of the program, a neighborhood list method is useful. 'Neighbors' of particle i are then updated during certain time steps. Particles within a little larger distance than the cutoff radius are considered in the stage of 'updating' the neighborhood list. In the NEMD simulation in our chemical reaction, we developed a useful neighborhood list method, named as NEIGHBOUR3. This new method enables effective calculations of 'neighbors' through all necessary loops for pairs and triples, see Chapter 3. Figure 2.2 shows a schematic

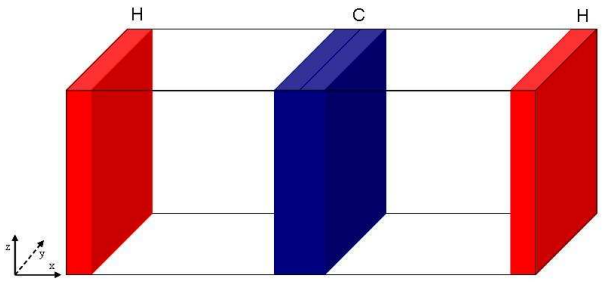

Figure 2.2: A schematic picture of a boundary-driven NEMD simulation box in the $x-$, $y-$ and $z-$ coordinates. H represents hot layers in high temperature and C represents cold layers in low temperature.

picture of a NEMD simulation box (or MD box). The MD box is rectangular (or cubic) with dimmensions L_x, L_y and L_z ($L_x > L_y = L_z$). Here x is the direction along the box, y is the vertical direction and z is the depth direction. The MD box contains N particles and is equally divided into many small volumes (layers) along the x-direction. The boundary regions lie in layers in the middle and near the ends of the MD box where H indicates 'hot' and L indicates 'cold'. The MD box is symmetric in the x direction and periodic boundary conditions are applied in all the three directions. Special attention has to be paid on extrapolation to the thermodynamic limit and to the limit of vanishing force, in the boundary regions. The boundaries like 'walls' formed by particles at fixed position or a layer of particles obeying perturbed equations of motion [32]. For example, in the boundaries, the temperature, chemical potential, or momentum can be set by a local perturbation of the system [37]. Many thermostat methods are suitable for the purpose of the temperature perturbation, like the Andersen thermostat [55], the Gaussian thermostat [56], the Nosé-Hoover thermostat [57], or a thermostat based on velocity scaling [58].

Until now we have given information on the defined interaction potential, periodic boundary conditions with 'minimum image convention' and neighborhood lists, and introduced our simulation box. Next, we shall briefly describe some other important features of NEMD.

In order to determine transport properties, we first need equilibrium properties of the system. NEMD (BD-NEMD) simulations are very suitable to find both type of data. In global equilibrium, the boundaries (H and C) are at the same conditions. Out of global equilibrium the boundaries are not the same. Hafskjold et al. proposed an efficient Heat EXchange (HEX) algorithm to create a temperature gradient in a MD box [35]. A heat (energy) flux is imposed by *adding* and *withdrawing* energy from boundary layers H and C respectively. In practice, we do this by perturbing the particle's momenta in H and C, while the total energy of the system is conserved. In this way, a heat flux is created in the force direction ($x-$coordinate). To model a particle flux from the vapor to the liquid (condensation), the MEX algorithm [4] is applied to remove a particle from the low temperature layers in the center and insert it into one of the high temperature layers at the

end of the cell. The particle maintains its $y-$ and $z-$ coordinates while its $x-$coordinate is changed by $L_x/2$. In order to avoid large perturbations of the energy of the system, the particle insertion shall be done with a probability given by the Boltzmann factor.

In NEMD, temperature, density, pressure, composition, enthalpy, fluxes, and other molecular properties of interest, are computed from the mechanical properties of the system. In a stationary state of a system, the fluxes of energy and mass are constant in the driving force direction. Using the symmetry of the system around the center of the box, the mean of the time averages of the properties (i.e. kinetic energies, potential energies and the number of particles) in each half can be calculated with a better statistics. All the variables in NEMD are in reduced units.

Non-equilibrium dynamics (NEMD) simulations as an efficient computation tool allow us to characterize non-equilibrium systems on the molecular scale. With the framework offered non-equilibrium thermodynamics (NET), the NEMD method is suitable to measure equilibrium as well as dynamic properties of nanoscale systems exposed to large gradients. In NEMD simulations, one does not a priori assume validity of thermodynamic relations, as thermodynamic properties are derived from a purely mechanical description. Therefore the NEMD method can serve as an independent verification of thermodynamic relations. The NEMD simulations have already been used in some studies to verify the assumption of local equilibrium which is of foundmental importance in NET. Examples of such NEMD studies can be found for pure component systems, binary fluid mixtures, as well as the bulk phases and the interface of a one-component system [32]. In these systems, heat and mass were transport in large gradients. With the NEMD technique, one can apply large temperature gradients in a magnitude of order of 10^{11}. When the equations of thermodynamics hold in local volume elements, transport coefficients can be defined from the relevant transport equations. With NEMD simulations, Onsager's reciprocal relations have already been validated for the pure component systems as well as binary fluid mixtures [32].

Chapter 3

Molecular dynamics simulations of a chemical reaction; conditions for local equilibrium in a temperature gradient

Jing Xu, Signe Kjelstrup and Dick Bedeaux

Department of Chemistry
Faculty of Natural Science and Technology,
Norwegian University of Science and Technology
NO-7491 Trondheim, Norway

This paper was published in
Physical Chemistry Chemical Physics,
Volume 8 (2006), pages 2017-2027.

We have examined a simple chemical reaction in a temperature gradient; $2F \rightleftarrows F_2$. A mechanical model was used, based on Stillinger and Weber's 2- and 3-body potentials. Equilibrium and non-equilibrium molecular dynamics simulations showed that the chemical reaction is in local thermodynamic as well as in local chemical equilibrium ($\Delta_r G$=0) in the supercritical fluid, for temperature gradients up to 10^{12} K/m. The reaction is thus diffusion-controlled. The velocity distributions of both components were everywhere close to being Maxwellian. The peak distributions were shifted slightly up or down from the average velocity of all particles. The shift depended on the magnitude of the temperature gradient. The results support the assumption that the entropy production of the reacting mixture can be written as a product sum of fluxes and forces. The temperature gradient promotes interdiffusion of components in the stationary state, a small reaction rate and an accumulation of the molecule in the cold region and the atom in the hot region.

3.1 Introduction

A chemical reaction that occurs far from global equilibrium, has a rate that is highly nonlinear in its driving force. Such reactions occur normally, not only in the presence of concentration gradients, but also in the presence of pressure and temperature gradients, *e.g.* in flames, combustors, turbines, reactors, in micro-porous or turbulent flow fields. For the modelling of these phenomena, it is important to have a well founded non-equilibrium description of the coupled transport processes. In nonequilibrium thermodynamics [1–3] it is assumed that, although the total system is not in equilibrium, there exists within small volume elements a state of 'local equilibrium', for which all normal thermodynamic relations hold. We then know that it is possible to write the entropy production of the system, the quantity that governs the transports, in terms of product sums of fluxes and forces.

The objective of the present work is to examine conditions for local equilibrium in a reacting system, to see how far these conditions can be assumed valid. Unless this assumption holds true, we cannot write the classical flux-force relations. The assumption is used in practice in all calculations of combustion processes [59]. Local equilibrium does not imply that the chemical reaction necessarily is in equilibrium. When a system that is in local thermodynamic equilibrium, is also in chemical equilibrium, the system is said to be in 'local *chemical* equilibrium'. There is local thermodynamic equilibrium in a volume element of the system, when all thermodynamics relations are valid in the volume element. Local chemical equilibrium means that, in addition, the reaction Gibbs energy is equal to zero in the volume element. Local chemical equilibrium is thus a subclass of local thermodynamic equilibrium. This special condition is also frequently used [59].

Local thermodynamic equilibrium was found to hold in systems exposed to large driving forces for heat and mass transport [4] and at surfaces [5, 6, 60]. For a homogeneous phase, non-equilibrium molecular dynamics (NEMD) simulations with Lennard-Jones spline particles were used to verify that local thermodynamic equilibrium was valid in a two-component mixture with a temperature gradient up to 10^8 K/m [4]. It was also found to apply to a heterogeneous system, a gas-liquid interface in a one-component system [5]. Chemical reactions have not been investigated before from this perspective, and

one may wonder how good the assumption of local equilibrium is in, for instance, flame composition calculations. The temperature gradient in flames is thought to be around 10^8 K/m. NEMD simulations are suitable for investigating problems of a thermodynamic nature, with the purpose of gaining molecular and statistical insight. For instance, one can find velocity distributions and compare them to a Maxwell distribution, a measure for thermodynamic equilibrium. This shall be done here. According to Ross and Mazur [61], the entropy production is bilinear in the fluxes and forces when the law of mass action holds. This is the case for reactions which do not disturb appreciably the Maxwell velocity distribution of the chemical components [1].

The purpose of this work is thus to use NEMD to study the precise nature of a chemical reaction exposed to large temperature gradients, up to 10^{12} K/m. How far is the reaction from local chemical equilibrium in the gradient? How can we characterize the behavior in the volume element, with an enormous energy flux, of about 10^8 kJ/m^{2}s, across it?

In order to accomplish such a study, we first have to establish NEMD procedures for a chemical reaction. For studies of the type we are after, quantum effects are not essential. A mechanical model may then be convenient for computational reasons. In order to capture the main thermodynamic property of the chemical reaction, namely its microscopic reversibility, the mechanical model must include not only 2, but also 3-body potentials [54, 62–64]. We chose therefore to use the reversible reaction;

$$2\mathrm{F} \rightleftarrows \mathrm{F}_2 \tag{3.1}$$

for method developments and first studies, as the 2 and 3-body interaction potential of fluorine atoms and fluorine molecules are well known and documented at equilibrium [49–53].

We shall thus report a first computational effort to build an effective reaction model to be used with NEMD. The impact of the 2 and 3-body potential on the calculation of fluxes and forces, and the algorithms used, shall first be reported. The state of the reaction shall next be studied for a fluid with a constant overall density (near 11 kmol/m^3) in various temperature gradients. The largest gradient was 1.1×10^{12} K/m and the corresponding total heat flux (or energy flux) was 9.9×10^8 kJ/m^{2}s. We shall see that the assumption of local thermodynamic equilibrium is fulfilled, as measured by the velocity distributions of both components, which were close to being Maxwellian. Local chemical equilibrium was also found to be valid for this particular reaction for a large range of conditions, within the accuracy of the calculation, and in spite of the net movement of components between the hot and the cold regions. The laws of thermodynamics at a local level can thus be safely applied, in spite of the extreme conditions.

3.2 Theory

3.2.1 Governing equations

De Groot and Mazur [1] give the expression for the entropy production rate for a two-component system with transports of heat and mass, and a chemical reaction:

$$\sigma = \mathbf{J}'_q \cdot \nabla \left(\frac{1}{T}\right) - \frac{1}{T}\sum_k \mathbf{J}_k \cdot \nabla \mu_{k,T} - \frac{r}{T}\Delta_r G \geq 0 \tag{3.2}$$

As is standard in non-equilibrium thermodynamics, σ is the sum of products of flux-force pairs. Here $\mathbf{J}'_q$ is the measurable heat flux, T the absolute temperature, $\mathbf{J}_k$ the molar component fluxes with respect to the wall (or the net movement of F and F_2), $\nabla \mu_{k,T}$ the gradient in chemical potential at a constant temperature, r the reaction rate, and $\Delta_r G$ is the reaction Gibbs energy. The symbol $\cdot$ between two vectors indicates a contraction of two vectors (a scalar product). The first two flux-force pairs are vectors. The reaction has one scalar flux-force pair, r and $\Delta_r G/T$. Our simple reaction is:

$$2\mathrm{F} \rightleftarrows \mathrm{F}_2 \tag{3.3}$$

In the molecular dynamics simulations we only considered gradients and fluxes in the $x-$direction. In that case the entropy production rate simplifies to

$$\sigma = J'_q \frac{\partial}{\partial x}\left(\frac{1}{T}\right) - \frac{1}{T}\sum_k J_k \frac{\partial}{\partial x}\mu_{k,T} - \frac{r}{T}\Delta_r G \geq 0 \tag{3.4}$$

The balance equations for the molar densities are thus:

$$\begin{aligned} \frac{\partial c_F(x,t)}{\partial t} &= -\frac{\partial\, J_F(x,t)}{\partial x} - 2r(x,t) = 0 \\ \frac{\partial c_{F_2}(x,t)}{\partial t} &= -\frac{\partial J_{F_2}(x,t)}{\partial x} + r(x,t) = 0. \end{aligned} \tag{3.5}$$

Here c_F and c_{F_2} are molar densities of component F and F_2 respectively. In our analysis we will focus on stationary states alone. The molar fluxes and the reaction rate are then only functions of x. No external forces were applied during the simulations, and there was no mass flux out of the box. Mass conservation gives in a stationary state:

$$\frac{\partial J_F(x)}{\partial x} = -2\frac{\partial J_{F_2}(x)}{\partial x} = -2r(x) \tag{3.6}$$

At every position, the divergence of each flux is therefore balanced by the reaction rate. From reaction kinetics, we can express the net reaction rate as

$$r = r_f - r_b \tag{3.7}$$

where r_f and r_b are unidirectional forward and backward reaction rate, respectively. By integrating Eq.(3.6), we have $J_F(x) = -2J_{F_2}(x) + C$, where C depends on the system boundaries. In this system, C=0, and as a consequence

$$J_F(x) = -2J_{F_2}(x) \tag{3.8}$$

We shall find that the divergences of the fluxes are finite and lead to nonzero molar fluxes in the system, of atoms to the cold side and molecules to the hot side.

In the stationary state, the measurable heat flux is related to the reaction enthalpy. This can be seen from the expression for the total heat flux, or energy flux:

$$J_q = J'_q + J_F H_F + J_{F_2} H_{F_2} = J'_q + J_{F_2} \Delta_r H \tag{3.9}$$

Here H_F and H_{F_2} are partial molar enthalpies of F and F_2, respectively. We have used Eq.(3.8) and $\Delta_r H = H_{F_2} - 2H_F$. At the boundaries used, both mass fluxes were zero. This allows us to use $J'_q{=}J_q$ at these locations. The energy flux through the system is constant.

3.2.2 Defining local equilibrium and local chemical equilibrium

There is local thermodynamic equilibrium in a volume element of a system when:

- All normal thermodynamic relations are valid in the volume element [65].

Criteria for local thermodynamic equilibrium were investigated by Hafskjold and Kjelstrup [4]. They found that the assumption was valid even when the temperature gradient was $\nabla T{=}10^8$ K/m. On the statistical level, local thermodynamic equilibrium means:

- The probability distribution of particle velocities is close to being Maxwellian everywhere in the system;

The Maxwell distribution of the $x-$component of the velocity is:

$$M(\mathrm{v_x}) = \sqrt{\frac{\mathrm{m}}{2\pi \mathrm{k_B T_x}}} \exp\left(-\frac{\mathrm{m}(\mathrm{v_x} - \langle \mathrm{v_x} \rangle)^2}{2\mathrm{k_B T_x}}\right). \tag{3.10}$$

Here k_B is Boltzmann's constant, m is the mass of the particle in question, v_x is the $x-$component of the particle's velocity, $\langle \mathrm{v}_x \rangle$ is its average and T_x is the temperature in the volume element calculated from the average kinetic energy in the x-direction. The distributions in the y and the z direction are similar.

There is local chemical equilibrium in a volume element of a system when:

- In addition to the two criteria above, the reaction Gibbs energy is zero, $\Delta_r G(x){=}0$.

This is a special case of local thermodynamic equilibrium. The velocity distribution should be close to Maxwellian for both particles also in this case [61] in order for the law of mass action to be valid. We can finally state that a system is in *global* equilibrium when all volume elements have the same thermodynamic state. This is what we normally understand as equilibrium.

3.2.3 The equilibrium constant and the reaction Gibbs energy

The chemical potentials of F and F_2 are needed to define the reaction Gibbs energy. For each of the components, we have:

$$\mu_k = \mu_k^{\ominus} + RT \ln f_k/p^{\ominus} \tag{3.11}$$

where f_k is the fugacity and k represents F or F_2 and the standard state is $p^{\ominus}$=1 bar.

The fluid that we are dealing with, has a relatively high overall density, 11 kmol/m^3. We are working with temperatures from 400 K and up, but with high pressures. At the critical point, the molar density of molecular fluorine is for comparison, near 15 kmol/m^3, the critical temperature is 144 K, and the critical pressure is 52 bar. It is thus necessary to use fugacities rather than partial pressures alone. The fugacity of the component with partial pressure p_k, is:

$$f_k = \gamma_k p_k = \gamma_k \frac{N_k}{N_F + N_{F_2}} p \tag{3.12}$$

We use particle numbers N_k to calculate the mole fraction x_k. The reaction Gibbs energy is:

$$\Delta_r G = \Delta_r G^{\ominus} + RT \ln Q \tag{3.13}$$

where $\Delta_r G^{\ominus}=\mu_{F_2}^{\ominus} - 2\mu_F^{\ominus}$ is the standard reaction Gibbs energy and Q is the reaction quotient, defined by

$$Q = \gamma_p \frac{N_{F_2}(N_F + N_{F_2})}{(N_F)^2} \frac{p^{\ominus}}{p} \tag{3.14}$$

and γ_p is the activity coefficient ratio γ_{F_2}/γ_F^2. When Δ_rG=0 we obtain

$$\Delta_r G^{\ominus} = -RT \ln K_{eq} \tag{3.15}$$

and

$$K_{eq} = \left[\gamma_p \frac{N_{F_2}(N_F + N_{F_2})}{(N_F)^2} \frac{p^{\ominus}}{p} \right]_{eq}. \tag{3.16}$$

The equilibrium constant is only a function of the temperature (with 1 bar standard state). When the activity coefficient ratio is unity, K_{eq}=K_p :

$$K_p = \left[\frac{N_{F_2}(N_F + N_{F_2})}{(N_F)^2} \frac{p^{\ominus}}{p} \right]_{eq}. \tag{3.17}$$

The value of K_p can be found from simulation data; components numbers and the pressure of the mixture. We can calculate

$$K_p' = \frac{N_{F_2}(N_F + N_{F_2})}{(N_F)^2} \frac{p^{\ominus}}{p} \tag{3.18}$$

also in simulations of systems which are not in global equilibrium. If K_p' is the same function of T as K_p is, one may conclude that the mixture in question is in chemical equilibrium, without having knowledge of $\gamma_p(T)$.

3.3 Model and simulation details

3.3.1 The reaction model

The reaction given in Eq.(3.3), is simple. Fluorine atoms and molecules react and form a mixture. In order to see why 2- and 3-body potential interactions are essential, we write the reaction mechanism for Eq.(3.3) by:

$$\mathrm{F} + \mathrm{F}_2 \rightleftarrows \mathrm{F}_2 + \mathrm{F} \tag{3.19}$$

This equation indicates that an atom can constantly hit a molecule, and form a new bond (a molecule) plus a new single atom. Alternatively, one may write for the same:

$$\mathrm{F} \cdots \mathrm{F} - \mathrm{F} \rightleftarrows \mathrm{F} - \mathrm{F} \cdots \mathrm{F}. \tag{3.20}$$

Stillinger and Weber [52] gave the potential surface Φ for the reaction as:

$$\Phi(\mathbf{r}_1, ..., \mathbf{r}_N) = \sum_{\text{pairs } i,j} u_2(r_{ij}) + \sum_{\text{triplets } i,j,k} u_3(r_{ij}, r_{ik}, r_{jk}) \tag{3.21}$$

Here u_2 is the two-atom potential, a function of the atom-atom distance $r_{ij} \equiv |\mathbf{r}_i - \mathbf{r}_j|$, and u_3 is the three-atom potential determined by three-atom distances r_{ij}, r_{ik} and r_{jk}. The subscripts i, j and k indicate different atoms. The pair potential u_2 was selected to give a good representation of isolated diatomic fluorine:

$$u_2(r_{ij}) = \begin{cases} A\epsilon_0 \left[(\sigma_0/r_{ij})^8 - (\sigma_0/r_{ij})^4\right] \exp\left[\sigma_o/(r_{ij} - r_{c1})\right] & ,0 < r_{ij} < r_{c1} \\ 0 & ,r_{ij} \geq r_{c1} \end{cases} \tag{3.22}$$

The value A=6.052463017 causes the reduced pair potential u_2^*=u_2/ϵ_0 to have a minimum with depth -1 at the normal fluorine bond distance $1.18199\sigma_0$ (1.435 Å). The function vanishes at a cutoff distance of r_{c1}=$3.6\sigma_0$. For the choice of these coefficients and a discussion of this choice we refer to Stillinger and Weber [52]. The reduced pair potential is plotted in Fig. 3.1.

Reduced units were used in the calculation. Basic units were the diameter of the fluorine atom, σ_0=1.214 Å, its potential energy depth ϵ_0=2.659×10^{-19} J and its particle mass, m_0=3.155×10^{-26} kg. Reduced units are indicated by a star symbol. The variables in real and reduced form are listed in Table 3.1. Using these reduced units the expression for the pair potential becomes

$$u_2^*(r_{ij}) = \begin{cases} A\left[\left(r_{ij}^*\right)^{-8} - \left(r_{ij}^*\right)^{-4}\right] \exp\left[1/(r_{ij}^* - r_{c1}^*)\right] & ,0 < r_{ij}^* < r_{c1}^* \\ 0 & ,r_{ij}^* \geq r_{c1}^* \end{cases} \tag{3.23}$$

The three-atom potential u_3 is the sum of three $h-$functions:

$$\begin{aligned} u_3(r_{ij}, r_{ik}, r_{jk}) &= h_i + h_j + h_k \\ &= h(r_{ij}, r_{ik}, \theta_i) + h(r_{ij}, r_{jk}, \theta_j) + h(r_{ik}, r_{jk}, \theta_k). \end{aligned} \tag{3.24}$$

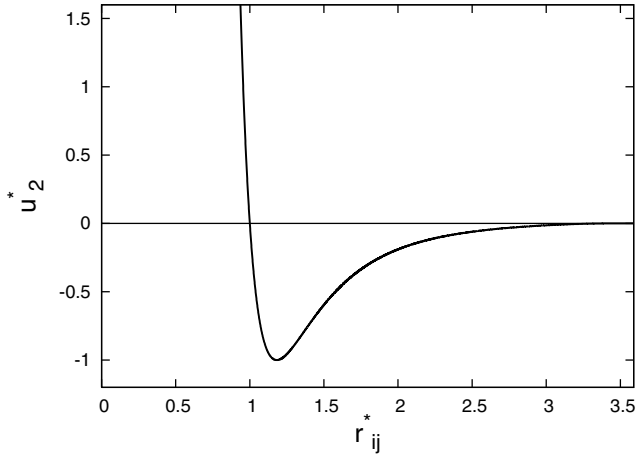

Figure 3.1: Pair potential used for the fluorine model. This function vanishes when $r^*_{ij} \geq r^*_{c1} = 3.6$.

Table 3.1: **Relations between reduced and real variables for fluorine**

Reduced variable, symbol	Formula
mass	$m^* = m/m_0$
distance	$r^* = r/\sigma_0$
energy	$U^* = U/\epsilon_0$
time	$t^* = (t/\sigma_0)\sqrt{\epsilon_0/m_0}$
temperature	$T^* = k_B T/\epsilon_0$
molar density of k	$c^*_k = N_A c_k \sigma_0^3$
pressure	$p^* = p\sigma_0^3/\epsilon_0$
velocity	$v^* = v\sqrt{m_0/\epsilon_0}$

The three-atom potential was scaled to fit fluorine, from the well-known potential surface of H+H_2 [52]. The three $h-$functions are symmetric in their first two variables, while θ_i in h_i represents the angle between r_{ij} and r_{ik}, and similarly for θ_j and θ_k. Figure 3.2 gives notations for the triple fluorine configuration. The expression for the reduced $h-$ function is:

$$h^*(a^*,b^*,\theta) = \begin{cases} 8.4(a^*b^*)^{-4}\exp\left[(a^*-r^*_{c1})^{-1}+(b^*-r^*_{c1})^{-1}\right] & \\ \quad +\left(50-25\cos^2\theta\right)\exp\left[3\,(a^*-r^*_{c2})^{-1}\right. & ,0<a^*,b^*<r^*_{c2} \\ \quad \left.+\,3\,(b^*-r^*_{c2})^{-1}\right] & \\ 8.4(a^*b^*)^{-4}\exp\left[(a^*-r^*_{c1})^{-1}+(b^*-r^*_{c1})^{-1}\right] & \text{,either } a^* \text{ or } b^* \text{ exceeds } r^*_{c2} \\ 0 & \text{,either } a^* \text{or } b^* \text{exceeds } r^*_{c1} \end{cases} \tag{3.25}$$

Here a (a=$a^*\sigma_0$) and b (b=$b^*\sigma_0$) are adjacent sides of the angle θ. The expression for $\cos^2\theta$=$(a^2+b^2-c^2)/(2ab)$, where c (c=$c^*\sigma_0$) is the third side of the triangle, was used to

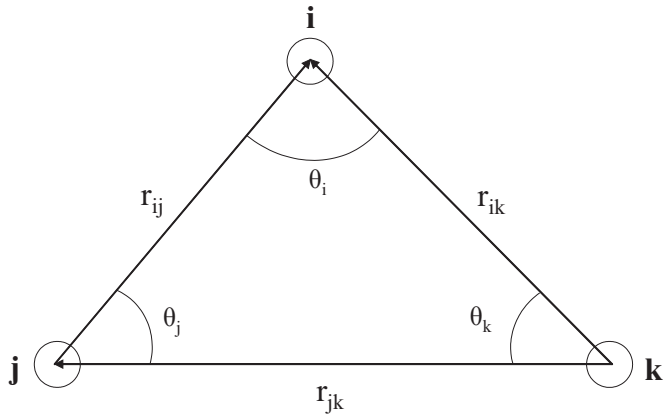

Figure 3.2: Notations used for a triple configuration.

make the formula for h dependent on positions only. The second cutoff distance r_{c2}=2.8σ_0 was obtained from the aforementioned scaling [52].

Using the 2-atom and 3-atom reaction model, we computed first the potential energy for the linear configuration of three fluorine atoms. The results were compared with those of Stillinger and Weber [52]. We found the same value as they, −1.04 (in reduced units), for the two triple potential minima. Figure 3.3 shows the contour plot of the potential energy for the linear 3-F configuration. Contours are given for reduced values −1.04, −1.01, and up. In this symmetrical configuration, the transition state for the reaction is found on the diagonal in the figure that separates the potential minima.

Stillinger and Weber [52] used a distance cutoff criterion to identify chemical bonds, and by default also identifying unbonded atoms produced by dissociation. The value was chosen in the low temperature pair correlation function gap, which gave the cutoff diameter r_c=1.7σ_0. Any pair of atoms with atom-atom distance less than or equal to r_c were thus defined as molecules, *i.e.* chemically bonded. Pairs with atom-atom distance larger than this value were considered as free atoms. An important role of the chosen three-atom potential is to prevent the formation of more than one covalent bond to each fluorine atom [52].

3.3.2 Simulation details

The MD box. Algorithms

The system had N=1000 fluorine atoms in a box with dimensions L_x, L_y, L_z, in the x, y and z direction, respectively. Stillinger and Weber [52] used the same number of fluorine atoms. The volume of the box was V=$L_xL_yL_z$=1000/(cN_A), where c is the overall molar density (11270.9 mol/m^3), and N_A is Avogadro's number. The molecular dynamics (MD)-box was non-cubic, with lengths L_y=L_z=L_x/2. It was divided into 128 equal planar

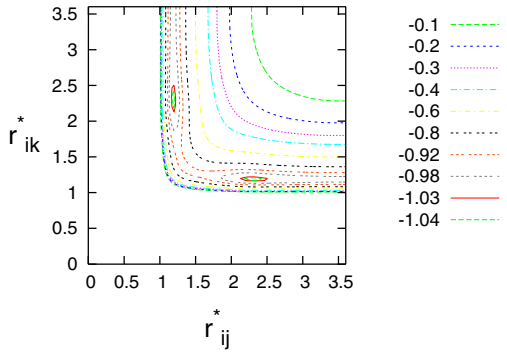

Figure 3.3: Potential energy contours for a linear arrangement three fluorine atoms.

volume layers in the $x-$direction, with a symmetry plane between layers 64 and 65. The volume of each layer is V_L=V/128.

When the system was thermostatted, equilibrium MD simulations produced a canonical ensemble (with constant number of particles N, volume V and temperature T). In order to test system size dependence, we did some of the equilibrium simulations with 1728 particles and L_y=L_z=L_x/8.

Ikeshoji /Hafskjold [39] periodic boundary conditions were applied to the x-direction and regular periodic boundary conditions were used in the y- and z-directions. In a stationary state the system is symmetric. Figure 4.4 shows a 3-dimensional snapshot of 1000 fluorine particles in the MD box. Layers 1-4 and 125-128 (the hot layers) at the ends of the box were thermostatted to the temperature T_H using the HEX algoritm [4]. The layers 61-69 (the cold layers) in the middle of the box were thermostatted to the temperature , where $T_C \leq T_H$. Thermodynamic properties were found by time averaging over the instantaneous values in elements that lie symmetric to the central plane in the box.

The Verlet 'Leap Frog' algorithm was used. Many particle pairs are out of the range r^*_{c1}=3.6 of each others pair potential, see Eq.(A.2). To restrict the computation time a list of pairs was made with a distance from each other smaller than a cut-off distance, r^*_{list}=4. Pair interactions were calculated when r^* was equal to or smaller than this value. A similar algorithm, called NEIGHBOUR3, was made to compute 3-body interactions. For this, a list of triplets was made by combining pairs from the pair list, which had one particle in common.

As long as the displacement of the particles was less than half of $r^*_{list} - r^*_{c1}$=0.4, we

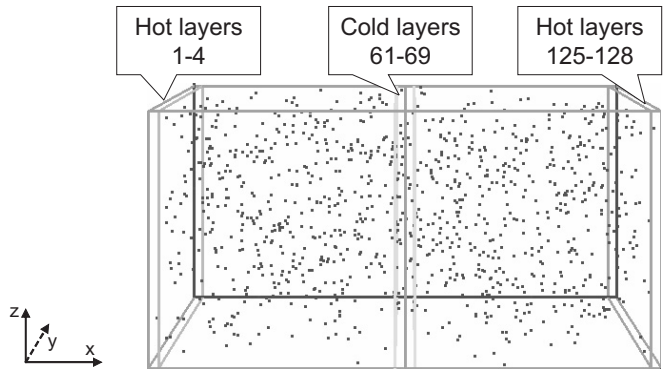

Figure 3.4: A snapshot of the MD box with 1000 fluorine atoms, partially reacted to molecules. The box has dimensions $L_y/L_x = L_z/L_x = 1/2$.

did not need to update the two lists. This procedure avoided unnecessary calculation of particle interactions. A time step length of 0.01 in reduced units (see Table 2) was used. This corresponds to 4.1817 ± 10^{-16} s in real time.

Equilibrium MD simulations

Equilibrium simulations were first done. These results are called EMD results. We used the NEMD program (see next section) thermostatting the hot and the cold layers to the same temperature, to find the EMD results. In the EMD simulations, the program gave the temperatures of each layer within 0.1%. A standard thermostat method (the velocity scaling algorithm [4]) was applied during the first 1000 time steps.

Thirteen equilibrium cases were studied, all with the same overall density, c^*=0.012147:

- Case 1: This case is identical to one of the cases of Stillinger and Weber [52]. The triple point of molecular fluorine is T_t^*=0.002779 and ρ_t^*=0.097173 [52], and we chose a state well above this point, with a temperature T^*=0.019.
- Cases 2-13 had temperatures varying from T^*=0.25, in steps by 0.05 to 0.80 in reduced units.

Case 1 was done to check reproducibility of the earlier EMD [52] results with our NEMD code. In all cases, we calculated compositions and velocities of atoms and molecules, temperature and pressure (see section on Calculation details). We also calculated the velocity distribution of the x -component of the velocity of atoms and molecules in equilibrium. They are given for Cases 4 and 13 in Fig. 3.9 for a position where the reduced temperatures were T^*=0.35 and T^*=0.8, respectively.

Non-equilibrium MD simulations

Details of the NEMD program have been described in earlier work [4,5,9,35,38]. Here we shall only give the main properties as well as the expressions which are modified due to contributions from the three particle interactions.

The thermostatting algorithm was now used to control the temperatures in the hot and in the cold layers. All NEMD simulations were performed over 10^7 time steps. We omitted the first 2×10^6 time steps, which showed transient effects. Mean values of properties, such as temperature and density, were computed for each layer of the box. The average value was then taken for mirror symmetric layers. Time averages were done every 5×10^5 time steps.

Nine NEMD simulations were performed, Cases 14-22. The temperatures in the hot and the cold layers for these cases, are listed in Table 3.2 . Cases 14, 15 and 16 had the smallest temperature difference, while Case 22 had the largest temperature difference. In the last case the temperature gradient was 1.1×10^{12} K/m and the heat flux through the system was then 9.9×10^8 kJ/m^{2}s. For even larger temperature differences the velocity distribution would no longer relax to a nearly Maxwellian distribution, so that nothing comparable to local equilibrium developed. In all cases the NEMD simulations were very far from global equilibrium. The velocity distributions of the x-component of the velocity of atoms and molecules were studied. They are given for the Cases 19 and 22 in Fig. 3.10 for a position where the reduced temperatures were T^*=0.488 and T^*=0.511, respectively.

Table 3.2: **NEMD simulation conditions. The temperature is given in reduced units.**

Case no.	14	15	16	17	18	19	20	21	22
T^*_H	0.30	0.35	0.40	0.40	0.50	0.60	0.80	1.00	0.80
T^*_L	0.25	0.30	0.35	0.30	0.40	0.40	0.60	0.70	0.30

Calculation details

The same NEMD program was used to calculate all properties, also equilibrium properties. In EMD simulations, the overall temperature, pressure and densities were determined by averaging layer properties over all 128 layers in the MD box. In NEMD simulations, local properties, such as temperature, pressure and densities, were calculated for each layer, and an average was then taken for pairs of layers that were mirror symmetric around the center of the box.

The molar density of component k in layer l, with l=1,...,128, is:

$$c_{k,l} = \frac{N_{k,l}}{N_A V_L} \tag{3.26}$$

where $N_{k,l}$ is the number of particles of component k (F or F_2) in the layer l. All the layers have the volume $V/128$. Furthermore N_A is Avogadro's number.

The temperature T_l of layer l was found from the average kinetic energy per degree of freedom:

$$T_l = \frac{1}{3k_B N_l} \sum_{i \in l} m_i v_i^2 \tag{3.27}$$

where $N_l = \sum_k N_{k,l}$ is the total number of particles in the layer l and $v_i^2 = v_{x,i}^2 + v_{y,i}^2 + v_{z,i}^2$.

From the virial theorem, the expression for the pressure tensor for layer l in the presence of 2- and 3-body interactions is:

$$\boldsymbol{p}_l = \frac{k_B T N_l}{V_L}\mathbf{1} + \frac{1}{V_L}\sum_{i \in l}\left(\sum_{j \text{ pair with } i} \boldsymbol{w}_{i(j)} + \sum_{j<k \text{ triplet with } i} \boldsymbol{w}_{i(j,k)}\right) \tag{3.28}$$

where $\mathbf{1}$ is the unit tensor. The first contribution on the right hand side is the kinetic contribution. The second and the third contribution are due to the two and the three particle interaction respectively. The summands in these terms are given by:

$$\begin{aligned} \boldsymbol{w}_{i(j)} &= -\frac{1}{2}\frac{\partial u_2(r_{ij})}{\partial\, r_{ij}}\hat{\boldsymbol{r}}_{ij}\boldsymbol{r}_{ij} \\ \boldsymbol{w}_{i(j,k)} &= -\frac{\partial h_i}{\partial r_{ij}}\hat{\boldsymbol{r}}_{ij}\boldsymbol{r}_{ij} - \frac{\partial h_i}{\partial r_{ik}}\hat{\boldsymbol{r}}_{ik}\boldsymbol{r}_{ik} - \frac{\partial h_i}{\partial r_{jk}}\hat{\boldsymbol{r}}_{jk}\boldsymbol{r}_{jk} \end{aligned} \tag{3.29}$$

where the hat indicates a unit vector, like $\hat{\boldsymbol{r}}_{ij} = \boldsymbol{r}_{ij}/r_{ij}$. In the expression for the contribution due to pair interactions we use the convention due to Irving and Kirkwood [66] and assign half of the force moment due to the pair ij to particle i and the other half to particle j. The interaction energy due to a triple, cf. Eq.(3.24), is the sum of three terms, h_i, h_j and h_k. In Eq.(3.28) we have assigned the force moments due to h_i to particle i, those to h_j to particle j and those to h_k to particle k . Though other choices are possible this seems like a natural choice. In the simulations we found the pressure to be independent of the position. A different choice would therefore lead to essentially the same results. Furthermore the pressure tensor was found to be diagonal and the same in all directions. Using Eq.(3.29) we find for the hydrostatic pressure in layer l one third of trace of the tensor given in Eq.(3.28)

$$p_l = \frac{k_B T N_l}{V_L} - \frac{1}{3V_L}\sum_{i \in l}\left[\frac{1}{2}\sum_{j \text{ pair with } i}\frac{\partial u_2(r_{ij})}{\partial\, r_{ij}} r_{ij} + \sum_{j<k \text{ triplet with } i}\left(\frac{\partial h_i}{\partial r_{ij}} r_{ij} + \frac{\partial h_i}{\partial r_{ik}} r_{ik} + \frac{\partial h_i}{\partial r_{jk}} r_{jk}\right)\right] \tag{3.30}$$

The positive direction of the fluxes is from the left to the right hand side of the MD-box. The molar flux of component k in layer l is:

$$\mathbf{J}_{k,l} = \frac{1}{N_A V_L}\sum_{i \in l \,,\, i \in \text{ component } k} \mathbf{v}_i \tag{3.31}$$

The total molar flux in layer l is given by

$$\mathbf{J}_l = \sum_k \mathbf{J}_{k,l} \tag{3.32}$$

The energy flux in layer l is

$$\begin{aligned} \mathbf{J}_{q,l} &= \frac{1}{V_L} \sum_{i \in l} \left[\mathbf{v}_i \left(\frac{1}{2} m_i \mathrm{v}_i^2 + \Phi_i \right) + \mathbf{v}_i \cdot \boldsymbol{p}_l \right] \\ &= \frac{1}{V_L} \sum_{i \in l} \mathbf{v}_i \left(\frac{1}{2} m_i \mathrm{v}_i^2 + \Phi_i + p_l \right) \end{aligned} \tag{3.33}$$

where the $\cdot$ now indicates a contraction of a vector and a tensor. Furthermore Φ_i is the potential energy of particle i

$$\Phi_i = \frac{1}{2} \sum_{j \text{ pair with } i} u_2(r_{ij}) + \sum_{j<k \text{ triplet with } i} h(r_{ij}, r_{ik}, \theta_i) \tag{3.34}$$

In the expression for the contribution due to pair interactions we assign half of the force moment due to the pair ij to particle i and the other half to particle j. The interaction energy due to a triplet, cf. Eq.(3.24), is the sum of three terms, h_i, h_j and h_k. In Eq.(3.34) we have assigned h_i to particle i, h_j to particle j and h_k to particle k. All these choices are analogous to the ones we made in the expression for the pressure, see Eqs.(3.28) and (3.30). In the expression for the energy flux, Eq.(3.33), it is crucial to use similar choices as those used in the pressure. This contributes to making the treatment self-consistent. It should be emphasized that other choices are possible, which should give essentially the same results.

The measurable heat flux in a volume element is related to the energy flux by

$$\mathbf{J}'_{q,l} = \mathbf{J}_{q,l} - \mathbf{J}_{\mathrm{F},l} H_{\mathrm{F},l} - \mathbf{J}_{\mathrm{F}_2,l} H_{\mathrm{F}_2,l} = \mathbf{J}_{q,l} - \mathbf{J}_{\mathrm{F}_2,l} \Delta_r H_l \tag{3.35}$$

where the reaction enthalpy in layer l is $\Delta_r H_l = H_{\mathrm{F}_2,l} - 2H_{\mathrm{F},l}$. It is impossible to calculate the partial enthalpies $H_{\mathrm{F}_2,l}$ and $H_{\mathrm{F},l}$ by simulations. We can, however, find the total enthalpy of F and of F_2 in layer l. The total enthalpy in J/mol is given by

$$H_l = N_A \left\{ \frac{1}{N_l} \sum_{i \in l} \Phi_i + \frac{p_l V_L}{N_l} + \frac{3}{2} k_B T \right\} \tag{3.36}$$

By allocating contributions to H_l from F or F_2, we found estimates for molar enthalpies. With this information, we estimated $\Delta_r H$ for each layer. With knowledge of the particle flux and total heat flux, we were then able to estimate the measurable heat flux. These estimates will be reliable when the gas is close to being ideal.

3.4 Results and discussion

3.4.1 An algorithm for a chemical reaction in a temperature gradient

The results of the EMD simulation for Case 1 are shown in Fig. 3.5. The results are identical to those of Stillinger and Weber [52] up to 70 psec. We continued the simulation

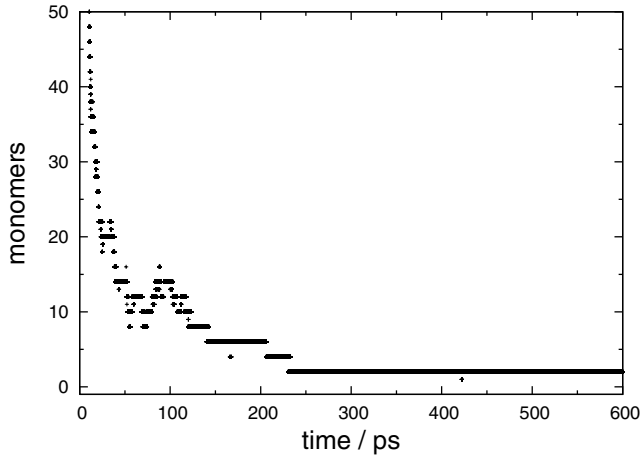

Figure 3.5: The decline of free fluorine atoms from a start with 1000 particles versus time (in pico seconds) at $T^* = 0.019$ and $c^* = 0.012147$. The number of fluorine atoms declined rapidly due to the reaction in the first 60 ps. The chemical reaction was limited by diffusion in the MD box. Two atoms remained at equilibrium at stationary state.

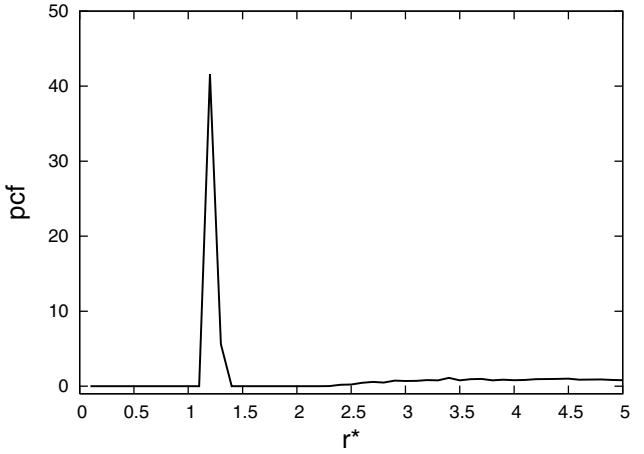

Figure 3.6: The pair correlation function in the reacting system at $T^* = 0.019$ and $c^* = 0.012147$. The peak represents chemically bonded atoms.

up to $4{\times}10^6$ time steps (1672.8 psec), and found a stationary state with only two atoms left, see Fig. 3.5. The corresponding pair correlation function (pcf) versus distance is shown for the long runs in Fig. 3.6. The sharp peak of the pcf curve is positioned at a reduced atom-atom distance of r^*=1.2. This represents the chemically bonded pairs, and corresponds to the minimum in Fig. 3.1.

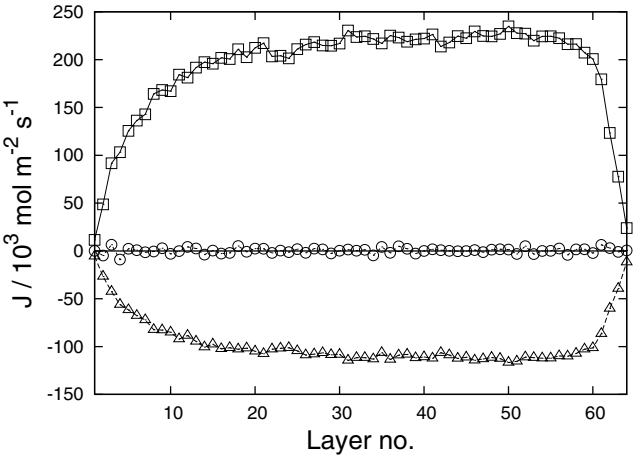

Figure 3.7: The molar fluxes in the NEMD simulation Case 18, at $c^* = 0.012147$. Symbols give values for the layers in MD box.

We have thus confirmed the equilibrium results of Stillinger and Weber [52] and consider our computations to be reliable.

3.4.2 The chemical reaction in the temperature gradient

The system we investigated had no net mass flux. In order to obey mass conservation (Eq.3.8), the flux of atoms was everywhere minus twice the flux of molecules. The calculations are reported for stationary state. The fluxes in Case 18 are shown in Fig. 4.3. The flux of atoms was directed to the cold side, while the flux of molecules was directed to the hot side. It is interesting that they are not constant across the box. This situation is very unlike the situation in the absence of a chemical reaction, where the fluxes of both components will be zero at stationary state. The variation is due to the chemical reaction. The total mass flux is proportional to two times the molar flux of F_2 plus the molar flux of F. This flux is, as expected within the accuracy of the calculation, equal to zero.

A net and varying reaction rate $r(x)$, was observed through the system, see Fig. 3.12 for Case 22. The series of events can be understood as the reaction being controlled by diffusion. The transport in and out of a volume element is limited by the fluxes. As soon as a composition is perturbed from its equilibrium value by an incoming flux, the reaction rate will bring the mixture back to equilibrium.

The largest temperature gradient used in the simulations was around 1.1×10^{12} K/m and the corresponding total heat flux was 9.9×10^{8} kJ/m^{2}s. The temperature gradient is larger by several orders of magnitude from what one may expect in flames. This gradient drives the chemical reaction by setting up thermal diffusion and interdiffusion of components. The distribution of components must be explained by the reaction in combination

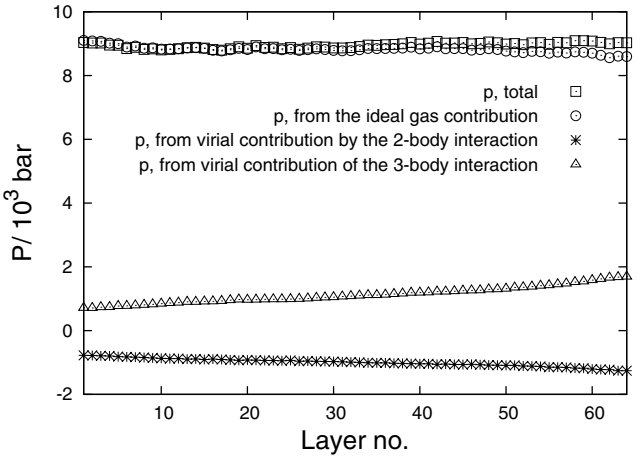

Figure 3.8: The three contributions to the pressure in the NEMD simulation Case 19, at $c^* = 0.012147$.

with a Soret effect [1, 35, 67]. A Soret effect often leads to a preference for the heavy component on cold side. The effect of the chemical reaction may have an impact on flame modelling through this. We shall elaborate on this in our next study.

3.4.3 The effect of the 3-body potential on calculation of thermodynamic properties

The model used to simulate the chemical reaction was described in the theoretical section 3.3.1. Unless a third particle is there to take away excess kinetic energy, a stable pair cannot be formed. Similarly, a molecule need be hit by a third particle, to break open and at the same time change its interaction potential. Calculations of system's properties are consistent with this. As our NEIGHBOUR3 algorithm and the expressions of the section reproduced earlier results we believe that it performs satisfactorily. The 3-body potential interaction had a significant effect on the thermodynamic properties. This is illustrated for the pressure for one condition in Fig. 3.8. The figure shows the varying contributions to the pressure; that is the ideal gas-, the 2-body interaction-, and the 3-body interaction-contribution. The different contributions have different temperature dependencies. The three-body contribution is more sensitive to the temperature than the two-body contribution is. This is expected, as this potential reflects much of the properties of the reaction.

3.4.4 Maxwell velocity distributions

The probability distributions for the $x-$components of the velocities of the atoms, F, and the molecules, F_2 in the system, $P(v_x^*)$=$N(v_x^*)/N$, are shown in Figs. 3.9 and 3.10. Figure

3.9 presents the equilibrium Cases 4 and 13, while Fig. 3.10 presents the nonequilibrium Cases 19 and 22, for layer 35 together with its mirror image. The Maxwell velocity distributions for the two components, $M(\mathrm{v}_x^*)$, were calculated from Eq.(4.2) using the average temperatures of the symmetric layers in question. These results are also shown in Figs. 3.9 and 3.10. These temperatures were found from the average kinetic energy in the x direction. Temperatures obtained from the average kinetic energies in the y and the z direction were found to be the same (as they should be).

Figure 3.9 shows results for global equilibrium, at a low and a high temperature, respectively (T^*=0.35 and T^*=0.8). The figure shows that the velocity distribution of the atoms and molecules have average velocity 0.0000 ±0.0001, and both are Maxwellian within 1% accuracy. This result is what we expect for equilibrium.

The non-equilibrium studies were done at a small temperature difference, ΔT^*=0.2, and the largest possible temperature difference, ΔT^*=0.5. The temperatures and velocities of the atoms and the molecules in the layer were calculated (Cases 19 and 22). We observed that a temperature gradient across the system shifted the velocity distributions. The shift for F_2 gave J_{F_2} as pictured in Fig. 4.3, while the shift for F gave J_F in this figure. The molecules had a sharper distribution than the atoms had in Fig. 3.10, and the molecules gave a negative average velocity, while the atoms gave a positive average velocity. Each distribution was still close to a Maxwellian one. The simulations in sub-figures 3.4.4 and 3.4.4 agreed with their respective Maxwell distribution within ±3% (3.4.4) and ±5% (3.4.4). The shift increased with the temperature gradient. For temperature gradients larger than 10^{12} K/m, we found that the velocity distribution did no longer relax to a nearly Maxwellian distribution.

We can thus conclude that the system is always in local *thermodynamic* equilibrium. This is true even for the largest temperature gradient investigated, 1.1×10^{12} K/m. The situation fits well with the situation described by Ross and Mazur [61]. We see that the chemical reaction perturbs the Maxwell distribution of velocities. The reason is removal (supply) of molecules with high (low) kinetic energy. The perturbation observed here does not alter the law of mass action (see section below) and must therefore be considered small enough. The small shift in the velocity distribution up or down, equal to the mean velocity of the component, does thus not affect the entropy production. It maintains its bilinear form in the fluxes and driving forces [61]. This is comforting to know for a further development of the transport properties of the system. We can use the familiar expression for the entropy production from classical non-equilibrium thermodynamics to define the fluxes and forces in the system. This shall be done in our next paper, when we discuss the transport properties of the mixture.

3.4.5 A distance from local chemical equilibrium?

The question is now whether one can speak of local *chemical* equilibrium in a system that has internal diffusion as described above. This question was investigated by comparing Cases 14-22 to Cases 2-13 (see the theoretical section 3.2.3). The ratio K_p was calculated as a function of T^* for all EMD simulations and plotted in Fig. 3.11. It was verified that

K_p was independent of the size of the system by an extra study with 1728 fluorine atoms in an elongated box. We found the same results as the EMD results with 1000 fluorine atoms (Fig. 3.11), within ±1%.

We next calculated the same ratio for Cases 14 (ΔT^*=0.05), 21 (ΔT^*=0.3) and 22 (ΔT^*=0.5), all as a function of the reduced temperature, T^*, in the box. These results are also shown as points in Fig. 3.11. We observed then that K_p of the EMD simulations and K'_p of the NEMD simulations coincided to a large extent, see Fig. 3.11. There was reasonable agreement (±5%) between the ratios from NEMD and EMD in the central part of the half-box, and less agreement (±10%) close to the thermostatted regions. Deviations were larger for the largest gradient (see Fig. 3.11). We can say on the basis of this, that the reaction is very close to local *chemical* equilibrium away from the boudaries.

By counting the formation of molecules over several thousand time steps at stationary state, we found a forward reaction rate, r_f, in case 22 of around 10^{16} to 10^{17} mol/m^{3}s, see Fig. 3.12. Compared to the value of the forward reaction rate r_f, a net rate of 10^{13} mol/m^{3}s is small. The system is therefore also very close to microscopic reversibility, in spite of having a net reaction rate. We verified this by plotting also the ratio $c^*_{\mathrm{F}_2}/(c^*_{\mathrm{F}})^2$ for EMD and NEMD conditions, shown in Fig. 3.13. Also these ratios were very similar.

3.4.6 Comment on the system's transport properties

The system with the reacting mixture has an enthalpy flux associated with the transport of each component, and therefore a substantial transfer of enthalpy takes place between the ends. The local reaction enthalpy was estimated using Eq.(4.45) for the separate components. The value varied across the box from -340 to -190 kJ/mol. The large enthalpy change has an effect on the measurable heat flux, estimated to be 5% for the largest heat flux. We shall return to a quantitative determination of the transport properties in the future.

3.5 Conclusion

NEMD simulations with various temperature gradients have been done to study the chemical reaction, 2F $\rightleftarrows$ F_2 using the 2-body and 3-body potentials of Stillinger and Weber [52], adding for an efficient MD program the NEIGHBOUR3 algorithm. Our NEMD code reproduced some of the equilibrium results obtained by others [52], indicating that our results can be trusted. Temperature gradients up to ∇T=1.1×10^{12} K/m were investigated.

The non-ideal reacting mixture was always in local thermodynamic as well as in local chemical equilibrium. This means that the reaction Gibbs energy is zero and all normal thermodynamic relations hold. Component velocity distributions remained close to Maxwellian. Statistical and thermodynamic evidence was thus presented that the transport processes are governed by an entropy production which is bilinear in the fluxes and forces of the system. The stationary state was characterized by nonzero average velocities

of the components. Thermal diffusion and interdiffusion of components were set up in the temperature gradient. A net reaction rate was observed much smaller than the forward and the backward reaction rates. The reaction was diffusion controlled.

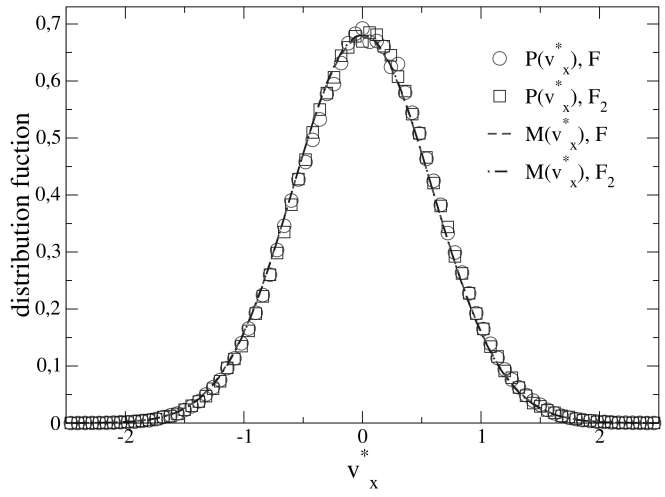

(a)

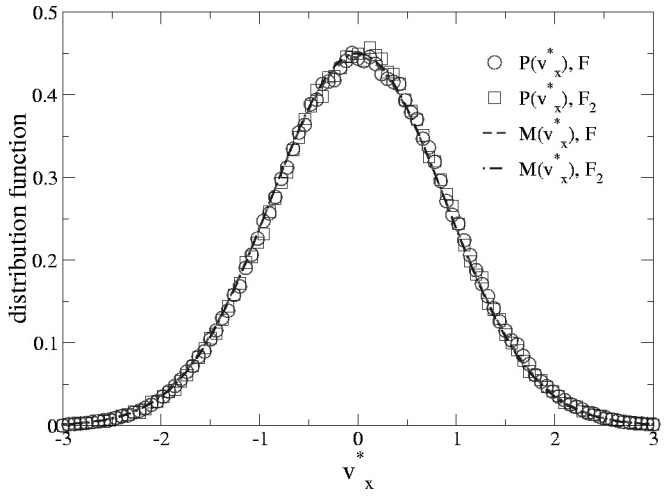

(b)

Figure 3.9: Distribution of the $x-$component of the velocity in layer number 35 of the MD box, which is at equilibrium. The dotted lines are Maxwell velocity distributions (eq. 4.2) in the layer. Symbols denote EMD simulations, Cases 4 and 13. (a) Case 4, $\langle T^* \rangle = 0.345$. (b) Case 13, $\langle T^* \rangle = 0.792$.

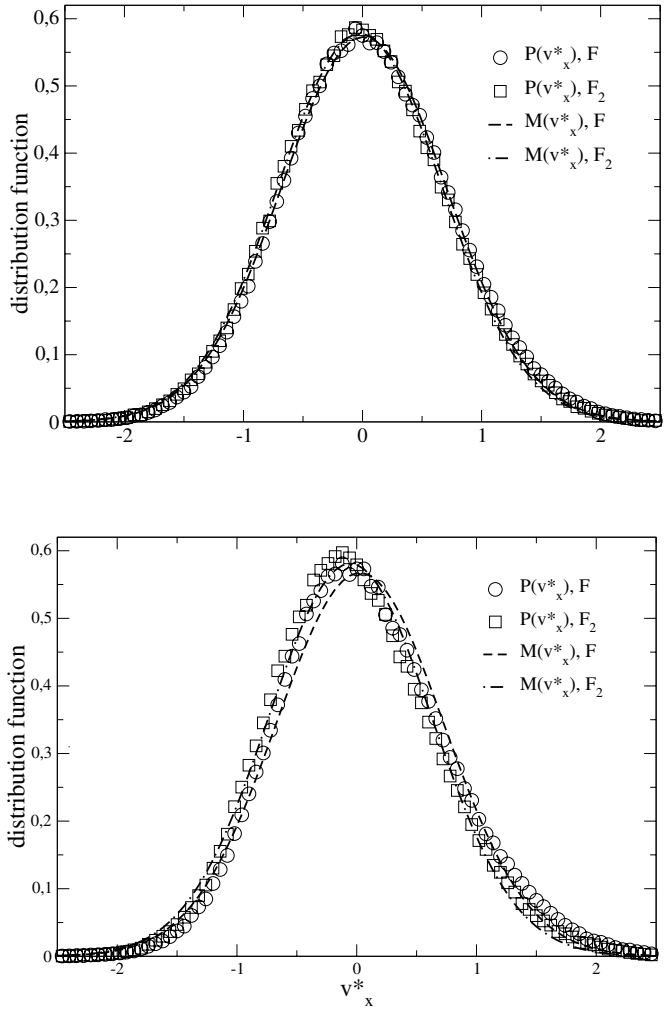

(b)

Figure 3.10: Distribution of the $x-$component of the velocity in layer number 35 of the MD box in a temperature gradient. The dotted lines are Maxwell velocity distributions (eq. 4.2) in the layer. Symbols denote NEMD simulations, Cases 19 and 22. (a) Case 19: $\langle T^* \rangle = 0.488$. (b) Case 22: $\langle T^* \rangle = 0.511$.

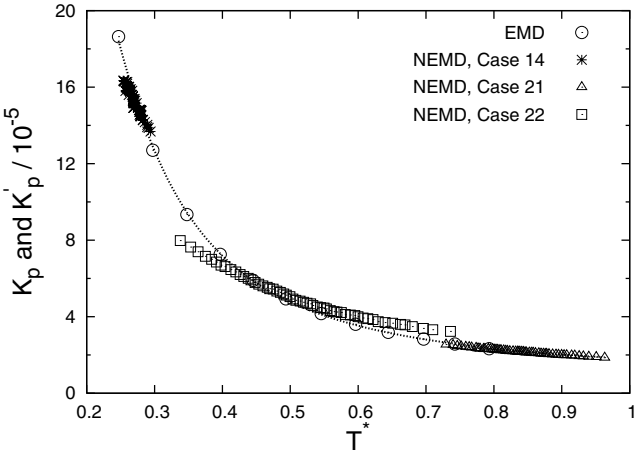

Figure 3.11: K_p and K_p' as a function of temperature, at $c^* = 0.012147$. The dotted curve is the fitted function and the symbols are from EMD simulations (Case 2 - Case 13) and NEMD simulations (Cases 14, 21 and 22).

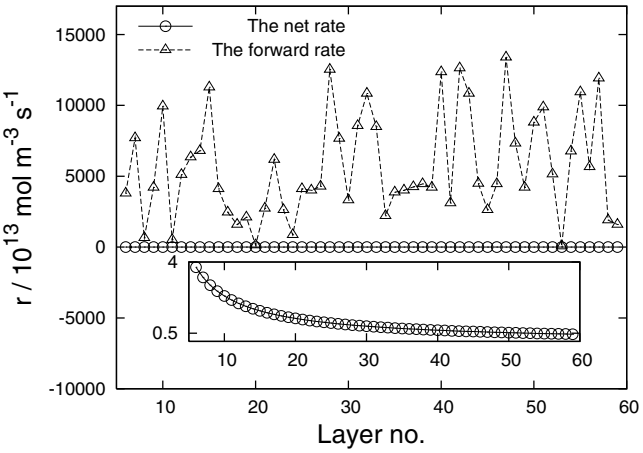

Figure 3.12: The net reaction rate $r(x)$ and the forward reaction rate $r_f(x)$ in NEMD simulation Case 22, at $c^* = 0.012147$. Symbols give values for layer 6 to 59 in the MD box.

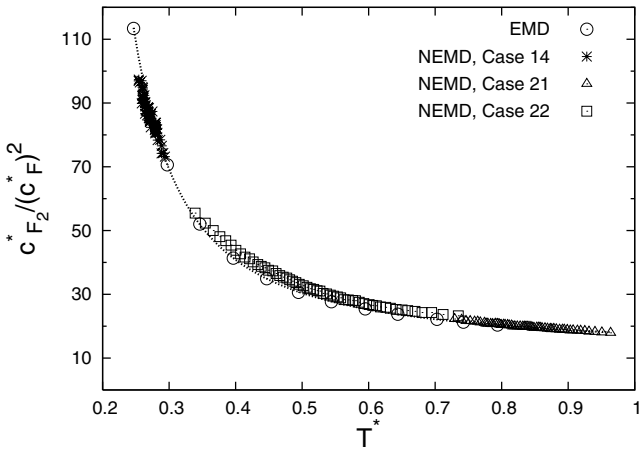

Figure 3.13: $c^*_{F_2}/(c^*_F)^2$ as a function of temperature, at $c^* = 0.012147$. The dotted curve is the fitted function and the symbols are from EMD simulations (Case 2 - Case 13) and NEMD simulations (Cases 14, 21 and 22).

Chapter 4

Transport properties of $F \rightleftarrows F_2$ in a temperature gradient as studied by molecular dynamics simulations

Jing Xu, Signe Kjelstrup, Dick Bedeaux and Jean-Marc Simon

Department of Chemistry
Faculty of Natural Science and Technology,
Norwegian University of Science and Technology
NO-7491 Trondheim, Norway

This paper was published in
Physical Chemistry Chemical Physics,
Volume 9 (2006), pages 1-13.

We calculate transport properties of a reacting mixture of F and F_2 from results of non-equilibrium molecular dynamics simulations. The reaction investigated is controlled by thermal diffusion and is close to local chemical equilibrium. The simmulations show that a formulation of the transport problem in terms of classical non-equilibrium thermodynamics theory is sound. The chemical reaction has a large effect on the magnitude and temperature dependence of the thermal conductivity and the interdiffusion coefficient. The increase in the thermal conductivity in the presence of the chemical reaction, can be understood as a response to an imposed temperature gradient, which reduces the entropy production. The heat of transfer for the Soret stationary state was more than 100 kJ/mol, meaning that the Dufour and Soret effects are non-negligible in reacting mixtures. This sheds new light on the transport properties of reacting mixtures.

4.1 Introduction

Transport properties have been widely studied by computer simulations with the aim to understand the underlying molecular mechanisms or avoid costly and dangerous experiments [68]. Various computing techniques have been used [56,69,70], and we may now say that molecular dynamics simulations are not only able to explain and generate trends, but to a large extent also predict accurate transport properties, at least for pure components and mixtures. This opens up the perspective, that also more sophisticated mixtures like those including a chemical reaction, may be better understood by this technique.

We have recently investigated a chemical reaction in a temperature gradient [44] using boundary driven non-equilibrium molecular dynamics simulations (NEMD). NEMD is made to mimic an experimental situation. As a model for the chemical reaction we took

$$2\mathrm{F} \rightleftarrows \mathrm{F}_2 \tag{4.1}$$

which according to Stillinger and Weber [52] can be satisfactorily modeled by a mechanical analogue (2- and 3-body potentials). In order for the reaction to occur, a collision of three particles was needed.

The study of such systems is important for at least two reasons. In the first place, one would like to confirm that there is a sound basis for the relevant transport equations. In the second place, one would like to learn about the specific transport coefficients, how they vary, and how they can be used in practical contexts; for instance in chemical reactor engineering, or in flame modeling. In such modelling, transport properties for reacting mixtures are central [59]. Also the understanding of dynamic structures may benefit from such a study. The aim of the present work is thus to calculate transport properties of a mixture where a chemical reaction takes place in a temperature gradient, and to contribute to the understanding of the nature of such systems, drawing on NEMD simulation results obtained already [44].

The outline of the paper is as follows: We describe the system and present the fundamental problems that shall be investigated (section 4.2) and give its governing equations (section 4.3). A full analytical solution can be found for stationary states near chemical equilibrium (section 4.3.3). This solution is equivalent to the one presented by de Groot

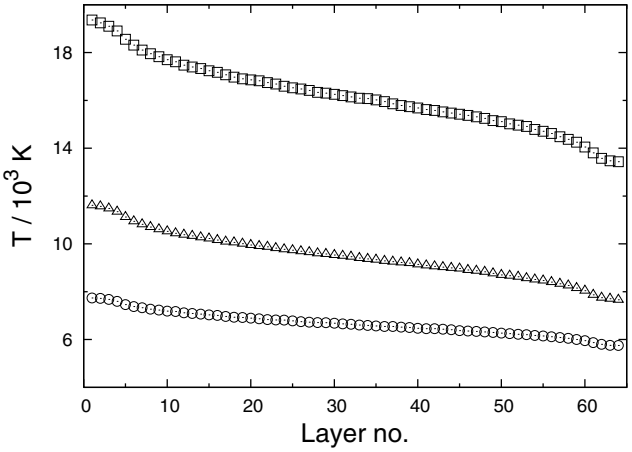

Figure 4.1: Temperature profiles for Cases 4 (circles), 6 (triangles) and 8 (squares), at $c_{\mathrm{F}} + 2c_{\mathrm{F}_2} = 11271$ mol m^{-3}. The symbols represent values in the layers in the MD box. The thickness of the layers is about 0.65 Å

and Mazur [1], but is given in terms of more commonly used variables and fluxes. The solution can be simplified when the system is everywhere in chemical equilibrium (section 4.3.3). The details of the NEMD simulations were given before [44], and are therefore only reviewed briefly here (section 4.4), before we present the results in section 4.5. A discussion (section 4.6) and conclusion (section 4.7) follow.

4.2 A reaction in a temperature gradient

We give first a qualitative description of the system [44], before the governing equations are derived. A thousand particles, reacting according to Eq. (4.1), were put inside a box, with an overall density, $c_{\mathrm{F}} + 2c_{\mathrm{F}_2} = 11271$ mol m^{-3}. For the temperatures considered the fluid is supercritical at this relatively high density [52]. An overall temperature gradient was applied to the $x-$direction of the box, the maximum value being around 6.6×10^{11} K/m (see Fig. 4.1). The temperature gradient led to variations in density and mole fractions, see Fig. 4.2. There was no net mass flux through the system in the states considered. We observed a flux of fluorine atoms to the cold side, while fluorine molecules were transported to the hot side. Both fluxes were functions of position. An example of these component fluxes, giving zero mass flux, is shown in Fig. 4.3. The fluxes are in the direction suggested by the mole-fraction distribution in Fig. 4.2.

The system therefore responds to the imposed boundary conditions by setting up the component fluxes. This is unlike the situation with two non-reacting components in a temperature gradient [4, 35, 39] where the component fluxes are zero in the stationary state. By setting up the varying component fluxes, we shall see that the reacting system

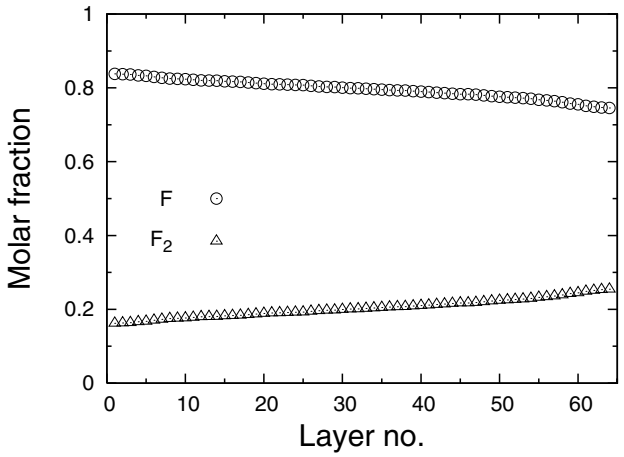

Figure 4.2: Mole fraction profiles for Case 6, at $c_{\mathrm{F}} + 2c_{\mathrm{F}_2} = 11271$ mol m^{-3}. The symbols represent values in the layers in the MD box.

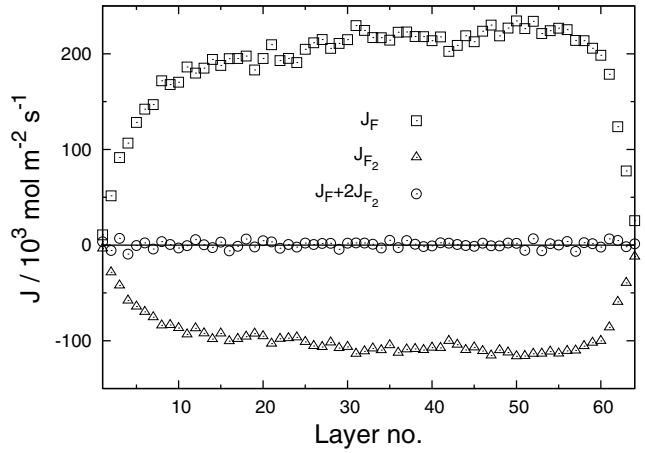

Figure 4.3: Molar flux profiles of F and F_2 for Case 4, at $c_{\mathrm{F}} + 2c_{\mathrm{F}_2} = 11271$ mol m^{-3}. The symbols represent values in the layers in the MD box.

increases its overall conductance of heat. The total heat flux becomes somewhat larger than the measurable heat flux. The non-equilibrium system has *a dynamic structure*, maintained by energy supply from the outside.

Several questions are of interest. How can we characterise and understand the dynamic structure? Can it be understood from the system's entropy production? Is it an example of Prigogine's dissipative structures [71]? The reaction is very exothermic, and according to Le Chatelier's principle, the equilibrium in such a reaction is shifted to the right (more

molecules) at low temperatures. One may wonder to which degree the observed distribution in the temperature gradient is a consequence of such a *shift* alone. We shall see that the shift of the reaction may offer much, but not all of the explanation for the mole fraction distributions in Fig. 4.2. The dynamic structure explains the cause of the shift.

In our first study [44], we mentioned that the reaction was diffusion controlled, but is it controlled by thermal diffusion or interdiffusion? The thermal force is the origin of all transport processes, but does this force alone explain the non-zero component fluxes? We shall see in this paper that precise answers can be given also to these questions. The reaction is controlled by thermal diffusion, and the dynamic structure can be seen as a response to the boundary conditions.

We shall also add evidence to the hypothesis that the assumption of local equilibrium, the basic assumption in non-equilibrium thermodynamics, is reliable [5, 6, 72]. We have earlier shown [44] that the system was nearly Maxwellian in its component velocity distributions. In order to have local equilibrium, this is central. We shall see now that the basis for a thermodynamic analysis can be further strengthened; by showing that the small shifts in the Maxwellians are directly proportional to the temperature gradient. According to kinetic theory, the Maxwell distribution for the $x-$component of the velocity of component k in layer l is:

$$f^0_{k,l}(\mathrm{v}_x) = \sqrt{\frac{m_k}{2\pi k_B T_l}} \exp\left(-\frac{m_k(\mathrm{v}_x - \langle \mathrm{v}_x\rangle_{k,l})^2}{2k_B T_l}\right) \tag{4.2}$$

Here k_B is Boltzmann's constant, m_k is the mass of the particle in question, v_x is the $x-$component of the particle's velocity, $\langle \mathrm{v}_x\rangle_{k,l}$ is the average velocity of particles of component k in layer l and T_l is the temperature in layer l calculated from the average kinetic energy. The Maxwell distributions in the $y-$ and the $z-$directions are similar. With a temperature gradient in the $x-$direction, kinetic theory uses a perturbation in this direction [1], setting:

$$f_{k,l}(\mathrm{v}_x) = f^0_{k,l}(\mathrm{v}_x)\,(1 + \phi_{k,l}) \tag{4.3}$$

where $\phi_{k,l}$ is a function of $(\mathrm{v}_x - \langle \mathrm{v}_x\rangle_{k,l})$, the temperature and composition of the layer, and is proportional to the temperature gradient in the layer:

$$\phi_{k,l} = -A_{k,l}\left(\frac{\partial T}{\partial x}\right)_l \tag{4.4}$$

We shall confirm this property. As explained by Ross and Mazur, this gives a sound basis for a description of the system within the context of classical non-equilibrium thermodynamics [1,61]. We shall also calculate the transport properties as functions of temperature. These coefficients are relevant for modelling of chemical reactions in a temperature gradient, i.e. in a flame [59].

4.3 Governing equations

We reported earlier [44] that the system was in local thermodynamic equilibrium; and that it was also close to chemical equilibrium. We found that the unidirectional rates of

the reaction were nearly the same in the center of the box, meaning that the distance to chemical equilibrium was small there. Away from the center, a larger deviation was seen. After a presentation of the entropy production (subsection 4.3.1), we shall therefore proceed to give equations for the system near, but not at chemical equilibrium (subsection 4.3.2). Coefficients that can be related to experiments are then developed (subsections 4.3.3 and 4.3.4).

4.3.1 The entropy production

The system is one-dimensional, since the temperature gradient is in the x-direction only. We shall describe the system in its stationary state only. The mass balances of the two components then satisfy

$$\frac{\partial}{\partial x} J_{\mathrm{F}_2} = -\frac{1}{2}\frac{\partial}{\partial x} J_{\mathrm{F}} = r \tag{4.5}$$

Here J_{F_2} and J_{F} are the molar fluxes of the molecules and atoms, respectively, and r is the reaction rate in Eq. (4.1). With no net mass flux through the system, we obtain

$$J_{\mathrm{F}} = -2J_{\mathrm{F}_2} \tag{4.6}$$

In the absence of external forces, the energy balance is

$$\frac{\partial}{\partial x} J_q = 0 \tag{4.7}$$

where J_q is the total heat flux. The total heat flux is equal to the measurable heat flux, J'_q, plus the enthalpies carried along with the components, H_{F_2} and H_{F}. With Eq. (4.6) we obtain

$$J_q = J'_q + J_{\mathrm{F}_2} H_{\mathrm{F}_2} + J_{\mathrm{F}} H_{\mathrm{F}} = J'_q + J_{\mathrm{F}_2} \Delta_r H \tag{4.8}$$

where $\Delta_r H$ is the enthalpy of reaction, $\Delta_r H = H_{\mathrm{F}_2} - 2H_{\mathrm{F}}$. We write the entropy production, σ, for transport of heat and two components with a chemical reaction [1] in different ways depending on the purpose. For calculation purposes it is convenient to use the constant total heat flux as a variable, giving:

$$\sigma = J_q \frac{\partial}{\partial x}\left(\frac{1}{T}\right) - J_{\mathrm{F}_2} \frac{\partial}{\partial x}\left(\frac{\Delta_r G}{T}\right) - r\frac{\Delta_r G}{T} \tag{4.9}$$

Here T is the temperature. The reaction Gibbs energy is

$$\Delta_r G = \mu_{\mathrm{F}_2} - 2\mu_{\mathrm{F}}$$

This form shall be used to find an analytical solution to the general transport problem. In order to explain real experiments, one will need the equivalent form of the entropy production, which uses the measurable heat flux as a variable:

$$\sigma = J'_q \frac{\partial}{\partial x}\left(\frac{1}{T}\right) - \frac{1}{T} J_{\mathrm{F}_2} \frac{\partial}{\partial x}\left(\Delta_r G\right)_T - r\frac{\Delta_r G}{T} \tag{4.10}$$

Subscript T on the central term means that the derivative should be taken at constant temperature. With local chemical equilibrium, the entropy production reduces to a one flux - one force expression. We introduce $\Delta_r G = 0$ in Eq. (4.9) and obtain:

$$\sigma = J_q \frac{\partial}{\partial x}\left(\frac{1}{T}\right) \tag{4.11}$$

We shall use this simplification as a reference for the more general case.

4.3.2 Transport properties near local chemical equilibrium

When the system is close to, but not at chemical equilibrium it is possible to find an analytical solution to the flux equations given by the entropy production. Such a solution was also presented by de Groot and Mazur [1]; but not in terms of commonly used variables. We return therefore to Eq. (4.9). The first two flux-force products are products of vectors, and the last product contains a scalar flux and force. There is no coupling of the vectorial forces to the scalar reaction Gibbs energy (the Curie principle). As flux equations in the system, we thus have the reaction rate which does not couple to any other flux, and the heat and mass fluxes which are coupled.

The reaction rate was earlier found [44] to obey the law of mass action:

$$r = k_{\mathrm{f}} c_{\mathrm{F}}^2 - k_{\mathrm{b}} c_{\mathrm{F}_2} \tag{4.12}$$

where c_k are molar densities of the components, and k_{f} and k_{b} are rate constants. In equilibrium we therefore have $k_{\mathrm{f}} c_{\mathrm{F},eq}^2 = k_{\mathrm{b}} c_{\mathrm{F}_2,eq}$, where the subscript eq denotes the equilibrium value. We assume that the activity coefficients are constant for the range of concentrations considered in the simulations. This gives

$$\mu_k = \mu_k^0 + RT \ln \frac{c_k}{c_k^0} = \mu_{k,eq} + RT \ln \frac{c_k}{c_{k,eq}} \tag{4.13}$$

It follows from Eqs. (4.12) and (4.13) that the reaction rate can be written as

$$r = k_{\mathrm{f}} c_{\mathrm{F}}^2 \left(1 - e^{\Delta_r G/RT}\right) \tag{4.14}$$

In chemical equilibrium we have $\Delta_r G_{eq} = 0$.

We introduce $\delta c_k \equiv c_k - c_{k,eq}$ for both components. When the reaction is near chemical equilibrium, the reaction rate becomes

$$r = -k_{\mathrm{f}} c_{\mathrm{F},eq}^2 \left(\frac{\delta c_{\mathrm{F}_2}}{c_{\mathrm{F}_2,eq}} - 2\frac{\delta c_{\mathrm{F}}}{c_{\mathrm{F},eq}}\right) = -\frac{k_{\mathrm{f}} c_{\mathrm{F},eq}^2}{R}\frac{\Delta_r G}{T} \tag{4.15}$$

to linear order.

The coupled fluxes of heat and mass are from Eq. (4.9):

$$\begin{aligned} \frac{d}{dx}\frac{1}{T} &= R_{qq}\ J_q + R_{q\mu} J_{\mathrm{F}_2} \\ -\frac{d}{dx}\frac{\Delta_r G}{T} &= R_{\mu q}\ J_q + R_{\mu\mu} J_{\mathrm{F}_2} \end{aligned} \tag{4.16}$$

or, in the inverse form:

$$\begin{aligned} J_q &= L_{qq}\frac{d}{dx}\frac{1}{T} + L_{q\mu}\left(-\frac{d}{dx}\frac{\Delta_r G}{T}\right) \\ J_{\mathrm{F}_2} &= L_{\mu q}\frac{d}{dx}\frac{1}{T} + L_{\mu\mu}\left(-\frac{d}{dx}\frac{\Delta_r G}{T}\right) \end{aligned} \tag{4.17}$$

The R and L-coefficient matrices are both symmetric according to Onsager. Taking the derivative of Eq. (4.16) using Eqs. (4.5) and (4.7), we obtain:

$$\begin{aligned} \frac{d^2}{dx^2}\frac{1}{T} &= R_{q\mu}\frac{\partial}{\partial x}J_{\mathrm{F}_2} = R_{q\mu}r \\ -\frac{d^2}{dx^2}\frac{\Delta_r G}{T} &= R_{\mu\mu}\frac{\partial}{\partial x}J_{\mathrm{F}_2} = R_{\mu\mu}r \end{aligned} \tag{4.18}$$

By substituting Eq. (4.15) valid close to chemical equilibrium into Eq. (4.18), we have

$$\begin{aligned} \frac{d^2}{dx^2}\frac{1}{T} &= -R_{q\mu}\frac{k_{\mathrm{f}}c^2_{\mathrm{F},eq}}{R}\frac{\Delta_r G}{T} \\ -\frac{d^2}{dx^2}\frac{\Delta_r G}{T} &= -R_{\mu\mu}\frac{k_{\mathrm{f}}c^2_{\mathrm{F},eq}}{R}\frac{\Delta_r G}{T} \end{aligned} \tag{4.19}$$

When the rate constant and the resistivities are constants, these equations can be solved. Boundary conditions for the solution are the temperatures and the zero value of the component fluxes at the ends ($x = 0,\ 2l$) and the middle ($x = l$) of the box. In the solution it is convenient to introduce the characteristic length d over which an atom can diffuse relative to other particles before it reacts

$$d \equiv \sqrt{\frac{R}{R_{\mu\mu}k_{\mathrm{f}}c^2_{\mathrm{F},eq}}} \tag{4.20}$$

This is the socalled penetration depth. The solution is for $0 \le x \le l$:

$$\begin{aligned} \frac{1}{T(x)} &= A_D + B_D x + C_D \sinh\left(\frac{2x-l}{2d}\right) \\ \frac{\Delta_r G(x)}{T(x)} &= -\frac{R_{\mu\mu}}{R_{q\mu}}C_D \sinh\left(\frac{2x-l}{2d}\right) \end{aligned} \tag{4.21}$$

For the fluxes and the reaction rate this gives

$$\begin{aligned} J_q &= L_{qq}B_D \\ J_{F_2} &= L_{\mu q}B_D + \frac{1}{R_{q\mu}d}C_D \cosh\left(\frac{2x-l}{2d}\right) \\ r &= \frac{1}{R_{q\mu}d^2}C_D \sinh\left(\frac{2x-l}{2d}\right) \end{aligned} \tag{4.22}$$

Using $T(0) = T_H$, $T(l) = T_L$ and $J_{F_2}(0) = J_{F_2}(l) = 0$, we find

$$\begin{aligned} A_D &= \frac{1}{T_H} + C_D \sinh \frac{l}{2d} \\ B_D &= -\frac{C_D}{L_{\mu q} R_{q\mu} d} \cosh \frac{l}{2d} \\ C_D &= \left(\frac{1}{T_L} - \frac{1}{T_H} \right) \frac{L_{\mu q} R_{q\mu}}{L_{\mu q} R_{q\mu} \sinh \frac{l}{2d} - \frac{l}{d} \cosh \frac{l}{2d}} \end{aligned} \tag{4.23}$$

A_D, B_D and C_D depend only on two parameters d and $L_{\mu q} R_{q\mu}$. The solution for the other half of the box, $l \leq x \leq 2l$ is the mirror image of the solution between $0 \leq x \leq l$.

In order to see how the reaction contributes to the heat transport across the system, we calculate J_q in the limit that there is no reaction ($d \to \infty$) and in the limit that the reaction is in equilibrium ($d \to 0$)

$$\begin{aligned} J_q(d &\to \infty) = \frac{1}{l R_{qq}} \left(\frac{1}{T(l)} - \frac{1}{T(0)} \right) = \frac{1}{l} \left(L_{qq} - \frac{L_{q\mu}^2}{L_{\mu\mu}} \right) \left(\frac{1}{T(l)} - \frac{1}{T(0)} \right) \\ J_q(d &\to 0) = \frac{L_{qq}}{l} \left(\frac{1}{T(l)} - \frac{1}{T(0)} \right) \end{aligned} \tag{4.24}$$

This shows that the effective thermal conductivity of the system increases when the reaction takes place, as $L_{qq} - \frac{L_{q\mu}^2}{L_{\mu\mu}} < L_{qq}$. The reason is the coupling coefficient $L_{q\mu}$. We shall see below that it can be linked to the reaction enthalpy.

4.3.3 The description using the measurable heat flux

With the alternative choice for the entropy production, Eq. (4.10), the chemical reaction rate is the same as above, but the set of vectorial force-flux relations changes to:

$$\begin{aligned} \frac{\partial}{\partial x} \left(\frac{1}{T} \right) &= r_{qq} J_q' + r_{q\mu} J_{\mathrm{F}_2} \\ -\frac{1}{T} \frac{\partial}{\partial x} \left(\Delta_r G \right)_T &= r_{\mu q} \; J_q' + r_{\mu\mu} J_{\mathrm{F}_2} \end{aligned} \tag{4.25}$$

where the reaction Gibbs energy at constant temperature is defined by

$$\frac{\partial}{\partial x} \left(\Delta_r G \right)_T = \Delta_r S \frac{\partial}{\partial x} T = \frac{\Delta_r H}{T} \frac{\partial}{\partial x} T = -T \Delta_r H \frac{\partial}{\partial x} \left(\frac{1}{T} \right) \tag{4.26}$$

The r-coefficient matrix of resistivities is also symmetric according to Onsager. We shall determine these coefficients as well as more convenient combinations of them. In order to do so, we rewrite the measurable heat flux, using Eq. (4.25)

$$J_q' = -\frac{1}{T^2 r_{qq}} \frac{\partial}{\partial x} T - \frac{r_{q\mu}}{r_{qq}} J_{\mathrm{F}_2} = -\lambda_J \frac{\partial}{\partial x} T + q^* J_{\mathrm{F}_2} \tag{4.27}$$

and define the thermal conductivity λ_J at zero component flux:

$$\lambda_J \equiv -\left[\frac{J'_q}{\partial T/\partial x}\right]_{J_{\mathrm{F}_2}=0} = \frac{1}{T^2 r_{qq}} \tag{4.28}$$

and the heat of transfer:

$$q^* \equiv \left[\frac{J'_q}{J_{\mathrm{F}_2}}\right]_{\nabla T=0} = -\frac{r_{\mu q}}{r_{qq}} \tag{4.29}$$

The remaining independent coefficient is $r_{\mu\mu}$.

One cannot speak of a Soret equilibrium in the traditional sense in this system. In the traditional sense there is a balance of a chemical and a thermal force in Soret equilibrium, and the component fluxes are zero. Here the component fluxes are non-zero (see figure 4.3) (but the total mass flux is still zero). One must rather speak of a *Soret stationary state*.

In the *limiting case of local chemical equilibrium* matters simplify considerably [73]. When $\Delta_r G(x) = 0$ everywhere in the system, there is only one independent flux and force in the entropy production Eq. (4.11). They are related by

$$J_q = \frac{1}{R_{qq}}\frac{\partial}{\partial x}(\frac{1}{T}) = -\frac{1}{R_{qq}T^2}\frac{\partial}{\partial x}T = -\lambda\frac{\partial}{\partial x}T \tag{4.30}$$

where the thermal conductivity is now given by $\lambda = 1/R_{qq}T^2$. All other coefficients in the r-resistivity matrix above, must now be linearly dependent on this coefficient. We can see this by introducing the measurable heat flux, Eq. (4.8) in Eq. (4.30):

$$\frac{\partial}{\partial x}\left(\frac{1}{T}\right) = R_{qq}J_q = R_{qq}J'_q + R_{qq}\Delta_r H J_{\mathrm{F}_2} \tag{4.31}$$

By comparing with Eq. (4.25a), we find that

$$r_{qq} = R_{qq} \quad \text{and} \quad r_{q\mu} = R_{qq}\Delta_r H \tag{4.32}$$

It follows that $\lambda = \lambda_J$. Using Eqs. (4.26) and (4.31), we furthermore have

$$\begin{aligned} -\frac{1}{T}\frac{\partial}{\partial x}\left(\Delta_r G\right)_T &= \Delta_r H\frac{\partial}{\partial x}\left(\frac{1}{T}\right) = R_{qq}\Delta_r H J_q \\ &= R_{qq}\Delta_r H J'_q + R_{qq}\left(\Delta_r H\right)^2 J_{F_2} \end{aligned} \tag{4.33}$$

By comparing with Eq. (4.25b), we find that

$$r_{\mu q} = R_{qq}\Delta_r H = r_{q\mu} \quad \text{and} \quad r_{\mu\mu} = R_{qq}\left(\Delta_r H\right)^2 \tag{4.34}$$

The heat of transfer is then obtained using Eq. (4.29):

$$q^* = \left[\frac{J'_q}{J_{\mathrm{F}_2}}\right]_{\nabla T=0} = -\frac{r_{q\mu}}{r_{qq}} = -\Delta_r H \tag{4.35}$$

The heat of transfer is now simply equal to minus the reaction enthalpy [73]. The ratio of fluxes is a ratio of zeros in the limit of a zero temperature gradient. This ratio is finite, however, as shown. In this paper we will establish that *the system is not in local chemical equilibrium*, only near enough to use Eq. (4.15).

4.3.4 Relations between sets of coefficients

Changing the set of variables leads to changes in the coefficients. One set can be derived from another, because the entropy production is invariant. Knowing the R_{ij} of Eq. (4.16) from the preceding section, we can calculate the r_{ij} coefficients of Eq. (4.25). The relation between the two resistivity matrices is

$$\begin{aligned} r_{qq} &= R_{qq} \quad , \; r_{q\mu} = r_{\mu q} = R_{q\mu} + R_{qq}\Delta_r H \\ r_{\mu\mu} &= R_{\mu\mu} + 2R_{q\mu}\Delta_r H + R_{qq}\left(\Delta_r H\right)^2 \end{aligned} \tag{4.36}$$

From the values of r_{ij} we compute the conductivity matrix l_{ij}. Inverting Eq. (4.25) gives

$$\begin{aligned} J'_q &= l_{qq}\,\frac{d}{dx}\left(\frac{1}{T}\right) - l_{q\mu}\frac{1}{T}\frac{d}{dx}\left(\Delta_r G\right)_T = l_{qq}\,\frac{d}{dx}\left(\frac{1}{T}\right) - l_{q\mu}\frac{\rho}{T\rho_{\mathrm{F}}}\frac{\partial\mu_{\mathrm{F}_2}}{\partial c_{\mathrm{F}_2}}\frac{d}{dx}c_{\mathrm{F}_2} \\ J_{\mathrm{F}_2} &= l_{\mu q}\,\frac{d}{dx}\left(\frac{1}{T}\right) - l_{\mu\mu}\frac{1}{T}\frac{d}{dx}\left(\Delta_r G\right)_T = l_{\mu q}\,\frac{d}{dx}\left(\frac{1}{T}\right) - l_{\mu\mu}\frac{\rho}{T\rho_{\mathrm{F}}}\frac{\partial\mu_{\mathrm{F}_2}}{\partial c_{\mathrm{F}_2}}\frac{d}{dx}c_{\mathrm{F}_2} \end{aligned} \tag{4.37}$$

Here ρ is the total mass density and ρ_F is the mass density of the F atoms. In the second equality we have used Gibbs-Duhem's equation. By comparing these relations to

$$\begin{aligned} J'_q &= -\lambda_G\,\frac{dT}{dx} - q^* D\frac{d}{dx}c_{\mathrm{F}_2} \\ J_{\mathrm{F}_2} &= -\frac{\rho_{\mathrm{F}} q^* D}{\rho T}\left(\frac{\partial\mu_{\mathrm{F}_2}}{\partial c_{\mathrm{F}_2}}\right)^{-1}\frac{dT}{dx} - D\frac{d}{dx}c_{\mathrm{F}_2} \end{aligned} \tag{4.38}$$

and using Eq. (4.36), we can finally identify the common transport coefficients, the thermal conductivity λ_G at zero variation in $\Delta_r G$, the interdiffusion coefficient in the two-component mixture, D, and the heat of transfer, in terms of the conductivities l_{ij} (or r_{ij}) and L_{ij} (or R_{ij}). We obtain

$$\begin{aligned} \lambda_G &= \frac{l_{qq}}{T^2} = \frac{1}{T^2}\left(L_{qq} - 2L_{q\mu}\Delta_r H + L_{\mu\mu}\left(\Delta_r H\right)^2\right) \\ D &= l_{\mu\mu}\frac{\rho}{T\rho_{\mathrm{F}}}\frac{\partial\mu_{\mathrm{F}_2}}{\partial c_{\mathrm{F}_2}} = L_{\mu\mu}\frac{\rho}{T\rho_{\mathrm{F}}}\frac{\partial\mu_{\mathrm{F}_2}}{\partial c_{\mathrm{F}_2}} \\ q^* &= \frac{l_{q\mu}}{l_{\mu\mu}} = -\frac{r_{q\mu}}{r_{qq}} = -\frac{R_{q\mu}}{R_{qq}} - \Delta_r H = \frac{L_{q\mu}}{L_{\mu\mu}} - \Delta_r H \end{aligned} \tag{4.39}$$

We see that the thermal conductivity has, in addition to L_{qq}, contributions from the reaction via thermal diffusion ($-2L_{q\mu}\Delta_r H$) and from diffusion ($L_{\mu\mu}\left(\Delta_r H\right)^2$). While the last term is always positive, the first term is found to be negative. According to Eq. (4.24), the presence of the reaction increases the thermal conductivity, meaning that the last term dominates the first.

The coefficient for interdiffusion, D, is determined by the mass conductivity $l_{\mu\mu} = L_{\mu\mu}$, cf. Eq. (4.17). The heat of transfer reduces to $-\Delta_r H$,in the limit that the reaction is in chemical equilibrium. This was the value given by Eq. (4.35) [73]. Away from chemical equilibrium, there is an additional term in the expression for the heat of transfer, which can be related to the thermal diffusion. Each coefficient can be determined from experiments or computer simulations according to their definition.

4.4 NEMD simulations

The details of the system and the NEMD simulations were described earlier [44]. We repeat the essentials here.

4.4.1 The system

The system had initially 1000 fluorine atoms in a non-cubic box, called the MD box, with lengths $L_y = L_z = L_x/2$. The box size (in m^3) was determined by the overall density, $L_x L_y L_z = 1000/(c_F + 2c_{F_2})/N_A$, where N_A is Avogadro's number and the overall density $c_F + 2c_{F_2}$ was 11271 mol/m^3. In the x-direction, the MD box was divided into 128 equal planar layers with a thickness of about 0.65 Å.

The reaction model was given by Stillinger and Weber [52]. The potential is a combined 2- and 3-body potential, see also our previous paper [44]. Basic units were the diameter of the fluorine atom, $\sigma_0 = 1.214$ Å, its potential energy depth $\epsilon_0 = 2.659 \times 10^{-19}$ J and its particle mass, $m_0 = 3.155 \times 10^{-26}$ kg. A default adjustment for un-bonded atoms was set using a distance cutoff criterion $r_c = 1.7\sigma_0$ [44]. A pair of atoms was defined as a molecule when the pair had a separation distance equal or less than r_c.

4.4.2 Simulation conditions

Periodic boundary conditions were applied in all directions [39] . The 'heat exchange' (HEX) algorithm was used to obtain the temperature profile [4]: The 'hot' layers 1-4 and 125-128, at the ends of the box, were thermostated to a high temperature, T_H, and the 'cold' layers 61-68, in the center of the box, were thermostated to a low temperature, T_L. The layers in the hot and cold regions in the MD box are shown in Fig. 4.4. The figure also displays a 3-dimensional snapshot of 1000 fluorine particles in the MD box. The NEIGHBOUR3 algorithm [44], that makes a neighborhood list of 3-body interactions, gave a saving of more than 50% in the computation time.

Different temperature gradients were applied across the MD box as described earlier [4, 9,35]. Stationary states were obtained after about 10^6 time steps. All NEMD simulations were performed over 10^7 time steps. We omitted the first 2×10^6 time steps, which showed transient effects. A time step length of 0.41817 femtoseconds was used.

All NEMD simulations were performed at constant overall density ($c_F + 2c_{F_2} = 11271$ mol/m^3), varying the temperature gradient up to 6.6×10^{11} K/m. The temperatures at the boundaries are listed in Table 4.1. Case 1 had the smallest imposed temperature gradient, 1.1×10^{11} K/m, while case 8 had the largest imposed temperature gradient, 6.6×10^{11} K/m. Case numbers refer to runs documented earlier [44].

For stationary states the time averaged temperature, pressure and density were found to be symmetric relative to the center of the box, while the fluxes were antisymmetric.

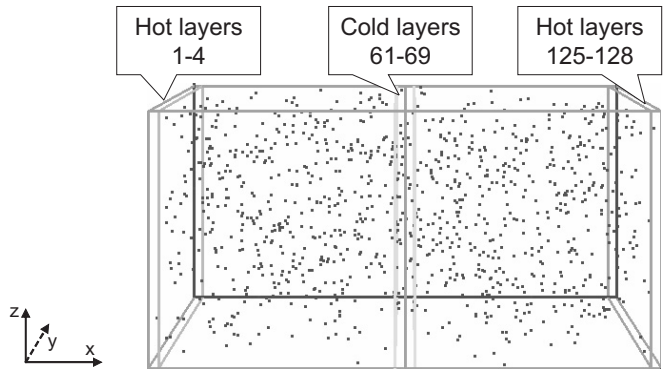

Figure 4.4: A snapshot of the MD box with 1000 fluorine atoms, partially reacted to molecules. The box has dimensions $L_y/L_x = L_z/L_x = 1/2$.

Table 4.1: Temperatures at the boundaries, T_H and T_L, and in the center $T(l/2)$, total heat flux and pressure in the studied cases. The case numbering refer to that of our previous paper.

Sim. No.	T_H (kK)	T_L (kK)	$T(l/2)$ (kK)	J_q (10^8 $\frac{\text{kJ}}{\text{m}^2\text{s}}$)	p (10^3 bar)
1	5.8	4.8	5.2	0.64	5.03
4	7.7	5.8	6.7	1.59	6.32
5	9.6	7.7	8.6	1.91	8.14
6	11.6	7.7	9.5	4.03	8.91
7	15.4	11.6	13.3	5.03	12.56
8	19.3	13.5	16.2	8.49	15.20

We were therefore able to use the appropriate averages for pairs of layers that were mirror symmetric around the center of the MD box. The molar flux of component k in layer l is:

$$\mathbf{J}_{k,l} = \frac{1}{N_A V_L} \sum_{i \in l \ , i \in \text{component} k} \mathbf{v}_i \tag{4.40}$$

Here $\mathbf{v}_i$ is the velocity of particle i. The volume of each layer is $V_L = V/128$. The total molar flux in layer l is then given by

$$\mathbf{J}_l = \sum_k \mathbf{J}_{k,l}. \tag{4.41}$$

The total heat flux in layer l is

$$\mathbf{J}_{q,l} = \frac{1}{V_L} \sum_{i \in l} \mathbf{v}_i \left(\frac{3}{2} m_i \mathrm{v}_i^2 + \Phi_i + p_l - \frac{k_B T N_l}{V_L} \right) \tag{4.42}$$

where Φ_i is the potential energy of particle i, p_l is the hydrostatic pressure in layer l and

$N_l = \sum_k N_{k,l}$ is the total number of particles in layer l.

$$\Phi_i = \frac{1}{2} \sum_{j \text{ pair with } i} u_2(r_{ij}) + \sum_{j<k \text{ triplet with } i} h(r_{ij}, r_{ik}, \theta_i). \tag{4.43}$$

Here u_2 is the 2-body potential, assigned half to each atom of the pair ij and the 3-body potential is composed by the h-functions, i.e. a sum of three terms, h_i, h_j and h_k, which are assigned to particles i, j and k, respectively [44].

From the virial theorem, the hydrostatic pressure p_l in layer l is:

$$p_l = \frac{k_B T N_l}{V_L} - \frac{1}{3V_L} \sum_{i \in l} \left[\frac{1}{2} \sum_{j \text{ pair with } i} \frac{\partial u_2(r_{ij})}{\partial r_{ij}} r_{ij} + \sum_{j<k \text{ triplet with } i} \left(\frac{\partial h_i}{\partial r_{ij}} r_{ij} + \frac{\partial h_i}{\partial r_{ik}} r_{ik} + \frac{\partial h_i}{\partial r_{jk}} r_{jk} \right) \right] \tag{4.44}$$

In this expression we have used that the hydrostatic pressure is scalar. This made it possible to replace the usual tensorial expression [5] by its trace divided by 3. The kinetic contribution then gives $k_B T N_l / V_L$. Like in Eq. (4.43), we assign half of the force due to the pair ij to particle i and the other half to particle j in the expression for the pair interaction. The interaction energy due to a triplet is the sum of three terms, h_i , h_j and h_k (see ref. [44]). In Eq. (4.44) we have assigned the force due to h_i to particle i, those to h_j to particle j and those to h_k to particle k.

The molar enthalpy of the mixture of F and F_2 in layer l is

$$H_l = N_A \left(\frac{1}{N_l} \sum_{i \in l} \Phi_i + \frac{p_l V_L}{N_l} + \frac{3}{2} k_B T \right) \tag{4.45}$$

By allocating contributions to H_l from F or F_2, we found estimates for the partial molar enthalpies and the reaction enthalpy. We discuss the estimates in Section 5.

4.4.3 Calculation procedures

Six NEMD simulations from our previous paper [44] (Cases 1, 4-8) were used as input for the calculations. The correctness of these data were discussed earlier [44]. We found, for instance, that the total heat flux and the pressure, cf. Eqs. (4.42) and (4.44) were constant. Their values are given in Table 4.1.

We estimated the reaction enthalpy $\Delta_r H_l = H_{F_2,l} - 2H_{F,l}$ for each layer (each temperature and pressure) using estimates of the contributions to H_l from F and F_2. With knowledge of the particle flux, the total heat flux and the reaction enthalpy we estimated the measurable heat flux in all layers using Eq. (4.8).

Examples of temperature profiles, mole fraction profiles, and component fluxes obtained from the NEMD simulations were shown in Figs. 4.1- 4.3. Such profiles were used to find transport coefficients. In this section we describe the calculation procedure we used.

Using Eq. (4.21a) we were able to obtain the coefficients A_D, B_D, C_D and d by fitting the analytical solution to the computational results. From the values of these coefficients we next obtained the penetration depth d and $L_{\mu q}R_{q\mu}$. The fit of the temperature profile was very good: The value of $T(x)$ differed from the analytical solution only close to $x = 0$ and $x = l$, due to the presence of the thermostats. Using the total heat flux, Eq. (4.22a) and the value of B_D, we could furthermore fit L_{qq}. The results for d, $L_{\mu q}R_{q\mu}$ and L_{qq} refer to the average temperature of the system they were derived for. The temperature dependence of the coefficients was found in this manner.

The reason that the temperature profile between 0 and l is antisymmetric around $l/2$ is that the $R_{q\mu}J_{\mathrm{F}_2}$ contribution to the inverse temperature gradient in Eq. (4.16) is small compared to $R_{qq}J_q$. We shall come back to this point below. By comparing Fig. 4.3 for the F_2 flux with the analytical solution given by Eq. (4.22b), we see that the data and the analytical solution do not agree with each other. These data were therefore not used in the fitting procedure.

We determined $R_{\mu\mu}$ using Eq. (4.20), which gives

$$R_{\mu\mu} = \frac{R}{k_{\mathrm{f}} d^2 c_{\mathrm{F},eq}^2} \tag{4.46}$$

In this equation d and $c_{\mathrm{F},eq}$ are already known at the temperature in the centre of the half box, at $x = l/2$, see our first paper [44] for the values of $c_{\mathrm{F},eq}$. We determined k_{f} using the forward reaction rate

$$r_{\mathrm{f}} = k_{\mathrm{f}} c_{\mathrm{F}}^2 \tag{4.47}$$

from the NEMD simulations. The NEMD values of r_{f} from layers 15 to 50 were practically constant with a scatter, in the order of 20%. We obtained the values of r_{f} in $x = l/2$ by averaging over all the layers. Using Eq. (4.46) then gave us $R_{\mu\mu}$ at the temperature in $x = l/2$.

It follows from Eqs. (4.14) and (4.47) that

$$\frac{\Delta_r G(l)}{RT(l)} = \ln\left(1 - \frac{r(l)}{r_{\mathrm{f}}}\right) \tag{4.48}$$

For r_{f} we used the constant value obtained above for all the layers and r we found from the F_2 flux using Eq. (4.5). The values of $\Delta_r G(l)/RT(l)$ make it possible to judge how close the system is to chemical equilibrium in each layer.

4.5 Results

4.5.1 Local thermodynamic equilibrium and local chemical equilibrium

The velocity distributions in this system are nearly Maxwellian, see also ref. [44]. This statement is now quantified by the results shown in Fig. 4.5. The figure shows how the velocity distributions were shifted in temperature gradients. The difference between

the observed distribution and the Maxwellian distribution, $\phi_{k,l}$, as defined by Eq.(4.3) is shown for two temperature gradients in Fig. 4.5. Subfigure 4.5c gives results for the atom and subfigure 4.5d gives results for the molecule. The parameter $A_{k,l}$ of Eq.(4.4) was determined from these plots. We see in subfigures a and b in Fig. 4.5 that $A_{k,l}$ is identical for both gradients for both the atom and the molecule. The value of $A_{k,l}$ varies across the box, however; i.e. with the temperature and composition. The system can thus be regarded as being in local *thermodynamic* equilibrium; i.e. any layer in the box can be described by standard thermodynamic equations.

In the previous paper, we argued that the chemical reaction was close to chemical equilibrium. This statement can now be quantified by Fig. 4.6. The figure shows that $\Delta_r G/RT << 1$ in all layers and in all cases. In the layers that are not thermostated the value is very small. It rapidly increases in the thermostated layers to an absolute value of not more than 0.03, which is still much smaller than one. The data are scattered, but we conclude that they confirm the prediction of Eq. (4.21). The data also confirm that a linear relation between the rate and the driving force is obeyed in all the layers. The component fluxes are not symmetric around $x = l/2$, however, see Fig. 4.3. We shall return to the reason for this in the discussion.

4.5.2 The total heat flux and its contributions

Figure 4.7 shows the total heat flux and the measurable heat flux for case 8. The measurable heat flux was around 5% smaller than the total heat flux, and varied slightly across the MD box, meaning that net enthalpy is moving to the cold side of the box.

The difference in the total heat flux and the measurable heat flux is due to the reaction enthalpy. The reaction enthalpy is shown in Fig. 4.8 . A large negative value is found, which is normal for a strongly exothermic reaction. The value changes with temperature as expected. The supercritical fluid is non-ideal, so the molar enthalpies will certainly deviate from the partial molar enthalpies. We consider therefore this figure as an estimate for the reaction enthalpy. The slope for each set of simulations gives a negative reaction heat capacity. The value is surprisingly independent of pressure, cf. Table 4.1. In the calculation of the resistivities r_{ij} and the conductivities l_{ij} below, we use this estimate of the reaction enthalpy.

4.5.3 Transport coefficients

The transport properties of the reacting system are shown in Tables 2-4 and Figs. 4.9-4.13. The results for R_{ij} and r_{ij} are given in Table 4.2, while Table 4.3 lists the corresponding results for the conductivity coefficients L_{ij} and l_{ij}. Finally, Table 4.4 shows the common transport properties λ_G, λ_J, D, q^*, $-\Delta_r H$. The quantities which are necessary to determine the coefficient $R_{\mu\mu}$, i.e. c_{F}, $c_{\mathrm{F,eq}}$, k_{f} and the length d, are shown in Table 4.5. The fitted penetration depth d has been checked to be larger than the mean free path of the same case, as we expected. All these quantities listed in Tables 4.2-4.5 are referred to the temperature at $x = l/2$, $T(l/2)$.

Figure 4.9 shows the thermal resistivity, R_{qq}=r_{qq}, from Eq. (4.31) (circles) and from fitting the analytical solution to the temperature profile (squares). The two methods gave within a few percent the same results. This shows that the $R_{q\mu}J_{\mathrm{F}_2}$ contribution in Eq. (4.16) is at most a few percent of the $R_{qq}J_q$ contribution. Using the values of $R_{q\mu}$, R_{qq} given in Table 4.2, the heat fluxes from Table 4.1 and the F_2 flux (see Fig. 4.3 for case 4) this was verified. The values of the other coefficients were found using the procedure described in the previous section.

Figure 4.10 shows results for the thermal conductivities λ_G and λ_J. Results from simple kinetic theory for a mixture are also shown for comparison. In all cases the values of λ_G are larger than the values of λ_J, within a difference of up to 40% for low temperatures. The order of magnitude of the results is that predicted by kinetic theory, however. The results for the diffusion coefficient D are shown in the Fig. 4.11. The value of D varies around a constant, 0.24×10^{-5} m^2/s. We demonstrate that also this coefficient has the same order of magnitude as that obtained from simple kinetic theory.

4.6 Discussion

4.6.1 Local thermodynamic equilibrium. Nearness to local chemical equilibrium

In our first article [44], we concluded from the small shift in the Maxwell velocity distributions that the system was always in local thermodynamic equilibrium; meaning that all normal thermodynamic relations were valid. Figure 4.5 shows that the shift in the velocity distribution was proportional to the temperature gradient everywhere, with a proportionality coefficient $A_{k,l}$. The coefficient was the same for both particles, and it varied with composition and temperature. This property is an important characteristic of the Maxwell distribution for a non-equilibrium state in kinetic theory, and was crucial in the analysis of transport and chemical reactions by Ross and Mazur [1, 61]. The fact that we can confirm this property, gives a statistical basis for the use of non-equilibrium thermodynamics in a reacting mixture.

In the first article we stated that the reaction was near local chemical equilibrium for many conditions in the MD box. In the present work, we assumed nearness to equilibrium and found analytical solutions for the temperature gradient, the reaction rate and the mass fluxes. The shape of the simulated temperature profile in Fig. 4.1 was such that it fitted well to the analytical solution obtained for the temperature profile under these conditions. From the values obtained for $\Delta_r G/RT$ (Fig. 4.6) we were able to conclude that the reaction rate was linear in the driving force in every layer for all cases considered. The data also confirmed the prediction of the analytical solutions. The criterion $\Delta_r G << RT$ is often used as a criterion for being close to chemical equilibrium, for instance in biology. We can conclude that our system is very near, but not at chemical equilibrium.

Somewhat surprisingly the component fluxes were not quite as symmetric around $x = l/2$ as one would expect on the basis of the analytical solution. One reason for this can

be the thermostatic procedure. In the thermostated layers the temperature is reset at the temperature of the thermostat every 10 time steps in the integration of the equations of motion. This brings the thermostated layers out of local equilibrium. As the reaction is relatively quick in these layers, it delivers or takes away energy, counteracting the action of the thermostats. How far the thermostated layers are away from local equilibrium depends on their temperature. As this temperature is different in the two thermostats, the strict symmetry suggested by the analytical solution can be broken for $\Delta_r G/RT$ and the component fluxes.

4.6.2 A chemical reaction controlled by thermal diffusion

The nearness to chemical equilibrium allowed us to calculate properties of the chemical reaction, for instance, the penetration depth d. This parameter expresses the average length a molecule diffuses before it reacts, around 4 Å in the present investigation. It was obtained from the temperature and the gradient of the temperature in $x = l/2$. Taking this distance constant one obtains a satisfactory fit of the whole temperature profile in the layers between the thermostats. The mean free path can be calculated to be between 3 and 6 Å for the molecule. Uncertainties considered, these lengths are the same, and indicate that particles can hardly collide with one another before a new molecule is formed. It is likely, that almost all collisions leads to a reaction in a fast reaction like ours, meaning that equilibrium is established (almost) immediately, when the reaction mixture is perturbed. This may then be seen as typical of diffusion controlled reactions. Clearly, also microscopic reversibility holds.

The non-zero component fluxes that characterize the stationary state of the system are not constant across the system. This is a true indication that the reaction plays a role. The divergences of the fluxes give a non-zero value for the reaction rate, the reaction can thus be seen as a sink or source for components. Is it the reaction that defines the flux divergence, or is it vice versa, the diffusion that determines the reaction rate? The two phenomena are not directly coupled, so one should be able to establish a cause-effect relationship. The value of d compared to the mean free path and the results for $\Delta_r G$, indicates that the latter explanation is most probable.

So, if the reaction is controlled by diffusion, the next question to ask is what kind of diffusion; normal interdiffusion or thermal diffusion? The question can be answered by looking at the contributions to the mass flux, J_{F_2}. Clearly, the values of the coefficients, in combination with the forces, tell that the thermal diffusion term is by far the most important contribution to the flux. We therefore conclude that the reaction is controlled by thermal diffusion. Thermal diffusion coefficients are normally at least one order of magnitude smaller that ordinary diffusion coefficients, but this is nor the case here (see section 6.4.2).

4.6.3 A dissipative structure

The system was found to respond to an applied temperature gradient by setting up fluxes of heat and of components. The nonzero component fluxes shown in Fig. 4.3 appear as futile cycling of mass. Clearly, energy is needed to maintain the dissipation represented by this transport. One interesting question is therefore why the transport occurs. What is governing it, and why is it preferred to other stationary states?

We may speak of a system with a dynamic structure, or a dissipative structure maintained by energy supply from the outside. It is then natural to examine the system's entropy production.

The dynamic properties of the system are governed by the system's entropy production. Prigogine showed that a globally linear system has a stationary state that is characterised by minimum entropy production [71]. This situation does not apply here, in particular because the reaction rate is not a linear function of $T_H - T_L$. The system is stationary, but the fluxes are not a linear function of the driving force across the whole box. The flux is a linear function of the forces in any volume element, however, with a coefficient that depends on the state variables.

We can, however, conclude from an interesting limiting case. In that case the reaction is in complete chemical equilibrium, and the temperature gradient becomes constant. The total heat flux is constant by definition, and the entropy production will then be constant through the box. We can then show that the entropy production becomes smaller in the presence of component interdiffusion, than in the absence of such interdiffusion. This is so because the total heat flux is larger than the measurable heat flux see Fig. 4.7. We are then in a situation that the dynamic structure of the reacting mixture in a temperature gradient is compatible with minimum entropy production.

Let us make the hypothesis that this remains true, also when the chemical reaction deviates from equilibrium, as is the case here. The system sets up thermal interdiffusion because there is a gain that compensates for the extra energy needed to cycle the components. The obvious gain is a facilitated transfer of heat. Equations (4.24) show that the total heat flux was enhanced in the presence of the chemical reaction. Also de Groot and Mazur [1] observed this. Equations (4.36) give explicit contributions to the conductivities from the enthalpy of reaction, meaning that there is an increase in the overall thermal conductivity of the system. This means that the entropy production of the system with thermal interdiffusion of components is smaller in the present simulated system than in a hypothetical system without such movement of components and the corresponding reaction. In other words, the system responds to the given boundary conditions by seeking a dynamic state (dissipative structure) with a low entropy production, most probably as low as possible. The distribution of components is a consequence of this rather than of a shift in the chemical equilibrium according to Chatelier's principle.

4.6.4 Transport properties

All transport coefficients in Tables 2-4 refer to the temperature at $x = l/2$. The cases represent different temperatures, so the temperature function could be plotted in Figures 9-13.

Table 4.2: Resistivity coefficients, R_{ij} and r_{ij}

Case	$T(l/2)$ (kK)	$R_{qq} = r_{qq}$ (10^{-8} $\frac{\mathrm{m}}{\mathrm{WK}}$)	$R_{q\mu} = R_{\mu q}$ (10^{-3} $\frac{\mathrm{ms}}{\mathrm{molK}}$)	$R_{\mu\mu}$ (10^{3} $\frac{\mathrm{Jms}}{\mathrm{mol^2K}}$)	$r_{q\mu} = r_{\mu q}$ (10^{-2} $\frac{\mathrm{ms}}{\mathrm{molK}}$)	$r_{\mu\mu}$ (10^{3} $\frac{\mathrm{Jms}}{\mathrm{mol^2K}}$)
1	5.2	10.13	0.80	2.96	-1.36	4.78
4	6.7	4.34	2.18	2.34	-0.52	2.84
5	8.6	2.29	1.56	2.93	-0.31	3.26
6	9.5	1.77	1.51	2.75	-0.24	2.96
7	13.3	0.76	0.76	3.84	-0.15	4.06
8	16.2	0.39	0.82	3.61	-0.05	3.51

Table 4.3: Conductivity coefficients, L_{ij} and l_{ij}

Case	$T(l/2)$ (kK)	L_{qq} (10^{7} $\frac{\mathrm{WK}}{\mathrm{m}}$)	$L_{q\mu} = L_{\mu q}$ ($\frac{\mathrm{molK}}{\mathrm{ms}}$)	$L_{\mu\mu} = l_{\mu\mu}$ (10^{-4} $\frac{\mathrm{mol^2K}}{\mathrm{msJ}}$)	l_{qq} (10^{7} $\frac{\mathrm{WK}}{\mathrm{m}}$)	$l_{q\mu} = l_{\mu q}$ ($\frac{\mathrm{molK}}{\mathrm{ms}}$)
1	5.2	0.99	-2.7	3.39	1.60	45.5
4	6.7	2.42	-22.5	4.49	2.94	53.4
5	8.6	4.53	-24.0	3.54	5.03	48.3
6	9.5	5.95	-32.7	3.81	6.39	52.6
7	13.3	13.41	-26.5	2.66	14.15	51.9
8	16.2	26.98	-61.5	2.91	26.25	40.5

Table 4.4: Thermal conductivity λ, interdiffusion coefficient D and heat of transfer q^*

Case	$T(l/2)$ (kK)	λ_G (Eq. 4.39a) ($\frac{\mathrm{W}}{\mathrm{mK}}$)	λ_J (Eq. 4.28) ($\frac{\mathrm{W}}{\mathrm{mK}}$)	D (Eq. 4.39b) (10^{-5} $\frac{\mathrm{m^2}}{\mathrm{s}}$)	q^* (Eq. 4.29) ($\frac{\mathrm{kJ}}{\mathrm{mol}}$)	$-\Delta_r H$ ($\frac{\mathrm{kJ}}{\mathrm{mol}}$)
1	5.2	0.58	0.41	0.20	130	140
4	6.7	0.67	0.50	0.27	120	170
5	8.6	0.68	0.59	0.23	140	210
6	9.5	0.71	0.56	0.25	140	220
7	13.3	0.80	0.75	0.19	200	300
8	16.2	1.01	0.94	0.22	140	350

The thermal conductivity and the interdiffusion coefficient

According to the theoretical sections a thermal conductivity can be defined for two different conditions. On the one hand Eq. (4.38a) defines the thermal conductivity λ_G in the absence of a concentration gradient, but in the presence of a chemical reaction. Definition 4.28, on the other hand, gives $\lambda_J = 1/(T^2 r_{qq}) = 1/(T^2 R_{qq})$ for zero component flow,

Table 4.5: Molar density of F, forward reaction rate constant and the fitted length d.

Case	$T(l/2)$ (kK)	k_f (10^7 $\frac{\mathrm{m}^3}{\mathrm{mols}}$)	c_F ($\frac{\mathrm{mol}}{\mathrm{m}^3}$)	$c_{\mathrm{F},eq}$ ($\frac{\mathrm{mol}}{\mathrm{m}^3}$)	d ()
1	5.2	1.45	5589	5515	2.5
4	6.7	0.49	6488	6517	4.1
5	8.6	0.36	7259	7287	3.8
6	9.5	0.32	7429	7513	4.1
7	13.3	0.27	8052	8104	3.5
8	16.2	0.21	8282	8361	4.0

i.e. also absence of a chemical reaction. The results in Fig. 10 must be seen on this background.

The thermal conductivities were plotted as a function of T. We see that λ_J and λ_G both increase with temperature. It is reassuring that kinetic theory gives a value of the same order of magnitude as we find for λ_J (no chemical reaction). Our fluid is like a dense gas. The most interesting feature is that λ_G was up to 40% larger than λ_J. Clearly the chemical reaction has a large impact on the thermal conductivity. The system conducts clearly better, when a chemical reaction is allowed. This may have an impact on how chemical reactions are now modelled in nonisothermal systems.

The interdiffusion coefficient for the reacting mixture is presented in Fig. 4.11. An important characteristic of D in the present system is its temperature independence. The order of magnitude of the coefficient is the same as that predicted by the kinetic theory, and D was proportional to the pressure (not shown), but other mechanisms are involved in heat transfer when a reaction is present. In kinetic theory the diffusion coefficient is proportional to the temperature to the power of 3/2 [74].

The heat of transfer near and at chemical equilibrium

In order to understand the heat of transfer in the system, q^*, it is again useful to consider the hypothetical case, when the reaction is in complete equilibrium. In this case, we showed that the heat of transfer is equal to minus of the reaction enthalpy (cf. Eq. 36) and [73].

The heat of transfer, calculated from Eq. (4.39c) and shown in Table 4.4, was therefore compared to the enthalpy of the reaction in Fig. 4.13. The heat of transfer, shown by squares in the figure, varies between 120 and 200 kJ/mol. The negative enthalpy of reaction, $-\Delta_r H$, was always larger in magnitude; varying between 140 and 350 kJ/mol. The discrepancy between the two numbers was largest at the higher temperatures. The heat of transfer has not only thermodynamic contributions, there are also contributions from the transport coefficients, cf. Eq. (4.39c).

The heat of transfer is a very large number, compared to heats of transfers that are typical for binary mixtures that do not react. This may cast doubt on the assumption

that is used in flame modeling (see i.e. [59, 75]); that the Dufour effect is negligible. Our results indicate that neglect of q^* may lead to errors in the heat as well as the mass flux.

The corresponding results for the coupling coefficient $r_{q\mu}$, plotted in Fig. 4.12, gives a smoother variation with temperature than q^*. Both values may be useful for improved thermodynamic modeling of chemical reactions. It is interesting to see that the square of this coefficient approaches the order of magnitude of the product of the main coefficients in Table 3, as the temperature decreases. The impact of the chemical reaction the thermal diffucion, is therefore larger the lower is the temperature, as evident also from Fig. 4.13.

The Onsager coefficients

Two sets of Onsager resistivity coefficients were calculated, one using the total heat flux and the fluorine flux as variables, the other with the measurable heat flux and the fluorine flux as variables. The inverse coefficients were also determined, before the more commonly known transport coefficients were found.

One may question the need to present also the Onsager coefficients. These are used here as intermediate values, from which we find the more commonly known coefficients. We claim that they are required for establishing well defined conditions for their measurement and calculation in this complex system. By starting with the entropy production, unique definitions can be obtained, and the relations between the coefficients can be given, like the Onsager relations.

4.7 Conclusions

We have derived transport properties for a chemical reaction in a temperature gradient. Their values can be explained by a reaction which is limited by thermal diffusion. This limitation brings the reaction into a regime, where all flux-force relations in a volume element of the system are linear, while the system on a global scale is far from equilibrium. The driving forces and fluxes vary largely across the box. The statistical basis for use of nonequilibrium thermodynanamics theory is found to be everywhere sound, in spite of the large gradients. When exposed to a temperature gradient, the system responds by increasing the thermal conductivity and reducing its entropy production. This property supports the hypothesis that the stationary system, which is far from global equilibrium, has minimum entropy production. It satisfies Prigogine's principle of minimum entropy production, which he was able to prove generally for stationary states close to global equilibrium [71].

Onsager coefficients are well suited to capture the difference between the presence and absence of the chemical reaction, and we suggest that these coefficients should be used systematically to define transport coefficients of reacting mixtures.

Acknowledgment

JX is grateful to The Research Council of Norway, grant no 153305/432 for financial support. JMS is grateful for grant no 167336/V30 also from The Research Council of Norway.

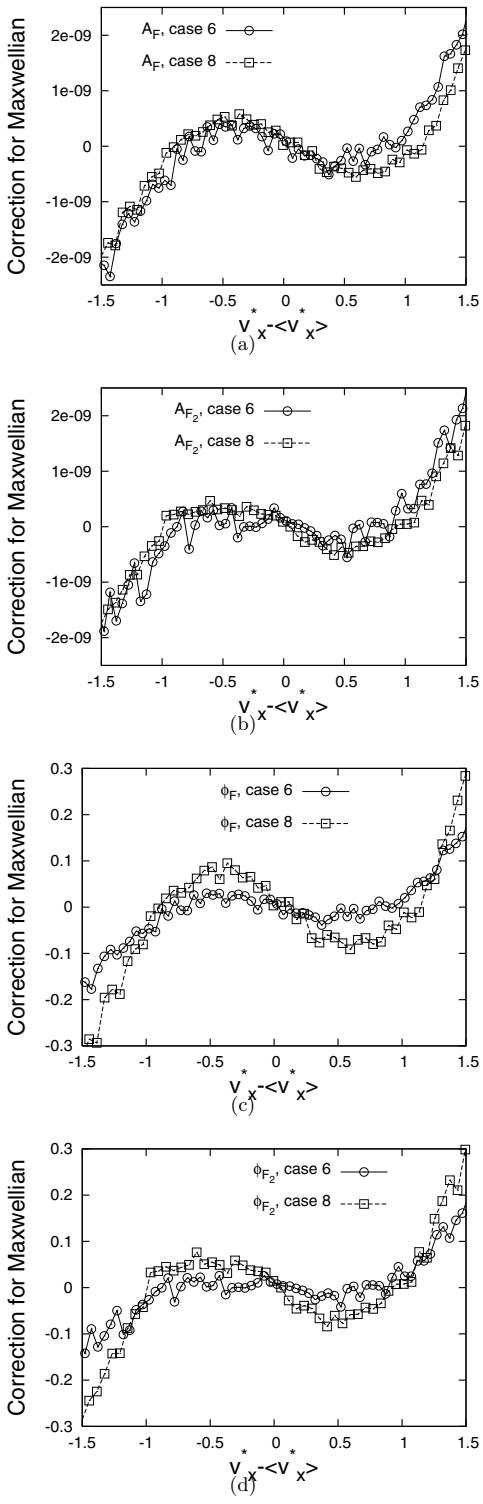

Figure 4.5: The parameter $A_{k,l}$ (figures a and b) and $\phi_{k,l}$ (figures c and d) for the atom and molecule calculated from two ∇T, Case 6 and Case 8, in layer no. 35.

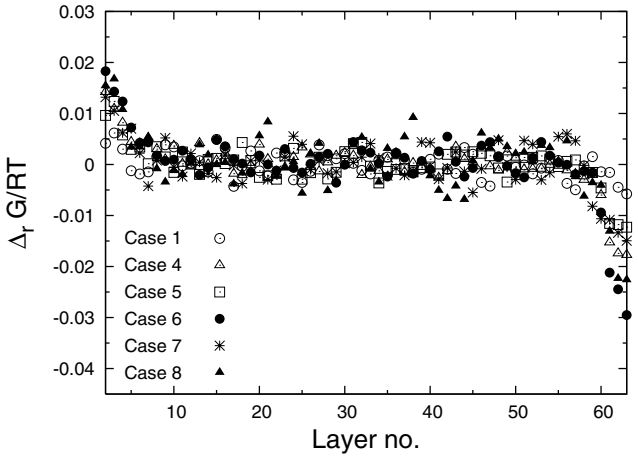

Figure 4.6: $\Delta_r G/RT$ in the MD box for all cases.

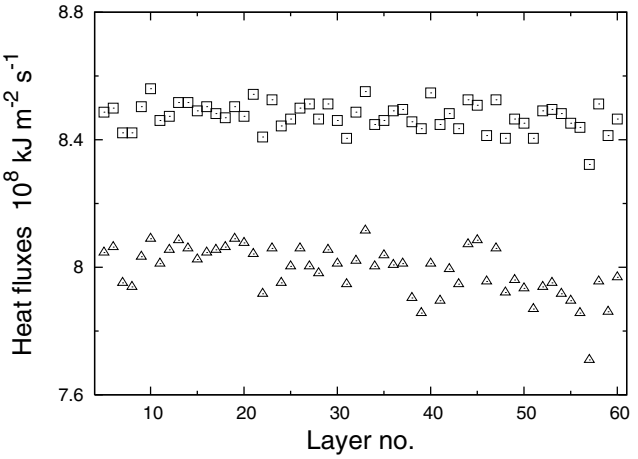

Figure 4.7: The total heat flux J_q (squares) and measurable heat flux J'_q (triangles) in the chemical reaction (Case 8), at $c_{\mathrm{F}} + 2c_{\mathrm{F}_2} = 11271$ mol m^{-3}. The symbols represent values in the layers in MD box.

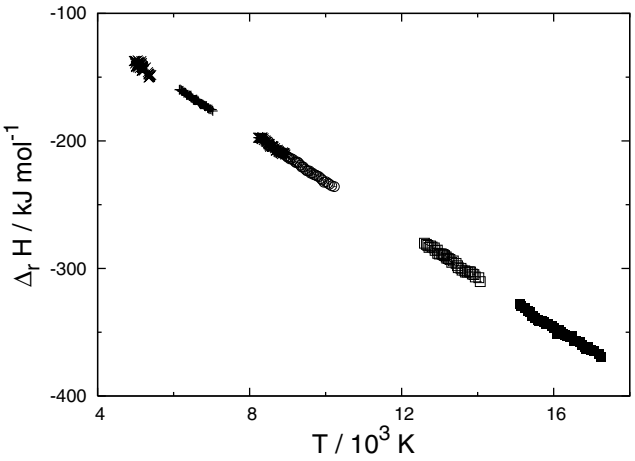

Figure 4.8: The local reaction enthalpy as a function of the temperature at the same location (Cases 1, 4-8), at $c_{\mathrm{F}} + 2c_{\mathrm{F}_2} = 11271$ mol m^{-3}. The symbols represent values in the layers in MD box.

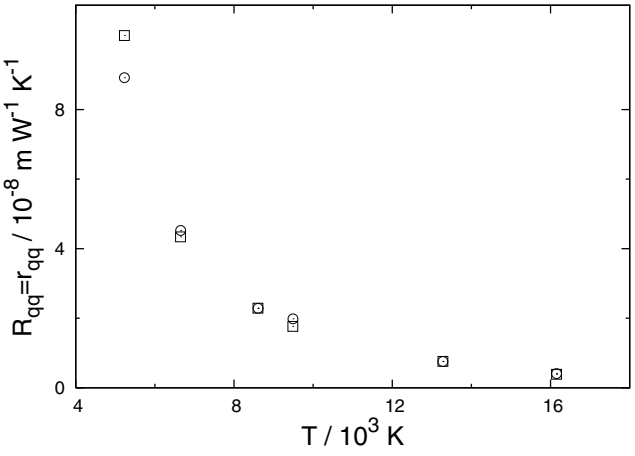

Figure 4.9: The thermal resistivity R_{qq}=r_{qq} from Eq. 32 (circles) and from fitting the analytical solution to the temperature profile (squares), at $c_{\mathrm{F}} + 2c_{\mathrm{F}_2} = 11271$ mol m^{-3}.

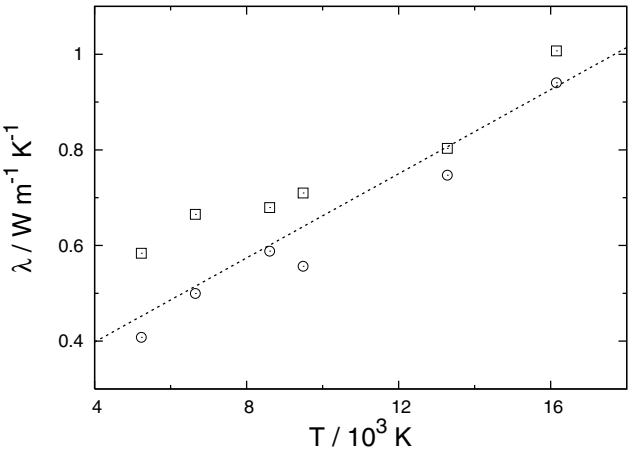

Figure 4.10: The thermal conductivities λ_G (squares) and λ_J (circles), at $c_{\mathrm{F}}+2c_{\mathrm{F}_2} = 11271$ mol m^{-3}. The dotted curve is from kinetic theory.

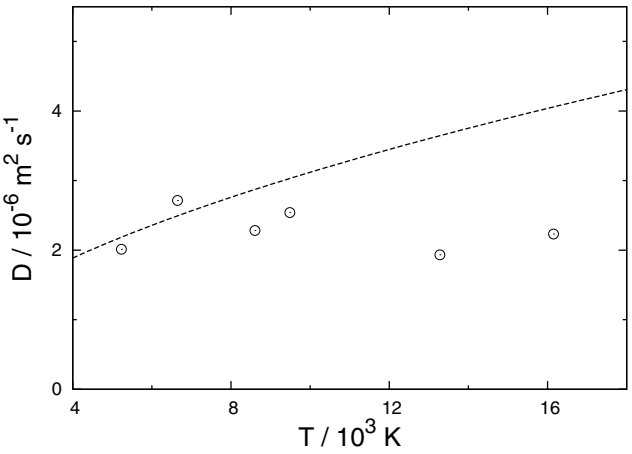

Figure 4.11: The diffusion coefficient, at $c_{\mathrm{F}} + 2c_{\mathrm{F}_2} = 11271$ mol m^{-3}. The dotted curve is from kinetic theory.

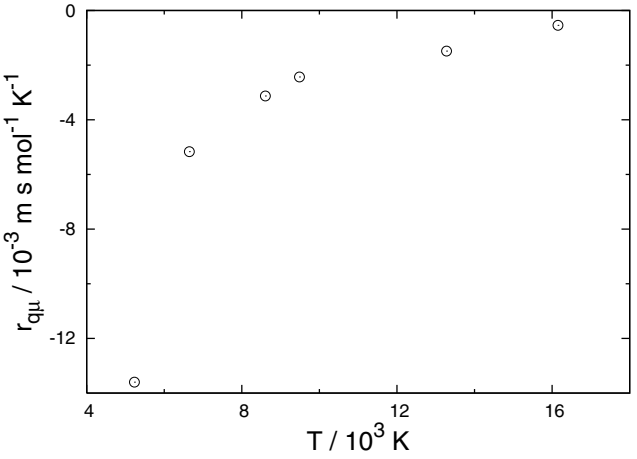

Figure 4.12: The resistivity coefficients $r_{q\mu}$, at $c_F + 2c_{F_2} = 11271$ mol m^{-3}.

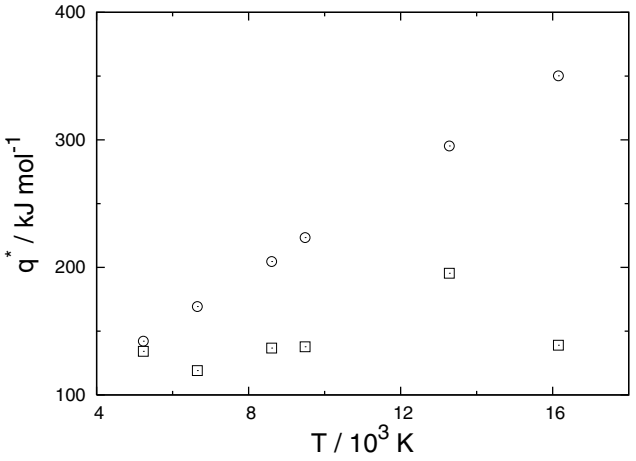

Figure 4.13: The heat of transfer (squares) and $-\Delta_r H$ (circles), at $c_F + 2c_{F_2} = 11271$ mol m^{-3}.

Chapter 5

Verification of Onsager's reciprocal relations for evaporation and condensation using non-equilibrium molecular dynamics

Jing Xu, Signe Kjelstrup, Dick Bedeaux, Audun Røsjorde and Live Rekvig

Department of Chemistry
Faculty of Natural Science and Technology,
Norwegian University of Science and Technology
NO-7491 Trondheim, Norway

This paper was published in
Journal of Colloid and Interface Science,
Volume 299 (2006), pages 452-463.

In this project work, we have used Non-equilibrium molecular dynamic (NEMD) simulations to study heat and mass transfer across a vapor-liquid interface for a one-component system using a Lennard-Jones spline potential. It was confirmed that the relation between the surface tension and the surface temperature in the non-equilibrium system was the same as in equilibrium (local equilibrium) [5]. Interfacial transfer coefficients were evaluated for the surface, which expressed the heat and mass fluxes in temperature and chemical potential differences across the interfacial region (film). In this analysis it was assumed that the Onsager reciprocal relations were valid [9]. In this work we extend the number of simulations such that we can calculate all four interface film transfer coefficients along the whole liquid-vapor coexistence curve. We do this analysis both for the case that we use the measurable heat flux on the vapor side and for the case where we use the measurable heat flux on the liquid side. The most important result we found is that the coupling coefficients are within the accuracy of the calculation equal. This is the first verification of the validity of the Onsager relations for transport through a surface using molecular dynamics. The interfacial film transfer coefficients are found to be a function of the surface temperature alone. New expressions are given for the kinetic theory values of these coefficients which only depend on the surface temperature. The NEMD values were found to be in good agreement with these expressions.

5.1 Introduction

In non-equilibrium thermodynamics, each thermodynamic force X_i is a linear function of all the conjugate thermodynamic fluxes

$$X_i = \sum_{j=1}^{n} R_{ij} J_j \tag{5.1}$$

Following Onsager, the matrix of resistivities R_{ij} is symmetric. These resistivities can in general be functions of the state variables, like for instance the temperature and the pressure, but not of the forces. The Onsager relations simplify transport problems by reducing the number of phenomenological coefficients needed to describe the process. In the study of the properties of surfaces it is therefore of great importance to verify their validity.

In homogeneous systems the Onsager relations have been verified both experimentally [1] and by non-equilibrium molecular dynamics (NEMD) [4]. For the surface such a verification has not yet been given, however. In the present work we will address this problem. We consider the vapor- liquid interface in a one-component system. We consider only transport across and not along the surface, so all fluxes and forces are in the direction normal to the surface.

Non-equilibrium molecular dynamics (NEMD) simulations is a technique to compute transport properties of classical many-body system. A model for the intermolecular potential is used. With these simulations, we can directly study variations of the temperature, pressure and density across the vapor-liquid interface and, important for our present purpose, get the surface tension and the resistivity coefficients for the transfer of heat and

mass across the surface. In general, NEMD simulations are virtual experiments in which one can apply, not only normal conditions, but also rather extreme conditions, which can not be realized in experiments. The computational results can be used to test theoretical results and the assumptions behind these. Experiments have been done, which confirm the presence of a temperature difference across the liquid-vapor interface. In experiments the problem becomes at least two dimensional. Phenomena like convection may occur. We refer to Ward et al. [76] and references there in. For a detailed analysis of the various theoretical descriptions and their application to the experiments we refer to Bond et al. [77].

Røsjorde et al. [5,9] studied condensation of Lennard-Jones spline particles using molecular dynamics simulations. Simon et al. [6] considered the case of more complicated particles (octane), while Kjelstrup et al. [8] and Tsuruta et al. [78–80] considered the longer ranged cut-off Lennard-Jones potentials. In most of these simulations the surface temperature T^{s} was defined using the average kinetic energy of molecules in the interface area. Both [5] and [6] found good agreement between the surface tension $\gamma\left(T^{\mathrm{s}}\right)$ from non-equilibrium simulations and the surface tension from equilibrium simulations at the same temperature. This verified that the surface is in local equilibrium. An important conclusion that can be drawn from this result is that the surface as described by excess densities is a separate thermodynamic system not only in equilibrium but also in nonequilibrium systems. This fact is a central assumption in the description of the nonequilibrium thermodynamics of such surfaces [17, 18].

Assuming Onsager's reciprocal relations, Røsjorde et al. [9] calculated the interface film transfer coefficients which describe heat and mass transfer across a surface. Along the coexistence curve the values of these coefficients were found to agree well with the values predicted by kinetic theory [81–85] for temperatures not too close to the critical temperature. The agreement with kinetic theory was for a simple fluid with a Lennard Jones spline potential. For more complicated particles [6] and longer range potentials [8] such agreement was not found.

Due to the time-consuming nature of the simulations, only a very limited number of simulations were done by Røsjorde et al. [5, 9] and by Simon et al. [6]. In the analysis of the data it was therefore not possible to verify the validity of the Onsager relations. In non-equilibrium thermodynamics the validity of the Onsager reciprocal relation is an essential point. The fact that these relations were not verified in these simulations was very unsatisfactory. It is the objective of this work to do so. For this purpose we have now done more simulations so that we are able to address this issue.

To determine the interface film transfer coefficients, linear force-flux equations derived from non-equilibrium thermodynamics shall be used. An important result of the work is that even for temperature gradients that are extremely large, a satisfactory description of the simulation data is found with these linear relations. There is absolutely no need to use nonlinear relations, as may be needed for other systems [86].

Another important finding is that we find that all interface film transfer coefficients for the surface can be given in terms of the temperature of the surface or alternatively as a

function of the surface tension alone. This simplifies the description and again establishes that the surface is a separate thermodynamic system with its own transport properties.

The report is organized as follows: In the second section we discuss the derivation of equations for transport of heat and mass through the surface. In addition to the equations given in our earlier work [1,2] using the measurable heat flux in the vapor close to the surface, we now also give equivalent equations using the measurable heat flux in the liquid close to the surface. New expressions are given for the interface film transfer coefficients of the surface which are obtained from kinetic theory. These new expressions depend only on the temperature of the surface, as they should, using the property of local equilibrium, and are found to be more appropriate than expressions used previously [9]. The details of our simulations and investigation procedure are presented in the third section. The fourth, fifth and sixth section contain the results, a discussion and conclusions respectively.

5.2 Transport equations for the surface

5.2.1 The excess entropy production rate for the surface

In the study of stationary states using molecular dynamics simulations we average over the time. On the molecular scale of Ångstroms these averages vary smoothly through the surface. In this way we obtain the profiles of, for instance, the temperature and the density through the surface. On a more macroscopic scale of microns some variables appear to change discontinuously across a phase boundary. Not only the density but also the temperature can have a surprisingly large jump across a surface on this scale.

In a macroscopic description not only the homogeneous phases but also the surface are separate thermodynamic systems. The properties of the surface are found by calculating excess densities and energies. Bedeaux and Kjelstrup [65,87,88] derived the excess entropy production rate per unit of surface area in a one component system and they found:

$$\sigma^{\mathrm{s}} = J_q'^{\mathrm{g}} \Delta\left(\frac{1}{T}\right) - J\frac{1}{T^{\mathrm{l}}}\Delta\mu_T(T^{\mathrm{l}}). \tag{5.2}$$

Here $J_q'^{\mathrm{g}}$ is the measurable heat flux from the vapor into the surface and J is the mass flux through the surface. The thermal driving force $\Delta(1/T)$ and chemical driving force $-\Delta\mu_T(T^{\mathrm{l}})/T^{\mathrm{l}}$ are respectively

$$\begin{aligned} X_q &= \Delta\left(\frac{1}{T}\right) = \frac{1}{T^{\mathrm{l}}} - \frac{1}{T^{\mathrm{g}}} \\ X_\mu^{\mathrm{g}} &= -\frac{1}{T^{\mathrm{l}}}\Delta\mu_T(T^{\mathrm{l}}) = -\frac{1}{T^{\mathrm{l}}}\left(\mu^{\mathrm{l}}(T^{\mathrm{l}}) - \mu^{\mathrm{g}}(T^{\mathrm{l}})\right). \end{aligned} \tag{5.3}$$

The vapor was taken on the left hand side and the liquid on the right hand side in Eqs. 5.2 and 5.3. The notation Δ gives the difference of a variable in the liquid minus the one in the vapor, both close to the surface. The temperatures T^{g} and T^{l} are the temperatures of the vapor and the liquid close to the surface. The chemical potential for the liquid and the

vapor, $\mu^{\rm l}$ and $\mu^{\rm g}$, are both evaluated at the temperature of the liquid close to the surface, $T^{\rm l}$. The subscript T indicates that this difference is taken at the same temperature.

Using the energy balance the measurable heat flux on the liquid side of the surface is given by

$$J_q'^{\rm l} = J_q'^{\rm g} + \Delta_{vap}HJ \tag{5.4}$$

where $\Delta_{vap}H = H^{\rm g} - H^{\rm l}$ is the enthalpy of evaporation and $\Delta_{vap}H$ is positive. Substituting Eq. 5.4 into Eq. 5.2 one obtains for the entropy production rate

$$\sigma^{\rm s} = J_q'^{\rm l}\Delta\left(\frac{1}{T}\right) - J\frac{1}{T^{\rm g}}\Delta\mu_T(T^{\rm g}) \tag{5.5}$$

where we used the thermodynamic identity

$$H^{\rm g}\Delta\left(\frac{1}{T}\right) = \frac{1}{T^{\rm l}}\mu^{\rm g}(T^{\rm l}) - \frac{1}{T^{\rm g}}\mu^{\rm g}(T^{\rm g}) \tag{5.6}$$

and the same equality for the liquid in order to obtain Eq. 5.5 from 5.2. Equation 5.5 contains the chemical driving force at the temperature of the vapor

$$X_\mu^{\rm l} = -\frac{1}{T^{\rm g}}\Delta\mu_T(T^{\rm g}) = -\frac{1}{T^{\rm g}}\left(\mu^{\rm l}(T^{\rm g}) - \mu^{\rm g}(T^{\rm g})\right). \tag{5.7}$$

The expressions for the chemical forces $X_\mu^{\rm g}$ and $X_\mu^{\rm l}$ are given above to linear order in the temperature difference across the surface. In view of the rather extreme temperature differences considered in the simulations, we will also take a contribution along which is of the second order in this difference. We clarify how we calculated the chemical forces in the appendix.

In the derivation of the above equations the surface is located following Gibbs [89] by choosing a so-called dividing surface. The values of the fluxes, the temperatures and the chemical potentials in the liquid and the vapor close to the surface are the extrapolated values of these quantities from the liquid and the vapor to this dividing surface [17]. In the nonequilibrium molecular dynamics simulations we found that one may distinguish a region with a finite thickness in which the particles are neither in the liquid or in the vapor. Extrapolation of the various quantities into this layer to for instance the equimolar surface is found to give values which have a larger computational error than the values of these quantities taken in positions just outside the interface region. It has been shown that the above equations are equally valid for the differences across the finite layer and the fluxes just outside this layer. These quantities are not identical to the extrapolated values. In practice the differences are usually small. The two descriptions can also be transformed into each other. We refer to Johannessen et al. [14] for this transformation.

5.2.2 The linear force-flux relations for the surface

Nonequilibrium thermodynamics gives linear relations between the thermodynamic driving forces and the heat and mass fluxes. In the vapor they are

$$\begin{aligned} \nabla\left(\frac{1}{T}\right) &= r^{\mathrm{g}}_{qq}\mathbf{J}'^{\mathrm{g}}_{q} + r^{\mathrm{g}}_{q\mu}\mathbf{J} \\ -\frac{1}{T}\nabla\mu_T &= r^{\mathrm{g}}_{\mu q}\mathbf{J}'^{\mathrm{g}}_{q} + r^{\mathrm{g}}_{\mu\mu}\mathbf{J} \end{aligned} \tag{5.8}$$

where vectors are indicated by bold symbols. Subscript T indicates that the differentiation is carried out for a constant temperature. Two main resistivities are r^{g}_{qq} and $r^{\mathrm{g}}_{\mu\mu}$ and the cross resistivities are $r^{\mathrm{g}}_{\mu q}$ and $r^{\mathrm{g}}_{q\mu}$. According to the Onsager relations $r^{\mathrm{g}}_{\mu q} = r^{\mathrm{g}}_{q\mu}$. We will consider only fluxes and gradients in the direction normal to the surface. The gradient ∇ can therefore be replaced by d/dx, and only the x-component of the fluxes is unequal to zero. Similar linear relations, in which all the g's should be replaced by l's, are valid for the liquid.

For the surface it follows from Eq. 5.2 that the linear relations between the thermodynamic forces and the conjugate fluxes is given by

$$\begin{aligned} X_q &= \Delta\left(\frac{1}{T}\right) = r^{\mathrm{s,g}}_{qq}J'^{\mathrm{g}}_{q} + r^{\mathrm{s,g}}_{q\mu}J \\ X^{\mathrm{g}}_{\mu} &= -\frac{1}{T^{\mathrm{l}}}\Delta\mu_T(T^{\mathrm{l}}) = r^{\mathrm{s,g}}_{\mu q}J'^{\mathrm{g}}_{q} + r^{\mathrm{s,g}}_{\mu\mu}J \end{aligned} \tag{5.9}$$

where $r^{\mathrm{s,g}}_{qq}$ and $r^{\mathrm{s,g}}_{\mu\mu}$ are the two main film resistivities for the surface and $r^{\mathrm{s,g}}_{q\mu}$ and $r^{\mathrm{s,g}}_{\mu q}$ are the coupling film resistivities for the surface. We use the notation *film resistivities for the surface* or *interface film resistivities* to indicate that they give the inverse temperature and chemical potential differences across the surface with a *finite thickness*. When we use the extrapolated values at the dividing surface we will use the notation *excess resistivities for the surface* or *interface excess resistivities*. If we express the fluxes in terms of the forces we replace *resistivities* by *conductivities*. And when we refer to either *resistivities* or *conductivities* we use *coefficients*.

In Eq.5.9 we deviate from expressions given earlier [5,9] in two ways. In the first place there is a sign difference in the film resistivities and in the second place the forces have been divided by the temperature of the liquid. One sees from this equation that condensation and evaporation not only gives a difference in chemical potential, but also a difference in the inverse temperature across the surface. It is therefore not correct to neglect such differences as is habitually done. According to the Onsager relations $r^{\mathrm{s,g}}_{\mu q} = r^{\mathrm{s,g}}_{q\mu}$. An interesting coefficient is the heat of transfer $q^{*\mathrm{s,g}}$ for the vapor side of the surface which is defined by:

$$q^{*\mathrm{s,g}} \equiv \left(\frac{J'^{\mathrm{g}}_{q}}{J}\right)_{\Delta T=0} = -\frac{r^{\mathrm{s,g}}_{\mu q}}{r^{\mathrm{s,g}}_{qq}}. \tag{5.10}$$

From Eq. 5.5 it follows that the linear relation between the thermodynamic forces and

the conjugate fluxes may alternatively be given by

$$\begin{aligned} X_q &= \Delta\left(\frac{1}{T}\right) = r_{qq}^{\mathrm{s,l}} J_q^{\prime\mathrm{l}} + r_{q\mu}^{\mathrm{s,l}} J \\ X_\mu^{\mathrm{l}} &= -\frac{1}{T^{\mathrm{g}}}\Delta\mu_T(T^{\mathrm{g}}) = r_{\mu q}^{\mathrm{s,l}} J_q^{\prime\mathrm{l}} + r_{\mu\mu}^{\mathrm{s,l}} J \end{aligned} \tag{5.11}$$

where $r_{qq}^{\mathrm{s,l}}$ and $r_{\mu\mu}^{\mathrm{s,l}}$ are the two main film resistivities for the surface and $r_{q\mu}^{\mathrm{s,l}} = r_{\mu q}^{\mathrm{s,l}}$ are the coupling film resistivities for the surface. Substitution of Eq. 5.4 into Eq. 5.9, using Eq. 5.6 and comparison with Eq. 5.11 gives the following relations between the interface film resistivities

$$\begin{aligned} r_{qq}^{\mathrm{s,l}} &= r_{qq}^{\mathrm{s,g}} \\ r_{q\mu}^{\mathrm{s,l}} &= r_{\mu q}^{\mathrm{s,l}} = r_{q\mu}^{\mathrm{s,g}} - \Delta_{vap} H r_{qq}^{\mathrm{s,g}} \\ r_{\mu\mu}^{\mathrm{s,l}} &= r_{\mu\mu}^{\mathrm{s,g}} - 2\Delta_{vap} H r_{\mu q}^{\mathrm{s,g}} + \left(\Delta_{vap} H\right)^2 r_{qq}^{\mathrm{s,g}} \end{aligned} \tag{5.12}$$

The heat of transfer $q^{*\mathrm{s,l}}$ for the liquid side of the surface is defined by:

$$q^{*\mathrm{s,l}} \equiv \left(\frac{J_q^{\prime\mathrm{l}}}{J}\right)_{\Delta T=0} = -\frac{r_{\mu q}^{\mathrm{s,l}}}{r_{qq}^{\mathrm{s,l}}} \tag{5.13}$$

Using Eq. 5.12 it follows that

$$q^{*\mathrm{s,g}} - q^{*\mathrm{s,l}} = \Delta_{vap} H \tag{5.14}$$

This equation shows most clearly that one violates thermodynamical laws by assuming that all the cross coefficients are zero.

In kinetic theory expressions have been derived [81–83] for the thermodynamic forces in terms of the fluxes in evaporation and condensation. These results can be used to find the following expressions for the interface film resistivities [84]:

$$\begin{aligned} r_{qq}^{\mathrm{s,g}}\left(T^{\mathrm{s}}\right) &= \frac{1.27640}{R\left(T^{\mathrm{s}}\right)^2 c^{\mathrm{g}}\left(T^{\mathrm{s}}\right)}\sqrt{\frac{M}{3RT^{\mathrm{s}}}} \\ r_{\mu q}^{\mathrm{s,g}}\left(T^{\mathrm{s}}\right) &= r_{q\mu}^{\mathrm{s,g}}(T^{\mathrm{s}}) = \frac{0.54715}{T^{\mathrm{s}} c^{\mathrm{g}}\left(T^{\mathrm{s}}\right)}\sqrt{\frac{M}{3RT^{\mathrm{s}}}} \\ r_{\mu\mu}^{\mathrm{s,g}}\left(T^{\mathrm{s}}\right) &= \frac{4.34161R(\sigma_c^{-1}\left(T^{\mathrm{s}}\right) - 0.39856)}{c^{\mathrm{g}}\left(T^{\mathrm{s}}\right)}\sqrt{\frac{M}{3RT^{\mathrm{s}}}} \end{aligned} \tag{5.15}$$

where $c^{\mathrm{g}}\left(T^{\mathrm{s}}\right)$ is the density of a vapor in coexistence with a liquid at the temperature of the surface. We refer to these coefficients as interface film resistivities rather than interface excess resistivities because they describe the changes across the Knudsen layer, which is also a layer with a finite thickness. For the condensation coefficient $\sigma_c\left(T^{\mathrm{s}}\right)$ values between 0.1 to 1.0 have been reported [85]. Furthermore M is the molar mass and R is the gas constant. In our simulations we evaluate T^{s}. In Eq. 5.15 we deviate from expressions we gave earlier [5, 9] by replacing all temperatures by the temperature of the surface. Also, the vapor concentration is now calculated as the value in phase equilibrium,

at the temperature of the surface. While this only leads to small corrections in the value of the coefficients, the coefficients are now a function of the temperature of the surface alone. The advantage of Eq. 5.15 is that we can now calculate the values predicted by kinetic theory given the temperature of the surface and $c^{\mathrm{g}}(T^{\mathrm{s}})$, as found from equilibrium simulations, alone. It is no longer necessary to use T^{l}, T^{g} and c^{g} from the non-equilibrium simulation, as we did in our previous work. We shall find the above expressions to be useful. The predictions from kinetic theory for the heat of transfer on the vapor side of the surface is:

$$q^{*\mathrm{s,g}}(T^{\mathrm{s}}) = -0.42867RT^{\mathrm{s}} \tag{5.16}$$

The reason to modify the predictions of kinetic theory for the interface film resistivities to contain only the temperature of the surface, is to make them dependent only on the state of the surface. According to the property of local equilibrium these coefficients should only depend on the state of the surface and this is accomplished in this way. This property is required in a proper description of the surface using non-equilibrium thermodynamics. In our analysis of the results of the NEMD simulations, this modification works well and as such our results support the validity of local equilibrium

5.3 Non-equilibrium molecular dynamics simulations

The basis of our nonequilibrium molecular dynamics simulations was described elsewhere [4, 35]. Here we shall only give a brief description of this method.

5.3.1 Model and simulation details

We simulated 4096 argon-like particles interacting with the pairwise additive intermolecular Lennard-Jones spline potential in an elongated box with lengths $L_y = L_z = L_x/16$. Normally the size of the box was about 10 molecular diameters (10σ) in the direction along the surface and about 160 molecular diameters (160σ) in the direction normal to the surface, the x-direction. The NEMD simulations were done with a constant number of particles N and volume V. In equilibrium the thermostatted regions were thermostatted to the same temperature. This produced then a canonical ensemble. Different overall densities of the model system were obtained by varying the size of the box.

A classical (12-6) Lennard-Jones spline potential model is used to describe the particle interaction. The potential is expressed in terms of the interparticle distance r_{ij} between any pair of particles i and j,

$$U(r_{ij}) = \begin{cases} 4\epsilon[(\sigma/r_{ij})^{12} - (\sigma/r_{ij})^{6}] & \text{for} \quad 0 < r_{ij} < r_c \\ a(r_{ij} - r_s)^2 - b(r_{ij} + r_s)^3 & \text{for} \quad r_c < r_{ij} < r_s \\ 0 & \text{for} \quad r_s < r_{ij} \end{cases} \tag{5.17}$$

Here the cutoff distance is $r_c = (26/7)^{1/6}\sigma \approx 1.24\sigma$ and the switch distance $r_s = (67/48)r_c \approx 1.73\sigma$. The two parameters $a = -(24192/3211)(\epsilon/r_c^2)$ and $b = -(387072/$

61009)/(ϵ/r_c^3) were chosen such that the potential and its first derivative are continuous in $r_{ij} = r_c$. The potential and its derivative are also continuous in $r_{ij} = r_s$. In our calculations we use for σ (the particle diameter), ϵ (the energy) and m_1 (the particle mass) values which are typical for argon; in which case one has $\epsilon/k_B = 124$ K, $\sigma = 3.42\times\ 10^{-10}$m and $m_1 = 6.64\times10^{-26}$kg where k_B is Boltzmann's constant. In the simulations all quantities are expressed in reduced units using σ , ϵ and m_1 as scaling factors.

The molecular dynamics simulation program makes use of dimensionless reduced variables which are defined in Table 5.1 where N_A is Avogrado's number. The reduced quantities are denoted with a superscript $*$.

The non-equilibrium simulations were done as described previously [5, 9]. The simulation box was divided into 128 equal planar layers parallel to the surface. In order to give the system a certain temperature gradient, energy was added or withdrawn in certain layers using the "heat exchange" (HEX) algorithm HafskjoldB1993. The layer numbers 1-4 and 125-128, named hot layers, were regulated to the temperature T_H^* while the layer numbers 61-68 in the middle of the box, named cold layers, were similarly regulated to the temperature T_L^* ($T_H^* > T_L^*$). Using periodic boundary conditions HafskjoldB1993 and the appropriate size of the box, two liquid-vapor interfaces appeared in the box with the liquid in the middle of the box. A condensation flux was induced using a "mass exchange" (MEX) algorithm which removed particles from the cold layers in the liquid phase and inserted them into the hot layers in the vapor phase [4]. The rate of transfer gives J in Table 2. As not all particle transfers are accepted by the algorithm, the actual J given in Table 3 is smaller. In figure 5.1, a 3−dimensional snapshot of 4096 particles is shown of our simulation box. In stationary simulations the system is symmetric and all properties are not only time averaged but also averaged with respect to the mirror plane in the middle of the simulation box.

Table 5.1: **Reduced Variables**

Variable	Reduction formula
mass	$m^* = m/m_1$
distance	$r^* = r/\sigma$
energy	$U^* = U/\epsilon$
time	$t^* = (t/\sigma)\sqrt{\epsilon/m_1}$
temperature	$T^* = k_B T/\epsilon$
molar density	$c^* = c\sigma^3 N_A$
pressure	$p^* = p\sigma^3/\epsilon$
velocity	$\mathrm{v}^* = \mathrm{v}\sqrt{m_1/\epsilon}$
surface tension	$\gamma^* = \gamma\sigma^2/\epsilon$

NEMD simulations were performed for over 10 million time steps using the Verlet 'Leap Frog' algorithm [90]. A time step length of 5×10^{-4} in reduced units was used, which corresponds to about 10^{-15} s in real time. Properties such as the temperature and the density in each layer of the box were monitored in intervals of 500,000 time steps each, in order to detect the stationary state. The first 2 million time steps were discarded to avoid transient effects. The simulation parameters such as the temperatures T_L^* and T_H^* and the overall densities were chosen using the phase diagram for the Lennard-Jones

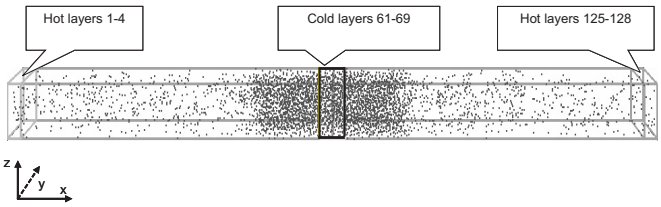

Figure 5.1: A snapshot of MD box with 4096 particles

spline fluid, in which the triple point temperature, the critical temperature and the critical pressure were found to be $T_t = 68.2$ K , $T_c = 111.2$ K and $p_c = 33.2 \times 10^5$ Pa [5]. For 48 simulations we give the simulation conditions in Table 5.2 both in reduced and in real units. We discarded some further simulations, which were either too close to the critical point or too close to the triple point, and would not properly go to a stationary state.

5.3.2 Equilibrium properties of the system

For the gas phase in the same Lennard-Jones spline system, Røsjorde et al. [5] found that the pressure was given in terms of the molar volume $v = 1/c$ and the temperature by the Soave-Redlich-Kwong (SRK) equation of state:

$$p = \frac{RT}{v-b} - \frac{a}{v(v+b)} \tag{5.18}$$

where the coefficients were given by

$$\begin{aligned} b &= 0.08664\frac{RT_c}{p_c} \\ a &= 0.42748\frac{R^2T_c^2}{p_c}\left[1 + 0.4866\left(1 - \sqrt{\frac{T}{T_c}}\right)\right]. \end{aligned} \tag{5.19}$$

The molar density given by the SRK equation of state, which is the inverse of the molar volume, was used to find the last layer in the vapor phase next to the surface. Figure 2 shows an example of such a determination of the surface extension. The layer next to the vapor had a substantially larger deviation of the density from the value found using the SRK equation. This method was formulated in the work by Røsjorde et al. [5]. For the liquid bulk, an appropriate equation of state has not been found. The last layer of the liquid was chosen by visual inspection from the density profiles. The layers between the vapor and the liquid will be referred to as the surface layers. Possible errors were estimated by changing these layers up or down one layer. For the vapor pressure of the liquid with a temperature T, Røsjorde et al. found $p^\star = p_0 \exp\left(-\Delta^p_{vap}H/RT\right)$, with $p_0 = 9.24 \cdot 10^8$ Pa and an "enthalpy of vaporization" $\Delta^p_{vap}H = 5205$ J mol^{-1}. It is important to realise that this enthalpy of evaporation is a temperature independent fit parameter. It should not be confused with the actual value of $\Delta_{vap}H = H^{\mathrm{g}} - H^{\mathrm{l}}$ which is found to be temperature dependent.

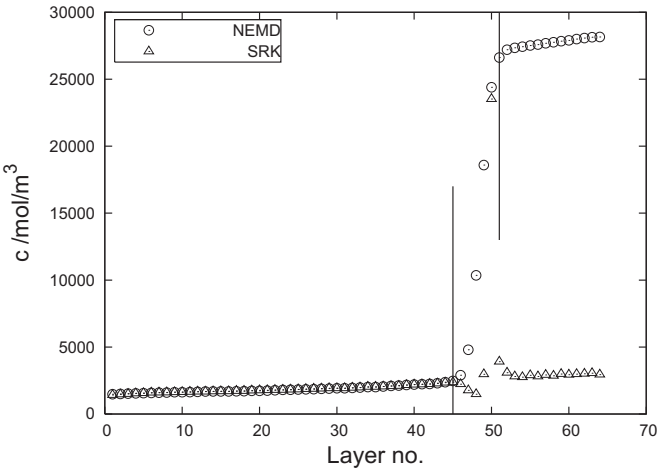

Figure 5.2: The density profile for simulation no. 1. The vertical lines indicate the surface extension.

The equation of state for the surface is:

$$\gamma^s = \gamma_0 \left(\frac{T_c - T}{T_c} \right)^{\nu} \tag{5.20}$$

where the universal critical exponent is given by $\nu = 1.26$. Røsjorde et al. [5] found $\gamma_0 = 2.48 \times 10^{-2}$ N/m . The surface tension varied between 1.1×10^{-3} N/m and 8.0×10^{-3} N/m in our simulations. We refer to [5] for a figure.

5.3.3 Calculation procedures

The molar density in layer ν, c_ν, for $\nu = 1, ..., 128$ was given by

$$c_\nu = \frac{128}{V N_A} \sum_{i \in \, layer \; \nu} 1 = \frac{128 N_\nu}{V N_A} \tag{5.21}$$

where $V = L_x L_y L_z$ is the volume and N_ν is the number of particles in layer ν. Using the symmetry of the system with respect to the surface between layer 64 and 65, we always used the averages of c_ν and $c_{129-\nu}$. The molar flux in layer ν, $\mathbf{J}_\nu$, was given by

$$\mathbf{J}_\nu = c_\nu \mathbf{v}_\nu = \frac{128}{V N_A} \sum_{i \in \, layer \; \nu} \mathbf{v}_i \tag{5.22}$$

and equals between layers 5 and 60 the layer independent value determined by the MEX algorithm. Between layers 69 and 124 the molar flux is minus this value. In this formula and the formulae below, $\mathbf{v}_i$ is the velocity of particle i and $\mathbf{v}_\nu$ is the average velocity in the layer.

The temperature of each layer ν , T_ν, is found from the kinetic energy of the layer

$$\frac{3}{2}N_\nu k_B T_\nu = \frac{1}{2}\sum_{i\,\in\,layer\;\nu} m\left|\mathbf{v}_i - \mathbf{v}_\nu\right|^2. \tag{5.23}$$

In view of the symmetry we again used the averages of T_ν and $T_{129-\nu}$. The temperatures T^{g} and T^{l} were chosen to be equal to the temperatures of the last layers of the vapor and the liquid next to the surface layers. These then give the thermal force X_q. For the temperature of the surface, T^{s}, we used the value which is found from the kinetic energy of the surface layers. In terms of the temperatures of the layers that are part of the surface this gives

$$T^{\mathrm{s}} = \sum_{\nu\,\in\,surface} N_\nu T_\nu \Big/ \sum_{\kappa\,\in\,surface} N_\kappa \tag{5.24}$$

where the sum of N_κ is the total number of particles in the surface. For the calculation of the chemical forces we refer to the appendix.

The pressure tensor was obtained using the formula

$$P_{\alpha\beta,\nu} = \frac{128}{V}\sum_{i\,\in\,layer\;\nu}\left(m\mathrm{v}_{i,\alpha}\mathrm{v}_{i,\beta} + \frac{1}{2}\sum_{j\neq i}\mathrm{F}_{ij,\alpha}r_{ij,\beta}\right) \tag{5.25}$$

where $\mathrm{v}_{i,\alpha}$ is the component of the velocity of particle i in the direction α and $\mathrm{F}_{ij,\alpha}$ is the component of the force exerted on particle i by particle j in the direction α. Furthermore $r_{ij,\beta}$ is the component of the vector from particle j to particle i in the direction β. The pressure tensor was found to be diagonal. In view of the symmetry we again use the averages of $P_{\alpha\beta,\nu}$ and $P_{\alpha\beta,129-\nu}$. The surface tension, γ, defined by $\gamma = \frac{L_x}{128}\sum_{\nu=1}^{64}(p_\parallel - p_\perp)$, is computed by

$$\gamma = \frac{1}{A}\sum_{i<j}(r_{ij} - 3{x_{ij}}^2/r_{ij})u'(r_{ij}) \tag{5.26}$$

where $A = L_y L_z$ is the surface area of the cross section in the y- and z- direction. The x direction is the direction normal to the surface. Furthermore $x_{ij} = |x_i - x_j|$, $u'(r_{ij})$ is the derivative of the pair potential with respect to the interparticle distance r_{ij}, $p_\parallel$ is the pressure parallel to the surface, and $p_\perp$ is the pressure normal to the surface. Equation [90] gives the surface tension of one of the two surfaces by restricting the particles to be either in layers 5 to 60 or in 69 to 124. If the sum is not restricted in this manner one must divide by $2A$.

The total heat flux $\mathbf{J}_q$ is constant while the measurable heat flux $\mathbf{J}'_q$ varies due to the temperature dependence of the enthalpy per mole H. The total heat flux is

$$\mathbf{J}_q = \mathbf{J}'_q + H\mathbf{J}. \tag{5.27}$$

The total heat flux in layer ν is calculated from

$$\begin{aligned}\mathbf{J}_{q,\nu} &= \frac{128}{V}\sum_{i\,\in\,layer\;\nu}\left[\mathbf{v}_i\left(\frac{1}{2}m\mathrm{v}_i^2 + \phi_i\right) + \mathbf{v}_i\cdot\left(m\mathbf{v}_i\mathbf{v}_i + \frac{1}{2}\sum_{j\neq i}\mathbf{F}_{ij}\mathbf{r}_{ij}\right)\right]\\ &= \frac{128}{V}\sum_{i\,\in\,layer\;\nu}\left[\mathbf{v}_i\left(\frac{3}{2}m\mathrm{v}_i^2 + \phi_i\right) + \frac{1}{2}\sum_{j\neq i}\mathbf{v}_i\cdot\mathbf{F}_{ij}\mathbf{r}_{ij}\right]\end{aligned} \tag{5.28}$$

where the potential energy of particle i is

$$\phi_i \equiv \frac{1}{2}\sum_j u(r_{ij}). \tag{5.29}$$

The enthalpy per mole in layer ν is found from

$$H_\nu = \frac{1}{N_A}\left[\frac{5}{2}k_B T_\nu N_\nu + \sum_{i\,\in\, layer\ \nu}\left(\phi_i + \frac{1}{6}\sum_j \vec{F}_{ij}\cdot\vec{r}_{ij}\right)\right]. \tag{5.30}$$

5.4 Results

We used 48 NEMD simulations to obtain the film resistivities for the surface. We verified that our calculations reproduced the results by Røsjorde et al. [5,9] by recalculating some of their data. In Table 5.3 we give the fluxes and the forces. The molar flux given in Table 5.2 is larger than the one given in Table 5.3. The reason for this is that Table 5.2 gives the number of particles that the MEX algorithm tries to transfer from the cold to the hot layer per second, while Table 5.3 gives the number of particles that is not rejected in this procedure. In Tables 5.4 and 5.5 we list the surface extension, i.e. the first and the last layer of the surface, the surface tension, the temperatures near and of the surface, the densities near the surface, the (normal) pressure and the vapor pressures. When we say near the surface we mean the value in the last layer before or in the first layer after the surface layers. For typical temperature, density and pressure profiles found in our simulations we refer to [5,9]. The normal pressure was always found to be constant.

In a one component system the equilibrium state of the surface is specified by the surface tension. The corresponding (equilibrium) surface temperature was found using Eq. 5.20 and vice versa. As was done by [5], we verified that also for the NEMD simulations in this work the relation between the surface tension and the surface temperature was given by the equilibrium relation, Eq. 5.20. The surface is therefore in local equilibrium. All properties of the surface, like the film resistivities, were therefore plotted as a function of the surface tension alone.

Part of the simulations were done for a zero rate of condensation, $J = 0$. In that case $J_q'^{\mathrm{g}} = J_q'^{\mathrm{l}}$, cf. Eq. 5.4. Using Eqs. 5.9 and 5.11 we were then able to determine $r_{qq}^{\mathrm{s,l}} = r_{qq}^{\mathrm{s,g}} \equiv r_{qq}^{\mathrm{s}}$, $r_{\mu q}^{\mathrm{s,g}}$ and $r_{\mu q}^{\mathrm{s,l}}$. The results are plotted in Figs. 5.3 and 5.4. In these figures we also plotted the predictions from kinetic theory, Eqs. 5.15 and 5.12 as well as those obtained by Røsjorde et al [9] for $J = 0$ on the vapor side. We see in these figures that our NEMD results agree well both with those obtained using kinetic theory as well as with those obtained by Røsjorde et al.

For the NEMD simulations with a finite condensation flux we used Eqs. 5.9 and 5.11 to determine the remaining interface film resistivities. From the NEMD results for zero condensation flux we know that kinetic theory gives a good prediction for $r_{qq}^{\mathrm{s,l}} = r_{qq}^{\mathrm{s,g}} \equiv r_{qq}^{\mathrm{s}}$, $r_{\mu q}^{\mathrm{s,g}}$ and $r_{\mu q}^{\mathrm{s,l}}$. In our analysis of the results for a finite condensation flux we used the

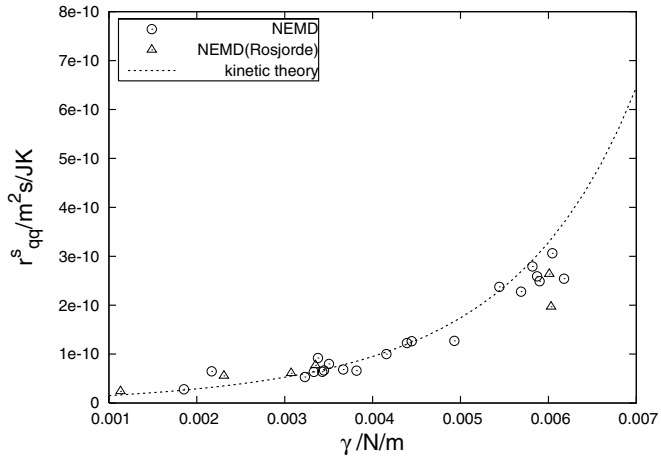

Figure 5.3: The main resistivity coefficient (r^{s}_{qq}) as a function of the surface tension. The symbols are from NEMD simulations. The dotted curve is from kinetic theory.

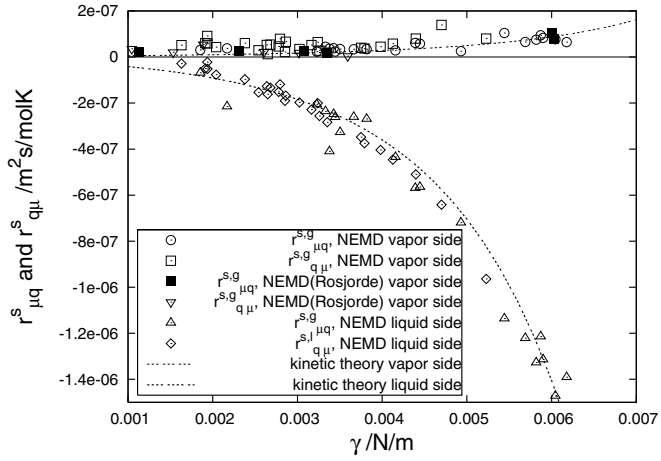

Figure 5.4: The coupling resistivity coefficient ($r^{\mathrm{s,g}}_{\mu q}$ and $r^{\mathrm{s,l}}_{\mu q}$) as a function of the surface tension. The symbols are from NEMD simulations. The dotted curves are from kinetic theory.

prediction of kinetic theory to calculate the first terms on the right hand side in Eqs. 5.9 and 5.11. This then made it then possible to calculate $r^{\mathrm{s,g}}_{q\mu}$, $r^{\mathrm{s,l}}_{q\mu}$, $r^{\mathrm{s,g}}_{\mu\mu}$ and $r^{\mathrm{s,l}}_{\mu\mu}$ from the remainder. This gave an independent determination of the cross coefficients $r^{\mathrm{s,g}}_{q\mu}$ and $r^{\mathrm{s,l}}_{q\mu}$. In figure 5.4 we also plotted these coefficients. From the figure it is clear that the cross coefficients satisfy, within the accuracy of the simulations, Onsager's reciprocal relations. The cross coefficients on the vapor side are rather small. Their accuracy is comparable with their size. The results for the liquid side gave the symmetry in a more convincing

manner.

In figure 5.5 we plotted the values obtained for $r^{s,g}_{\mu\mu}$ and $r^{s,l}_{\mu\mu}$. In this case we did not plot the prediction from kinetic theory as this depends on the condensation coefficient. The NEMD values of $r^{s,g}_{\mu\mu}$ and $r^{s,l}_{\mu\mu}$ made it possible to calculate this condensation coefficient. The resulting values for σ_c are plotted in figure 5.6.

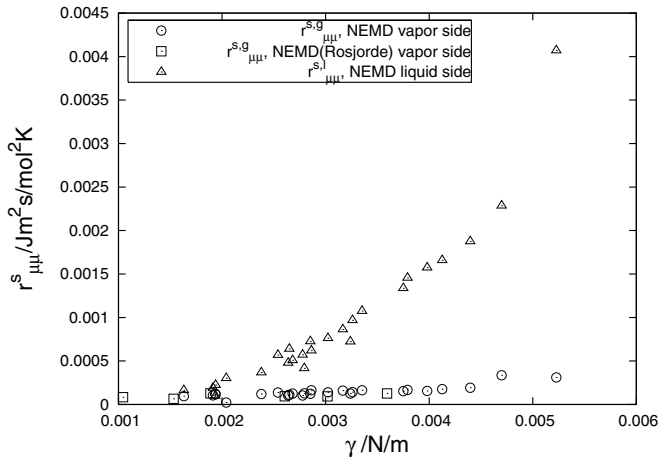

Figure 5.5: The mass resistivity coefficient for mass transfer ($r^{s,g}_{\mu\mu}$ and $r^{s,l}_{\mu\mu}$) as a function of the surface tension.

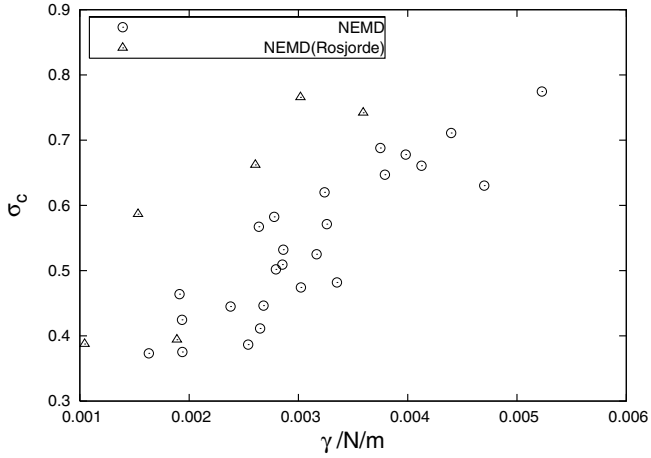

Figure 5.6: The condensation coefficient (σ_c) as a function of the surface tension.

5.5 Discussion

As in our first article [5] our present results for the NEMD simulations confirmed that the relation between the surface tension and the temperature of the surface is the same as in equilibrium. One may verify this property from the values given for these properties in Table 5.4. This verifies that the surface is in local equilibrium also in a temperature gradient. It confirms that the surface is a separate thermodynamic system.

Using the property of local equilibrium it follows that also the interface film resistivities should be a function of the surface temperature or alternatively the surface tension alone. In reporting these resistivities we have therefore chosen to plot them as a function of the surface tension. In the study of all the properties of these coefficients, like the Onsager symmetry relations, this procedure gave values within the accuracy of the calculation.

The standard formulae given by kinetic theory to describe the transport of heat and mass, use coefficients which depend on the temperatures of the vapor and the liquid [14-16,18]. The formulae which can be derived from their expressions for the interface film resistivities have the same property [2,17]. Given that the surface was also in the nonequilibrium simulations in local equilibrium, formulae depending only on the temperature of the surface are more appropriate. In Eq. 5.15 we proposed new formulae which have that property. The interface film resistivities $r_{qq}^{\mathrm{s,g}}$ and $r_{\mu q}^{\mathrm{s,g}}$ found from NEMD simulations for zero condensation flux were predicted with these new formulae with a good accuracy. A similar agreement with kinetic theory was also found by [9]. Close to the critical point, where the surface tension is small, the prediction from kinetic theory is less good. This is not clearly visible in the figures because the interface film resistivities of the NEMD simulations, as well as the kinetic theory values, both become small. The fact that the new kinetic theory formulae based on local equilibrium work so well is further evidence that the surface is in local equilibrium.

The agreement of the interface film resistivities $r_{qq}^{\mathrm{s,g}}$ and $r_{\mu q}^{\mathrm{s,g}}$, found from NEMD simulations with a zero condensation flux, with the predictions from kinetic theory, enabled us to use the prediction of kinetic theory for $r_{qq}^{\mathrm{s,g}} = r_{qq}^{\mathrm{s,l}}$ to calculate the first term on the right hand side in Eqs. 5.9 (a) and 5.11(a) for the NEMD simulations with a finite condensation flux. From the remaining value we then determined the interface film resistivities $r_{q\mu}^{\mathrm{s,g}}$ and $r_{q\mu}^{\mathrm{s,l}}$. In figure 5.4 we plotted the resulting cross coefficients. It is clear from this figure that $r_{q\mu}^{\mathrm{s,g}} = r_{\mu q}^{\mathrm{s,g}}$ and $r_{q\mu}^{\mathrm{s,l}} = r_{\mu q}^{\mathrm{s,l}}$ within the accuracy of the calculations. As the cross coefficients were found independently, this is a convincing confirmation of the validity of Onsager's reciprocal relations. It also verifies that the new kinetic theory formula for $r_{qq}^{\mathrm{s,g}} = r_{qq}^{\mathrm{s,l}}$ is correct.

Using that $r_{\mu q}^{\mathrm{s,g}}$ and $r_{\mu q}^{\mathrm{s,l}}$, found from the NEMD simulations with a zero condensation flux, were also well predicted by kinetic theory we could similarly calculate $r_{\mu\mu}^{\mathrm{s,g}}$ and $r_{\mu\mu}^{\mathrm{s,l}}$ from the NEMD simulations with a finite condensation flux from Eqs. 5.9 (b) and 5.11(b). The resulting values were plotted in figure 5.5. Using the kinetic theory prediction for $r_{\mu\mu}^{\mathrm{s,g}}$ given in Eq. 5.15(c) we can then calculate the condensation coefficient. The resulting value σ_c is plotted in figure 5.6. It is found to increase approaching the triple point. The values reported by [9] are slightly larger. This is probably due to the fact that the new

expressions for the kinetic theory coefficients were then not yet available. The difference is not larger than the accuracy of the coefficients. The values of σ_c were smaller than unity as is required. They increase from a value of about 0.4 close to the critical point to a value of about 0.8 close to the triple point. Tsuruta et al. [91] followed individual particle paths to obtain this coefficient and found a very similar result close to the triple point.

Far from global equilibrium the system becomes nonlinear for a variety of reasons. To quote from the preface of the second edition of the monograph by de Groot and Mazur [1] systems described by nonequilibrium thermodynamics are nonlinear for reasons such as "(i) the presence of convection terms and of (ii) quadratic source terms in,e.g., the energy equation, (iii) the nonlinear character of the equations of state and (iv) the dependence of the phenomenological transport coefficients on the state variables". One possible origin for nonlinearity is excluded in this list and that is that the thermodynamic forces are nonlinearly related to their conjugate forces. In the system we consider that would imply, to be precise, that $\Delta(1/T)$ and $\Delta(\mu/T)$ are nonlinear functions of the total heat flux J_q and the mass flux J; see the entropy production given in Eq. 5.31 in the appendix. Even though we went to temperature gradients up to 5×10^9 K/m we did not need such nonlinear dependence on the fluxes.

5.6 Conclusions

Using NEMD simulations we have obtained the interface film resistivities for heat and mass transfer along the liquid-vapor coexistence curve for an argon like fluid using a Lennard-Jones spline potential. Our results confirm earlier results of [5, 6] that also when the system is not in equilibrium the surface tension is the same function of the surface temperature as in equilibrium. The surface is in other words in local equilibrium. We furthermore find that the interface film resistivities are functions of the surface tension or alternatively the surface temperature alone. This further confirms that the surface is a separate thermodynamic system with its own properties. We proposed new expressions for the interface film resistivities obtained using kinetic theory, which only depend on the temperature of the surface. We find that these new formulae from kinetic theory predict the results of the NEMD simulations well as long as one is not to close to the critical point. These results are similar to those obtained by [9] for the same system. We were able to independently calculate the cross coefficients. The Onsager reciprocal relations could then be checked and were found to be satisfied. This is the first time that such a result is obtained for a surface.

Table 5.2: **Simulation Conditions, in Reduced and Real Units**

Sim. no.	c^*	T_H^*	T_L^*	J^*	c ($\frac{\text{mol}}{\text{m}^3}$)	T_H (K)	T_L (K)	J ($\frac{\text{kmol}}{\text{m}^2\text{s}}$)
1	0.20	1.10	0.75	0.001	8302	136.5	93.0	6.67
2	0.20	1.10	0.70	0.001	8302	136.5	86.8	6.67
3	0.30	1.20	0.65	0.002	12453	148.9	80.6	13.33
4	0.30	1.20	0.65	0.003	12453	148.9	80.6	20.00
5	0.30	1.35	0.65	0.002	12453	167.5	80.6	13.33
6	0.30	1.50	0.65	0.003	12453	186.1	80.6	20.00
7	0.30	1.03	0.57	0.002	12453	127.8	70.7	13.33
8	0.30	1.10	0.63	0.002	12453	136.5	78.2	13.33
9	0.15	1.10	0.65	0.001	6226	136.5	80.6	6.67
10	0.15	1.15	0.65	0.002	6226	142.7	80.6	13.33
11	0.15	1.05	0.75	0.002	6226	130.3	93.0	13.33
12	0.30	1.30	0.70	0.002	12453	161.3	86.8	13.33
13	0.20	1.10	0.65	0.002	8302	136.5	80.6	13.33
14	0.30	1.30	0.60	0.001	12453	161.3	74.4	6.67
15	0.20	1.20	0.70	0.003	8302	148.9	86.8	20.00
16	0.30	1.25	0.60	0.003	12453	155.1	74.4	20.00
17	0.30	1.25	0.62	0.003	12453	155.1	76.9	20.00
18	0.20	1.13	0.72	0.001	8302	140.2	89.3	6.67
19	0.25	1.05	0.70	0.002	10378	130.3	86.8	13.33
20	0.25	1.25	0.72	0.002	10378	155.1	89.3	13.33
21	0.25	1.15	0.75	0.002	10378	142.7	93.0	13.33
22	0.25	1.06	0.70	0.002	10378	131.5	86.8	13.33
23	0.25	1.25	0.70	0.002	10378	155.1	86.8	13.33
24	0.25	1.30	0.68	0.002	10378	161.3	84.4	13.33
25	0.25	1.20	0.70	0.004	10378	148.9	86.8	26.66
26	0.30	1.28	0.62	0.003	12453	158.8	76.9	20.00
27	0.15	1.10	0.60	0	6226	136.5	74.4	0
28	0.20	1.10	0.60	0	8302	136.5	74.4	0
29	0.20	1.10	0.75	0	8302	136.5	93.0	0
30	0.20	1.05	0.70	0	8302	130.3	86.8	0
31	0.20	1.10	0.68	0	8302	136.5	84.4	0
32	0.20	1.15	0.70	0	8302	142.7	86.8	0
33	0.25	1.30	0.80	0	10378	161.3	99.2	0
34	0.30	1.10	0.68	0	12453	136.5	84.4	0
35	0.30	1.00	0.70	0	12453	124.1	86.8	0
36	0.30	1.40	0.70	0	12453	173.7	86.8	0
37	0.30	1.60	0.75	0	12453	198.5	93.0	0
38	0.13	1.20	0.60	0	5189	148.9	74.4	0
39	0.18	1.20	0.60	0	7264	148.9	74.4	0
40	0.23	1.20	0.60	0	9340	148.9	74.4	0
41	0.28	1.20	0.60	0	11415	148.9	74.4	0
42	0.18	1.25	0.60	0	7264	155.1	74.4	0
43	0.18	1.10	0.65	0	7264	136.5	80.6	0
44	0.23	1.10	0.65	0	9340	136.5	80.6	0
45	0.28	1.10	0.65	0	11415	136.5	80.6	0
46	0.18	1.20	0.70	0	7264	148.9	86.8	0
47	0.23	1.20	0.70	0	9340	148.9	86.8	0
48	0.28	1.20	0.70	0	11415	148.9	86.8	0

Table 5.3: **Fluxes and Forces from MD Simulations**

Sim. no.	$J_q'^g$ $(\frac{\mathrm{MJ}}{\mathrm{m^2 s}})$	$J_q'^l$ $(\frac{\mathrm{MJ}}{\mathrm{m^2 s}})$	J $(\frac{\mathrm{kmol}}{\mathrm{m^2 s}})$	X_q $(\frac{1}{\mathrm{kK}})$	X_μ^g $(\frac{\mathrm{J}}{\mathrm{molK}})$	X_μ^l $(\frac{\mathrm{J}}{\mathrm{molK}})$
1	15.06	38.91	5.87	0.955	0.85	-2.80
2	12.65	39.77	6.20	1.169	1.02	-4.12
3	23.28	80.05	12.27	1.771	2.20	-5.68
4	33.07	111.91	17.93	1.990	2.72	-5.62
5	30.46	87.96	12.33	2.208	2.64	-7.28
6	48.00	129.31	17.86	2.453	3.10	-7.19
7	8.57	74.56	12.66	2.728	4.42	-9.72
8	15.83	75.21	12.53	1.802	2.32	-6.15
9	9.64	40.63	6.33	1.668	1.56	-7.19
10	14.04	75.26	12.46	2.157	2.62	-8.79
11	12.73	58.77	11.47	1.041	1.31	-2.87
12	32.75	80.52	11.73	1.550	1.76	-4.16
13	13.10	72.21	12.40	1.781	2.30	-6.15
14	14.17	49.40	6.53	2.959	2.79	-13.47
15	22.21	97.88	17.60	1.868	2.40	-5.26
16	23.00	114.28	18.60	2.624	3.71	-8.69
17	25.64	114.20	18.40	2.460	3.40	-7.74
18	13.68	39.42	6.07	1.119	0.99	-3.78
19	14.37	65.03	11.87	1.211	1.44	-3.50
20	27.11	72.83	11.53	1.435	1.61	-3.78
21	21.16	59.15	11.00	1.053	1.22	-2.31
22	14.08	64.31	11.93	1.225	1.43	-3.54
23	24.48	75.27	11.87	1.708	1.84	-5.10
24	25.33	77.77	12.06	1.773	2.13	-5.35
25	26.43	118.19	22.73	1.761	0.78	-4.26
26	26.88	114.99	18.26	2.506	3.42	-7.91
27	5.11	5.11	0	1.298	0.33	-7.10
28	5.20	5.20	0	1.593	0.40	-7.66
29	12.49	12.49	0	0.809	0.47	-2.68
30	8.08	8.08	0	0.539	0.19	-2.11
31	8.92	8.92	0	0.591	0.31	-2.40
32	11.11	11.11	0	0.887	0.38	-3.63
33	27.02	27.02	0	0.838	0.81	-1.71
34	11.32	11.32	0	1.134	0.32	-4.92
35	9.44	9.44	0	0.646	0.32	-2.46
36	24.38	24.38	0	1.553	1.09	-5.75
37	50.32	50.32	0	1.415	1.53	-3.44
38	5.97	5.97	0	1.546	0.56	-7.25
39	6.45	6.45	0	1.605	0.53	-8.47
40	7.25	7.25	0	1.650	0.47	-8.85
41	7.92	7.92	0	1.879	0.82	-9.00
42	7.01	7.01	0	1.958	0.53	-9.31
43	6.94	6.94	0	0.882	0.18	-4.99
44	7.95	7.95	0	1.004	0.46	-4.49
45	8.15	8.15	0	1.000	0.50	-4.64
46	12.12	12.12	0	1.116	0.44	-4.97
47	13.06	13.06	0	0.834	0.49	-3.24
48	14.70	14.70	0	0.781	0.34	-3.04

Table 5.4: **Surface Extension, Surface Tension and Temperature near and on the Surface**

Sim. no.	Surface layers	$\gamma(10^{-3})$ (N/m)	T^l (K)	T^g (K)	T^s (K)
1	45-51	1.935	95.5	105.1	96.5
2	45-50	3.239	89.3	99.7	90.1
3	37-41	3.260	88.3	104.7	90.0
4	36-42	2.853	90.9	111.0	93.4
5	36-41	3.352	88.7	110.3	90.8
6	36-42	2.540	92.8	120.2	96.1
7	38-42	5.227	76.1	96.1	77.2
8	37-41	3.750	84.9	100.2	86.2
9	50-54	4.397	82.5	95.6	83.3
10	50-54	4.126	83.8	102.3	85.3
11	50-56	1.912	95.1	105.5	96.9
12	35-41	2.649	95.4	112.0	97.9
13	45-50	3.981	84.8	99.9	86.3
14	37-41	4.700	78.4	102.0	79.2
15	45-51	2.379	92.9	112.4	95.7
16	37-42	3.791	84.2	108.1	86.2
17	36-42	2.862	86.9	110.6	89.4
18	44-50	2.794	91.9	102.4	93.1
19	40-46	2.778	91.9	103.4	93.5
20	40-46	1.938	96.2	111.6	98.6
21	38-47	1.631	98.9	110.4	101.2
22	40-46	2.638	92.3	104.0	93.8
23	40-46	2.681	93.1	110.8	95.1
24	40-46	3.023	90.8	108.3	92.9
25	40-47	2.040	96.8	116.7	100.3
26	36-42	3.166	87.3	111.8	89.8
27	49-54	6.178	74.7	82.7	74.8
28	46-51	6.045	74.7	84.8	74.9
29	42-52	2.169	93.7	101.4	94.3
30	46-51	3.446	87.5	91.8	87.5
31	46-50	3.816	85.2	89.7	85.4
32	45-50	3.503	87.5	94.9	87.8
33	37-48	0.980	101.7	111.2	103.4
34	36-41	4.157	85.4	94.5	85.7
35	35-42	3.665	87.4	92.7	87.8
36	32-41	3.331	89.0	103.3	90.3
37	34-45	1.853	97.7	113.4	99.6
38	52-57	5.871	74.6	84.3	74.7
39	48-52	5.900	74.9	85.1	75.1
40	44-48	5.689	74.9	85.4	75.0
41	40-44	5.442	75.1	87.5	75.3
42	48-52	5.818	74.8	87.6	74.8
43	48-52	4.930	80.9	87.1	81.1
44	43-48	4.445	81.1	88.3	81.4
45	39-43	4.390	81.4	88.7	81.8
46	47-52	3.378	87.4	96.9	87.9
47	43-48	3.427	87.5	94.4	87.9
48	38-43	3.229	88.4	94.9	88.7

Table 5.5: **Concentrations near the Surface and Pressures**

Sim. no.	c^l ($\frac{\text{kmol}}{\text{m}^3}$)	c^g ($\frac{\text{kmol}}{\text{m}^3}$)	p (bar)	$p^\star(T^l)$ (bar)	$p^\star(T^g)$ (bar)
1	27.35	2.099	14.91	23.87	13.12
2	29.08	1.312	9.54	17.33	8.34
3	29.36	1.291	10.23	23.34	7.70
4	28.78	1.662	13.63	32.75	9.42
5	29.27	1.294	11.01	31.76	7.97
6	28.32	1.778	16.33	50.57	10.89
7	32.00	0.518	4.11	13.68	2.48
8	30.13	1.001	7.76	17.94	5.81
9	30.68	0.753	5.60	13.27	4.67
10	30.39	0.899	7.17	20.31	5.26
11	27.49	2.256	15.78	24.50	12.77
12	27.40	2.145	17.06	34.54	13.09
13	30.19	1.004	7.67	17.50	5.74
14	31.50	0.485	4.08	20.00	3.14
15	28.21	1.889	15.35	35.25	10.95
16	30.37	0.984	8.42	28.16	5.45
17	29.77	1.220	10.45	32.14	6.89
18	28.36	1.595	11.65	20.48	10.17
19	28.43	1.725	12.51	21.68	10.16
20	27.19	2.265	17.69	33.79	13.76
21	26.28	2.870	20.61	31.89	16.49
22	28.33	1.771	12.85	22.50	10.45
23	28.12	1.787	14.28	32.42	11.13
24	28.76	1.552	12.50	28.46	9.38
25	27.10	2.561	20.59	43.15	14.32
26	29.67	1.246	10.75	34.14	7.11
27	32.24	0.327	2.18	4.77	2.12
28	32.24	0.317	2.18	5.75	2.12
29	27.90	1.750	12.34	19.21	11.58
30	29.56	1.101	7.38	10.09	7.20
31	30.10	0.917	6.16	8.58	5.93
32	29.54	1.063	7.54	12.58	7.22
33	25.13	3.227	23.21	33.12	19.60
34	30.05	0.882	6.21	12.30	6.05
35	29.56	1.102	7.49	10.77	7.19
36	29.18	1.153	9.25	21.58	8.16
37	26.73	2.387	19.71	36.95	15.24
38	32.28	0.320	2.20	5.50	2.09
39	32.21	0.321	2.27	5.92	2.17
40	32.21	0.326	2.24	6.07	2.16
41	32.17	0.345	2.39	7.21	2.22
42	32.23	0.309	2.20	7.27	2.13
43	31.02	0.600	4.09	7.00	4.03
44	30.98	0.629	4.33	7.72	4.12
45	30.90	0.645	4.49	7.93	4.24
46	29.55	1.029	7.50	14.42	7.17
47	29.56	1.084	7.68	12.16	7.21
48	29.31	1.154	8.09	12.65	7.76

5.7 Appendix

When the excess entropy production is calculated for a stationary state one obtains

$$\sigma^{\rm s} = J_q \Delta\left(\frac{1}{T}\right) - J\Delta\frac{\mu}{T} \tag{5.31}$$

where $J_q = J_q'^{\rm g} + H^{\rm g}J = J_q'^{\rm l} + H^{\rm l}J$ is the total heat flux, which is independent of the position in a stationary state. Substituting $J_q = J_q'^{\rm g} + H^{\rm g}J$ one obtains

$$\begin{aligned}\sigma^{\rm s} &= J_q'^{\rm g}\Delta\left(\frac{1}{T}\right) - J\left(\Delta\frac{\mu}{T} - H^{\rm g}\Delta\left(\frac{1}{T}\right)\right)\\ &= J_q'^{\rm g}\Delta\left(\frac{1}{T}\right) - J\left[\frac{\mu^{\rm l}}{T^{\rm l}} - \frac{\mu^{\rm g}}{T^{\rm g}} - H^{\ {\rm g}}\left(\frac{1}{T^{\rm l}} - \frac{1}{T^{\rm g}}\right)\right]\end{aligned} \tag{5.32}$$

Next we use that

$$\frac{\mu^{\rm g}\left(T^{\rm l}\right)}{T^{\rm l}} = \frac{\mu^{\rm g}\left(T^{\rm g}\right)}{T^{\rm g}} + H^{\rm g}\left(T^{\rm g}\right)\left(\frac{1}{T^{\rm l}} - \frac{1}{T^{\rm g}}\right) - \frac{1}{2}c_p^{\rm g}\left(T^{\rm g}\right)\left(1 - \frac{T^{\rm g}}{T^{\rm l}}\right)^2 \tag{5.33}$$

to second order in the temperature difference. It follows that

$$X_\mu^{\rm g} = -\frac{\mu^{\rm l}(T^{\rm l}) - \mu^{\rm g}(T^{\rm l})}{T^{\rm l}} + \frac{1}{2}c_p^{\rm g}\left(T^{\rm g}\right)\left(1 - \frac{T^{\rm g}}{T^{\rm l}}\right)^2 \tag{5.34}$$

to second order in the temperature difference. For $X_\mu^{\rm l}$ we similarly obtain

$$X_\mu^{\rm l} = -\frac{\mu^{\rm l}(T^{\rm g}) - \mu^{\rm g}(T^{\rm g})}{T^{\rm g}} + \frac{1}{2}c_p^{\rm l}\left(T^{\rm l}\right)\left(1 - \frac{T^{\rm l}}{T^{\rm g}}\right)^2 \tag{5.35}$$

Due to the extremely large temperature gradients used we find that the second order term may contribute up to 25% of the value of the chemical forces.

In order to calculate the first order contribution to the chemical forces we use for the gas

$$\mu^{\rm g}(T_1, p) = \mu^0(T_1) + RT_1 \ln\frac{p\phi(T_1, p)}{p^0} \tag{5.36}$$

where μ^0 and p^0 are standard values, which are chosen such that $\phi(T_1, p) \to 1$ in the ideal gas limit. Eq. 5.36) may be considered as a definition of $\phi(T_1, p)$.

For the liquid at temperature T_2 we use a vapor in coexistence with the liquid at this temperature and write

$$\mu^{\rm l}(T_2, p^\star(T_2)) = \mu^{\rm g}(T_2, p^\star(T_2)) = \mu^0(T_2) + RT_2 \ln\frac{p^\star(T_2)\phi^\star(T_2)}{p^0} \tag{5.37}$$

where $\phi^\star(T_2) \equiv \phi(T_2, p^\star(T_2))$. For the chemical force $X_\mu^{\rm g}$ we may then write to first order

$$\begin{aligned}X_\mu^{\rm g} &= -\frac{\mu^{\rm l}(T^{\rm l}, p) - \mu^{\rm g}(T^{\rm l}, p)}{T^{\rm l}} = -\frac{\mu^{\rm l}(T^{\rm l}, p^\star(T^{\rm l})) - \mu^{\rm g}(T^{\rm l}, p)}{T^{\rm l}}\\ &+ \frac{\mu^{\rm l}(T^{\rm l}, p^\star(T^{\rm l})) - \mu^{\rm l}(T^{\rm l}, p)}{T^{\rm l}}\\ &\quad + R\ln\frac{p\phi(T^{\rm l}, p)}{p^\star(T^{\rm l})\phi^\star(T^{\rm l})} + \frac{\mu^{\rm l}(T^{\rm l}, p^\star(T^{\rm l})) - \mu^{\rm l}(T^{\rm l}, p)}{T^{\rm l}}\end{aligned} \tag{5.38}$$

For the second term on the right hand side we use

$$\mu^{\rm l}(T^{\rm l},p^\star(T^{\rm l}))-\mu^{\rm l}(T^{\rm l},p)=\int_p^{p^\star(T^{\rm l})}v^{\rm l}(T^{\rm l},p')dp' \tag{5.39}$$

Using that the molar volume of the liquid does not depend very much on the pressure one obtains

$$\mu^{\rm l}(T^{\rm l},p^\star(T^{\rm l}))-\mu^{\rm l}(T^{\rm l},p)=v^{\rm l\star}(T^{\rm l})\left(p^\star(T^{\rm l})-p\right) \tag{5.40}$$

where $v^{\rm l\star}(T^{\rm l})=v^{\rm l}(T^{\rm l},p^\star(T^{\rm l}))$. Substituting Eqs. 5.38 and 5.40 into Eq. 5.34 we obtain to second order

$$X_\mu^{\rm g}=R\ln\frac{p\phi(T^{\rm l},p)}{p^\star(T^{\rm l})\phi^\star}(T^{\rm l})+\frac{v^{\rm l\star}(T^{\rm l})\left(p^\star(T^{\rm l})-p\right)}{T^{\rm l}}+\frac{1}{2}c_p^{\rm g}\left(T^{\rm g}\right)\left(1-\frac{T^{\rm g}}{T^{\rm l}}\right)^2 \tag{5.41}$$

For the chemical force on the liquid side we similarly obtain

$$X_\mu^{\rm l}=R\ln\frac{p\phi(T^{\rm g},p)}{p^\star(T^{\rm g})\phi^\star(T^{\rm g})}+\frac{v^{\rm l\star}(T^{\rm g})\left(p^\star(T^{\rm g})-p\right)}{T^{\rm g}}+\frac{1}{2}c_p^{\rm l}\left(T^{\rm l}\right)\left(1-\frac{T^{\rm l}}{T^{\rm g}}\right)^2 \tag{5.42}$$

The last two contributions in Eqs. 5.41 and 5.42 were always found to have an opposite sign. They therefore partially compensated each other. Their contribution to the final value was rather substantial in many cases.

In order to calculate $\phi(T,p)$ we use that the SRK equation of state is a good approximation for the gas phase. We will approximate $\phi(T,v)$ by $\phi_{SRK}(T,v)$, where p,v and T are related by the SRK equation of state, Eq. 5.18. We use

$$\begin{aligned}\mu(T,v_2)-\mu(T,v_1) &= \int_{p_1}^{p_2}vdp=\int_{(pv)_1}^{(pv)_2}dpv-\int_{v_1}^{v_2}pdv\\ &= p(T,v_2)v_2-p(T,v_1)v_1-\int_{v_1}^{v_2}pdv\end{aligned} \tag{5.43}$$

Using the SRK equation of state we have

$$\int_{v_1}^{v_2}pdv=\int_{v_1}^{v_2}\left(\frac{RT}{v-b}-\frac{a}{v(v+b)}\right)dv=RT\ln\frac{v_2-b}{v_1-b}-\frac{a}{b}\ln\frac{v_2\left(v_1+b\right)}{v_1\left(v_2+b\right)} \tag{5.44}$$

Substitution into Eq. 5.43 gives

$$\begin{aligned}\mu(T,v_2)-\mu(T,v_1) &= p(T,v_2)v_2-p(T,v_1)v_1-RT\ln\frac{v_2-b}{v_1-b}+\frac{a}{b}\ln\frac{v_2\left(v_1+b\right)}{v_1\left(v_2+b\right)}\\ &= RT\ln\frac{p(T,v_2)}{p(T,v_1)}+RT\ln\frac{\phi(T,v_2)}{\phi(T,v_1)}\end{aligned} \tag{5.45}$$

In order to find $\phi(T,v_1)$ we now take $v_2\gg b$ (the ideal gas limit) and use the Eq. 5.18, which gives an expression in which v_2 drops out. Replacing v_1 by v, one finds:

$$RT\ln\phi(T,v)=RT\left[\frac{b}{v-b}+\ln\frac{v}{v-b}-\ln\frac{vp(T,v)}{RT}\right]-\frac{a}{v+b}+\frac{a}{b}\ln\frac{v}{v+b} \tag{5.46}$$

Chapter 6

Conclusion

In this thesis, the coupled transport phenomena of heat and mass were investigated for a chemical reaction and a liquid-vapor interface where large temperature gradients were applied. Non-equilibrium molecular dynamics (NEMD) simulations have been used to measure thermodynamic and transport properties of the modeling systems at stationary non-equilibrium states. An overview and basic concepts of the modeling systems and non-equilibrium thermodynamics (NET) were given in the first Chapter. Some molecular simulation techniques, and in particular, boundary-driven NEMD, were described next (Chapter 2). In Chapters 3, 4 and 5 consistent and systematic studies of the two systems were presented. The purpose of the thesis for a better understanding of the transport problems in the studied systems has been achieved.

In Chapters 3 and 4, we examined heat and mass transfer in a chemical reaction, $2F \rightleftarrows F_2$. In order to accomplish such a study, our first computational effort has been made to build an efficient NEMD program with a mechanical reaction model given by Stillinger and Weber [52]. In this model, not only 2, but also 3-body potentials are included to effectively represent the main thermodynamic features of the chemical reaction, namely its microscopic reversibility. Because of the impact of the 2- and 3-body potentials on the calculations of forces and fluxes, we created a new MD program, namely NEIGHBOUR3, to save the CPU time. The results from our NEMD simulations reproduced some of the equilibrium results obtained by others [52], indicating that our simulations are trustable. By NEMD simulations, various temperature gradients up to ∇T=1.1×10^{12} K/m were investigated. Thermal diffusion and interdiffusion of components were set up in the temperature gradient. We observed a flux of fluorine atoms to the cold side, while fluorine molecules were transported to the hot side. There was no net mass flux through the system in the stationary state, which was characterized by nonzero average velocities of the components. We have shown how the Soret equilibrium was defined for the stationary state. Definitions of '*Local*' equilibrium and specifically '*local chemical*' equilibrium have been discussed in detail. The results from NEMD simulations showed that the system was nearly Maxwellian in its component velocity distributions. In order to have local equilibrium, we see this criterion is central. We also observed that the small shifts in the Maxwellians were directly proportional to the temperature gradient. Furthermore, we

found that the unidirectional rates of the reaction were nearly the same in the center of the box, meaning that the distance to chemical equilibrium was small there. A net reaction rate was observed much smaller than the forward and the backward reaction rates. For this study, we concluded that the system was in local thermodynamic equilibrium; and that it was also close to chemical equilibrium in large temperature gradients, typically 10_{11} K/m. Statistical and thermodynamic evidence was thus presented that the transport processes are governed by an entropy production which is bilinear in the fluxes and forces of the system.

With a sound basis for the relevant transport equations, in Chapter 4, we derived transport coefficients for the chemical reaction in large temperature gradients. From the NEMD results, the non-equilibrium reacting system was seen as limited by a thermal diffusion and its dynamic structure was maintained by energy supply from the outside. When exposed to a temperature gradient, the system responded to the given boundary conditions by seeking a dynamic state (dissipative structure) with a low entropy production, most probably as low as possible. We stated that the distribution of components is a consequence of this rather than of a shift in the chemical equilibrium according to Chatelier's principle. When the system was close to, but not at chemical equilibrium, we found an analytical solution to the flux equations given by the entropy production. Using this analysis, we determined resistivity coefficients (R_{ij} and r_{ij}), conductivity coefficients (L_{ij} and l_{ij}) and some common transport properties (λ_J, λ_G, D, q^*, and $-\Delta_r H$), in the chemical reaction. The thermal conductivities λ_J and λ_G were found and increased with temperature. From kinetic theory, we obtained a value in the same order of magnitude as in λ_J(absence of chemical reaction). We also pointed out that λ_G was up to 40% larger than λ_J. This most interesting feature leads us to clearly see that a reacting system can conduct better than a non-reacting system. For the heat of transfer, we found this transport property is equal to the negative enthalpy of reaction, $-\Delta_r H$, in the limiting case of *local chemical equilibrium*. Away from chemical equilibrium, the heat of transfer was computed not only by the thermodynamic contributions, but also by the contributions from the transport coefficients which can be related to the thermal diffusion. For the chemical reaction, we found the heat of transfers were much larger (varying between 120 and 200 kJ/mol), compared to the ones typical for non-reacting binary mixtures. Our results indicate that the Dufour and Soret effects are non-negligible in the reacting system. Onsager coefficients were discussed as their important role on systematically defining transport coefficients of reacting mixtures. The values of the transport coefficients derived from this Chapter may be useful for improved thermodynamic modeling of chemical reactions.

In Chapter 5, we studied simultaneous transfer of heat and mass across a surface. NEMD simulations with a Lennard-Jones spline potential have been performed to model a liquid-vapor phase transition in a one-component argon like fluid, exposed to a temperature gradient or/and a concentration gradient. We first established the surface boundaries, the proper equation of state, and the equilibrium properties of the surface. A comparison between non-equilibrium and equilibrium results showed that the surface was in local equilibrium also under temperature gradients of the order of 10^8 K/m. Our results confirmed earlier results of Røsjord et al. that also when the system is not in global equilibrium the surface tension is the same function of the surface temperature as in equilibrium [5]. Next, in the description of the transfer coefficients, we used non-equilibrium thermodynamics

theory as developed by Kjelstrup and Bedeaux for the surface [3]. This work aimed to give information about the coefficient that describes coupling of heat and mass and add a proof on the validity of ORR at surfaces. The coupling coefficient influences the value of the heat fluxes into the homogeneous phases. It is important to know its value and understand its origin. With available NEMD results, all four interfacial film transfer coefficients were independently determined along the whole liquid-vapor coexistence curve for the first time. We derived two sets of the interface film resistivities by using the measurable heat flux on the vapor side as well as on the liquid side. Moreover, we found that these coefficients are functions of the surface tension or alternatively the surface temperature alone. Large resistivities of the surface to heat and mass transfer were reported. We gave evidence in the important coupling of heat and mass at the surface. Most importantly, we found that the coupling coefficients are within the accuracy of the calculation equal. This is the first verification of the validity of the Onsager relations for transport through a surface using molecular dynamics. Furthermore, we proposed new expressions for the interface film resistivities obtained using kinetic theory, which only depend on the surface temperature. We found that these new formulae from kinetic theory predict the results of the NEMD simulations well as long as one is not to close to the critical point.

According to the purpose of this thesis, we have reached all sub goals. We succeeded in developing new NEMD algorithms with the combined 2- and 3-body potentials to model the chemical reaction (Chapter 3). With suitable NEMD techniques we were able to generate large temperature gradients, as high as 6.6×10^{11} K/m (Chapter 3), and use large mass fluxes about 26.7 kmol/m^{2}s (Chapter 5). We have verified the assumption of local equilibrium in both the chemical reacting system and the surface where heat and mass were transported (Chps. 3 and 5). Transport coefficients of the irreversible systems were derived in the framework offered by non-equilibrium thermodynamics (Chps. 4 and 5). A dissipative structure of the chemical reaction was displayed and transport properties of the reacting mixture were derived by assuming Onsager relations (Chapter 4). It was also tested that transport properties did not depend on the values of the flux, i.e. that the force-flux relation was linear (Chapter 4). Onsager's reciprocal relations were validated at the surface for the first time (Chapter 5). With the best knowledge from this thesis, we can further study another chemical reaction with the same type, $2H \rightleftarrows H_2$, in a direction of general interest and investigate particular wall effects on the chemical reaction. Moreover, we are now able to study coupled transport of heat and mass with a chemical reaction at a surface.

Bibliography

[1] S.R. de Groot and P. Mazur. *Non-Equilibrium Thermodynamics*. Dover, London, 1984.

[2] K. S. Førland, T. Førland, and S. Kjelstrup. *Irreversible Thermodynamics. Theory and Application*. Tapir, Trondheim, Norway, 3rd. edition, 2001.

[3] S. Kjelstrup and D. Bedeaux. *Non-Equlibrium Thermodynamics of Heterogeneous Systems*. World Scientific Publishing Co. Pte. Ltd., 2008.

[4] B. Hafskjold and S.K. Ratkje. Criteria for local equilibrium in a system with transport of heat and mass. *J. Stat. Phys.*, 78:463–494, 1995.

[5] A. Røsjorde, D. W. Fossmo, S. Kjelstrup, D. Bedeaux, and B. Hafskjold. Nonequilibrium molecular dynamics simulations of steady-state heat and mass transport in condensation: I. Local equilibrium. *J. Colloid Interf. Sci.*, 232:178–185, 2000.

[6] J.M. Simon, S. Kjelstrup, D. Bedeaux, and B. Hafskjold. Thermal flux through a surface of n-octane. a non-equilibrium molecular dynamics study. *J. Phys. Chem. B*, 108(22):7186–7195, 2004.

[7] T.M. Reed and K.E. Gubbins. *Applied Statistical Mechanics. Thermodynamic and transport properties of fluids*. Kingsport Press, Inc., 1973.

[8] S. Kjelstrup, T. Tsuruta, and D Bedeaux. The inverted temperature profile across a vapor/liquid surface analysed by molecular dynamics computer simulations. *J. Colloid Interface Sci.*, 256:451–461, 2002.

[9] A. Røsjorde, S. Kjelstrup, D. Bedeaux, and B. Hafskjold. Nonequilibrium molecular dynamics simulations of steady-state heat and mass transport in condensation: II. Transfer coefficients. *J. Colloid Interf. Sci.*, 240:355–364, 2001.

[10] R. Krishna and J.A. Wesselingh. The maxwell-stefan approach to mass transfer. *Chem. Eng. Sci.*, 52:861–911, 1997.

[11] G. Fang and C.A. Ward. Temperature measured close to the interface of an evaporating liquid. *Phys. Z.*, 59:417–428, 1999.

[12] G. Fang and C.A. Ward. Examination of the statistical rate theory expression for liquid evaporation rates. *Phys. Z.*, 59:441–453, 1999.

[13] R.A. James and L.F. Phillips. Onsager heat of transport for water vapour at the surface of sulfuric acid. *Chem. Phys. Lett.*, 407:358–361, 2005.

[14] E. Johannessen and D. Bedeaux. The nonequilibrium van der waals square gradient model. (iii). heat and mass transfer coefficients. *Physica A*, 336:252–270, 2004.

[15] L. Onsager. Reciprocal relations in irreversible processes. ii. *Phys. Rev.*, 38(12):2265–2279, 1931.

[16] D. Bedeaux, A.M. Albano, and P. Mazur. Boundary conditions and nonequilibrium thermodynamics. *Physica A*, 82:438–462, 1976.

[17] D. Bedeaux. Non-equilibrium thermodynamics and statistical physics of surfaces. *Adv. Chem. Phys.*, 64:47–109, 1986.

[18] A.M. Albano and D. Bedeaux. Non-equilibrium electro-thermodynamics of polarizable multicomponent fluids with an interface. *Physica A*, 147:407–435, 1987.

[19] N. Metropolis., A.W. Rosenbluth, M.N. Rosenbluth, A.H. Teller, and E. Teller. Equation of state calculations by fast computing machines. *J. Chem. Phys.*, 21:1087–1092, 1953.

[20] D. Frenkel and B. Smit. *Understanding Molecular Simulations: from Algorithms to Applications.* Academic Press, San Diego, 2002.

[21] C.H. Turnera, J.K. Brennanb, M. Lisal, W.R. Smithe, J.K. Johnsonf, and K.E. Gubbins. Simulation of chemical reaction equilibria by the reaction ensemble monte carlo method: a review. *Molecular Simulation*, 34(2):119–146, 2008.

[22] J.K. Johnson, A.Z. Panagiotopoulos, and K.E. Gubbins. Reactive canonical monte carlo: a new simulation technique for reacting or associating fluids. *Mol. Phys.*, 81:717, 1994.

[23] W.R. Smith and B. Triska. The reaction ensemble method for the computer simulation of chemical and phase equilibria. i. theory and basic examples. *J. Chem. Phys.*, 100:3019, 1994.

[24] A.Z. Panagiotopoulos. Direct determination of phase coexistence properties of fluids by monte carlo simulation in a new ensemble. *Mol. Phys.*, 61:813, 1987.

[25] A.Z. Panagiotopoulos, N. Quirke, M. Stapleton, and D.J. Tildesley. Phase-equilibria by simulation in the gibbs ensemble - alternative derivation, generalization and application to mixture and membrane equilibria. *Mol. Phys.*, 63(4):527–545, 1988.

[26] B.J. Alder and T.E. Wainwright. Phase transition for a hard sphear system. *J. Chem. Phys.*, 27:1208–1209, 1957.

[27] B.J. Alder and T.E. Wainwright. Studies in moleclar dynamics. i. general method. *J. Chem. Phys.*, 31:459–466, 1959.

[28] A. Rahman. Correlations in the motion of atoms in liquid argon. *Phys. Rev.*, 136(2A):405–411, 1964.

[29] A. Rahman. Liquid structure and self-diffusion. *J. Chem. Phys.*, 45:258–263, 1966.

[30] D.C. Rapaport. *The Art of Molecular Dynamics.* Cambridge: Cambridge University Press, 1995.

[31] R. Kubo. Statistical-mechanical theory of irreversible processes. i. general theory and simple applications to magnetic and conduction problems. *J. Phys. Soc. Japan*, 12(6):570–586, 1957.

[32] B. Hafskjold. *Computer Simulations of Thermal Diffusion in Binary Mixtures*, chapter Chap. 1, in Concepts, Theory and Computer Simulations, Lecture Notes in Physics, pages 3–23. Springer-Verlag Berline Heidelberg, 2002.

[33] J.K Brennan, M. Lisal, K.E. Gubbins, and B.M.Rice. Reaction ensemble molecular dynamics: direct simulation of the dynamic equilibrium properties of chemically reacting mixtures. *Phys. Rev. E*, 70, 2004.

[34] M. Lisal, J.K. Brennan, W.R. Smith, and F.R. Siperstein. Dual control cell reaction ensemble molecular dynamics: a method for simulations of reactions and adsorption in porous materials. *J. Chem. Phys.*, 121(10):4901–4912, 2004.

[35] B. Hafskjold, T. Ikeshoji, and S.K. Ratkje. On the molecular mechanism of thermal diffusion in liquids. *Molecular Physics*, 80(6):1389–1412, 1993.

[36] W.T. Ashurst and W.G. Hoover. Dense-fluid shear viscosity via nonequilibrium molecular dynamics. *Phys. Rev. A*, 11:658–678, 1975.

[37] A. Tenenbaum, G. Ciccotti, and R. Gallico. Stationary nonequilibrium states by molecular dynamics. fourier's law. *Phys. Rev. A*, 25:2778–2787, 1982.

[38] B. Hafskjold and T. Ikeshoji. Non equilibrium molecular dynamics simulation of coupled heat- and mass transport across a liquid-vapor interface. *Mol. Sim.*, 16:139–150, 1996.

[39] T. Ikeshoji and B. Hafskjold. Non-equilibrium molecular dynamics calculation of heat conduction in liquid and through liquid-gas interface. *Mol. Phys.*, 81:251–261, 1994.

[40] A. Baranyai. Heat flow studies for large temperature gradients by molecular dynamics simulation. *Phys. Rev. E*, 54:6911–6917, 1996.

[41] F. Müller Plathe. A simple nonequilibrium molecular dynamics method for calculating the thermal conductivity. *J. Chem. Phys.*, 106:6082–6086, 1997.

[42] F. Müller Plathe and D. Reith. Cause and effect reversed in non-equilibrium molecular dynamics: an easy route to transport coefficients. *Comp. Theor. Polymer Sci.*, 9:203–209, 1999.

[43] J.M. Simon, D.K. Dysthe, A.H. Fuchs, and B. Rousseau. Thermal diffusion in alkane binary mixtures. *Fluid Phase Equilibria*, 150-151:151–159, 1998.

[44] J. Xu, S. Kjelstrup, and D. Bedeaux. Molecular dynamics simulations of a chemical reaction; conditions for local equilibrium in a temperature gradient. *Phys. Chem. Chem. Phys.*, 8:2017–2027, 2006.

[45] J. Xu, S. Kjelstrup, D. Bedeaux, and J.M. Simon. Transport properties of $2F \rightleftarrows F_2$ in a temperature gradient as studied by molecular dynamics simulations. *Phys. Chem. Chem. Phys.*, 9:1–13, 2007.

[46] I. Inzoli, J.M. Simon, S. Kjelstrup, and D. Bedeaux. Thermal effects during the adsorption of n-butane on a silicate-1 membrane: a non-equilibrium molecular dynamics study. *J Colloid Interface Sci*, 313:1–11, 2007.

[47] F. Goujon, P. Malfrey J.M. Simon, A. Boutin, B. Rousseau, and A.H. Fuchs. Monte carlo versus molecular dynamics simulations in heterogeneous systems: an application to the n-pentane liquid-vapor interface. *J Chem Phys*, 121:12559–12571, 2004.

[48] J. Ge, S. Kjelstrup, D. Bedeaux, J.M. Simon, and B. Rousseau. B. rousseau. transfer coefficients for evaporation of a system with a lennard-jones long-rane spline potential. *Phys. Rev. E.*, 75:061604, 2007.

[49] F.H. Stillinger and T.A. Weber. Computer simulation of local order in condensed phases of silicon. *Phys. Rev. B*, 31(8):5262–5271, 1985.

[50] F.H. Stillinger, T.A. Weber, and R.A. Laviolette. Chemical reactions in liquids: Molecular dynamics simulation for sulfur. *J. Chem. Phys.*, 85:6460–6469, 1986.

[51] F.H. Stillinger and T.A. Weber. Molecular dynamics study of chemical reactivity in liquid sulfur. *J. Phys. Chem.*, 91:4899–4907, 1987.

[52] F.H. Stillinger and T.A. Weber. Molecular dynamics simulation for chemically reactive substances. fluorine. *J. Chem. Phys.*, 88:5123–5133, 1988.

[53] F.H. Stillinger and T.A. Weber. Fluorination of the dimerized si(100) surface studied by molecular dynamics simulation. *Phys. Rev. Lett.*, 62:2144–2147, 1989.

[54] F.H. Stillinger, H. Sakai, and S. Torquato. Statistical mechanical models with effective potentials: Definitions, applications, and thermodynamic consequences. *J. Chem. Phys.*, 117:288–296, 2002.

[55] H.C. Andersen. Molecular dynamics simulations at constant pressure and/or temperature. *J. Chem. Phys.*, 72:2384–2393, 1980.

[56] D.J. Evans and G.P. Morriss. *Statistical Mechanics of Nonequilibrium Liquids.*, chapter Chap. 6. Academic Press, London, 1990.

[57] S. Nosé. A molecular dynamics method for simulations in the canonical ensemble. *Mplec. Phys.*, 52:255–268, 1984.

[58] L.V. Woodcock. Isothermal molecular dynamics calculations for liquid salts. *Chem. Phys. Lett.*, 10:257–261, 1971.

[59] J. Warnatz, U. Maas, and R.W. Dibble. *Combustion: physical and chemical fundamentals, modeling and simulation, experiments.* Springer, 3 ed. edition, 2001.

[60] J. Xu, S. Kjelstrup, D. Bedeaux, A. Røsjorde, and L. Rekvig. Verification of onsager's reciprocal relations for evaporation and condensation using non-equilibrium molecular dynamics. *J. Colloid. Interface Sci.*, 299:452–463, 2006.

[61] J. Ross and P. Mazur. Some deductions from a formal statistical mechanical theory of chemical kinetics. *J. Chem. Phys.*, 35(1):19–28, 1961.

[62] M.V. Bobetic and J.A. Barker. Lattice dynamics with three-body forces: Argon. *Phys. Rev. B*, 2:4169, 1970.

[63] J.A. Barker, R.A. Fisher, and R.O. Watts. Liquid argon: Monte carlo and molecular dynamics calculations. *Mol. Phys.*, 21:657–673, 1971.

[64] J.A. Barker and M.L. Monte carlo calculations for solid and liquid argon. *Phys. Rev. B*, 7:4707–4712, 1973.

[65] D. Bedeaux and S. Kjelstrup. Heat, mass and charge transport, and chemical reactions at surfaces. *Int. J. of Thermodynamics*, 8:25–41, 2005.

[66] J.H. Irving and J.G. Kirkwood. The statistical mechanical theory of transport processes. IV. The equations of hydrodynamics. *J. Chem. Phys.*, 18:817–829, 1950.

[67] J. Kincaid, X. Li, B. Hafskjold, and T. Ikeshoji. *Fluid Phase equilibria*, 76:113, 1992.

[68] D. K. Dysthe, A. H. Fuchs, and B. Rousseau Durandeau. Fluid transport properties by equilibrium molecular dynamics. ii. multicomponent systems. *J. Chem. Phys.*, 110:4060–4067, 1999.

[69] G. Scheidler, W. Kob, A. Latz, J. Horbach, and K. Binder. Stationary nonequilibrium states by molecular dynamics. fourier's law. *Physical Review B*, 267:104204, 2001.

[70] A. Polian, D. Vo-Tanh, and P. Richter. Elastic properties of α-so$_2$ up to 2300 k from brillouin scattering measurements. *Europhys. Lett.*, 57:375–381, 2002.

[71] I. Prigogine. *Introduction to nonequilibrium thermodynamics.* Wiley, New York, 1962.

[72] F. Bresme. Equilibrium and nonequilibrium molecular-dynamics simulations of the central force model of water. *J. Chem. Phys.*, 115:7564–7574, 2001.

[73] J. Xu, S. Kjelstrup, D. Bedeaux, and J.M. Simon. The heat of transfer in a chemical reaction at equilibrium. *J. Non-Equilibrium Thermodyn.*, 32:1–9, 2007.

[74] R. Taylor and R. Krishna. *Multicomponent Mass Transfer.* Wiley, New York, 1993.

[75] Y. Demirel. Non-isothermal reaction diffusion systems with thermodynamically coupled heat and mass transfer. *Chem. Eng. Sci.*, 61:3379–3385, 2006.

[76] F. Duan, V.K. Badam, F. Durst, and C. Ward. Thermocapillary transport of energy during water evaporation. *Phys. Rev. E*, 72:056303, 2005.

[77] M. Bond and H. Struchtrup. Mean evaporation and condensation coefficients based on energy dependent condensation probability. *Phys. Rev. E*, 70:061605, 2004.

[78] T. Tsuruta, H. Tanaka, and T. Masuoka. Condensation/evaporation coefficient and velocity distribution at liquid-vapor interface. *Int. J. Heat Mass Transfer*, 42:4207–4116, 1999.

[79] T. Tsuruta and G. Nagayama. Dsmc analysis of interface mass transfer in evaporation/condensation based on molecular dynamics study. *Therm. Sci. Eng.*, 10:9–15, 2002.

[80] G. Nagayama and T. Tsuruta. A microscopic formulation of condensation coefficient and interface transport phenomena. *J. Chem. Phys.*, 118:1392–1399, 2003.

[81] Y.P. Pao. Applications of kinetic theory to the problem of evaporation and condensation. *Fluids*, 14:306–312, 1971.

[82] Y.P. Pao. Temperature and density jumps in the kinetic theory of. gases and vapors. *Fluids*, 14:1340–1346, 1971.

[83] J.W. Cipolla Jr., H. Lang, and S.K. Loyalka. A variational calculation of temperature and pressure jumps during evaporation and condensation using kinetic theory. *J. Chem. Phys.*, 61:69, 1974.

[84] D. Bedeaux and L.F.J. Hermans. Slow evaporation and condensation. *Physica A*, 169:263–280, 1990.

[85] T. Ytrehus and Multiphase. Molecular flow effects in evaporation and condensation at interfaces. *Multiphase Sci. Technol.*, 9:205–227, 1997.

[86] D. Jou, J. Casas-Vázquez, and G. Lebon. *Extended Irreversible Thermodynamics*. Springer, Berlin, 1996.

[87] D. Bedeaux and S. Kjelstrup. Transfer coefficients for evaporation. *Physica A*, 270:413–426, 1999.

[88] D. Bedeaux and S. Kjelstrup. Irreversible thermodynamics - a tool to describe phase transitions far from global equilibrium. *Chem. Eng. Sci.*, 59:109–118, 2004.

[89] J.W. Gibbs. *The Scientific Papers of J.W. Gibbs*. Dover, Inc. New York, 1961.

[90] M.P. Allen and D.J. Tildesley. *Computer Simulations of Liquids*. Clarendon Press, Oxford, 1987.

[91] T. Tsuruta and G. Nagayama. In Tsing Hua Univ., editor, *Proc. 11th Int. Symp. Transport Phenom.*, pages 527–532. Hsinchu, Taiwan, 1998.

Appendix A

2- and 3-body potential implementation in NEMD for fluorine reaction.

According to the purposes of the thesis, we shall establish NEMD procedures for the chemical reaction, $F \rightleftarrows F_2$. In this appendix, we first summarize expressions of the 2- and 3-body potential that we used in NEMD for the fluorine reaction. We then show how to implement the 2- and 3-body potential (Weber and Stillinger potential) in our NEMD programs. Finally, we simply illustrate our algorithms using pseudo codes for the two and three body force routine.

A.1 The 2- and 3-body potential

Stillinger and Weber gave a general expression of the potential surface Φ for the type of fluorine reaction as a linear combination of two and three-atom interactions:

$$\Phi(\mathbf{r}_1, ..., \mathbf{r}_N) = \sum_{\text{pairs } i,j} u_2(r_{ij}) + \sum_{\text{triplets } i,j,k} u_3(r_{ij}, r_{ik}, r_{jk}). \tag{A.1}$$

Here the two-atom potential u_2 is a function of the atom-atom distance ($r_{ij} \equiv |\mathbf{r}_i - \mathbf{r}_j|$) with constant $A = 6.052463017$ and the first cut-off distance $r_{c1} = 3.6\sigma$,

$$u_2(r_{ij}) = \begin{cases} A\epsilon \left[(\sigma/r_{ij})^8 - (\sigma/r_{ij})^4\right] \exp\left[\sigma/(r_{ij} - r_{c1})\right] & , \ 0 < r_{ij} < r_{c1} \\ 0 & , \ r_{ij} \geq r_{c1} \end{cases} \tag{A.2}$$

The three-atom potential u_3 determined by three-atom distances r_{ij}, r_{ik} and r_{jk} is given as the sum of three $h-$functions,

$$u_3(r_{ij}, r_{ik}, r_{jk}) = h_i + h_j + h_k \tag{A.3}$$

The general expression for the $h-$function is:

$$h(a,b,\cos\theta) = \begin{cases} 8.4\varepsilon\left(\frac{\sigma^2}{ab}\right)^4 \exp\left[\left(\frac{\sigma}{a-r_{c1}}\right)+\left(\frac{\sigma}{b-r_{c1}}\right)\right] & \\ \quad +(50-25\cos\theta^2)\exp\left[3\left(\frac{\sigma}{a-r_{c2}}\right)+3\left(\frac{\sigma}{b-r_{c2}}\right)\right] & , \ 0<a,b<r_{c2} \\ 8.4\varepsilon\left(\frac{\sigma^2}{ab}\right)^4 \exp\left[\left(\frac{\sigma}{a-r_{c1}}\right)+\left(\frac{\sigma}{b-r_{c1}}\right)\right] & , \text{ either } a \text{ or } b \text{ exceeds } r_{c2} \\ 0 & , \text{ either } a \text{ or } b \text{ exceeds } r_{c1} \end{cases} \tag{A.4}$$

, where a and b are adjacent sides of the angle θ. In the right side of the Eq. A.4, the first expression is called as two terms $h-$function and the second as one term $h-$function.

A.2 2-body and 3-body contributions

A.2.1 2-body contributions

Expressing the 2-body force (due to atom j) on atom i in the x direction

$$\begin{aligned} f2_{xi} &= -\frac{du2}{dx_i} \\ &= -\frac{\partial u2}{\partial r_{ij}}\frac{\partial r_{ij}}{\partial x_i} \end{aligned} \tag{A.5}$$

, and the 2-body force (due to atom i) on atom j in the x direction

$$\begin{aligned} f2_{xj} &= -\frac{du2}{dx_j} \\ &= -\frac{\partial u2}{\partial r_{ij}}\frac{\partial r_{ij}}{\partial x_j}, \end{aligned} \tag{A.6}$$

we derive

$$f2_{xi} = -f2_{xj} \tag{A.7}$$

The relation between the derivatives of r_{ij} in the coordinates is:

$$\frac{\partial r_{ij}}{\partial x_i} = -\frac{\partial r_{ij}}{\partial x_j} = \frac{r_{xij}}{r_{ij}} \tag{A.8}$$

here $r_{ij} = \sqrt{(x_i-x_j)^2+(y_i-y_j)^2+(z_i-z_j)^2}$ and $r_{xij} = x_i - x_j$.

Similarly, we have expressions in the y and z directions,

$$f2_{yj} = -f2_{yj} \quad \frac{\partial r_{ij}}{\partial y_i} = -\frac{\partial r_{ij}}{\partial y_j} \quad r_{yij} = y_i - y_j \tag{A.9}$$

$$f2_{zj} = -f2_{zj} \quad \frac{\partial r_{ij}}{\partial z_i} = -\frac{\partial r_{ij}}{\partial z_j} \quad r_{zij} = z_i - z_j \tag{A.10}$$

When the intermolecular distance satisfies $r_{ij} < r_{c1}$, the partial derivative of $u2$ is,

$$\begin{aligned} -\frac{\partial u2}{\partial r_{ij}} &= 4A\varepsilon\frac{1}{r_{ij}}\exp\left(\frac{\sigma}{r_{ij}-r_{c1}}\right)\left[2\left(\frac{\sigma}{r_{ij}}\right)^8-\left(\frac{\sigma}{r_{ij}}\right)^4\right] \\ &\quad +A\varepsilon\frac{\sigma}{(r_{ij}-r_{c1})^2}\exp\left(\frac{\sigma}{r_{ij}-r_{c1}}\right)\left[\left(\frac{\sigma}{r_{ij}}\right)^8-\left(\frac{\sigma}{r_{ij}}\right)^4\right] \end{aligned} \tag{A.11}$$

A.2.2 3-body contributions

From Eq. A.3, we write the total 3-body force (due to atoms j and k) on atom i in the x direction:

$$\begin{aligned} f3_{xi} &= -\frac{\partial u3}{\partial x_i} \\ &= -\frac{\partial h_i}{\partial x_i}-\frac{\partial h_j}{\partial x_i}-\frac{\partial h_k}{\partial x_i} \end{aligned} \tag{A.12}$$

With the two terms $h-$function in Eq. A.4, we have

$$\frac{\partial h_i}{\partial x_i} = \frac{\partial h_i}{\partial r_{ij}}\frac{\partial r_{ij}}{\partial x_i}+\frac{\partial h_i}{\partial r_{ik}}\frac{\partial r_{ik}}{\partial x_i}+\frac{\partial h_i}{\partial\cos\theta_i}\frac{\partial\cos\theta_i}{\partial x_i} \tag{A.13}$$

$$\begin{aligned} \frac{\partial h_j}{\partial x_i} &= \frac{\partial h_j}{\partial r_{ij}}\frac{\partial r_{ij}}{\partial x_i}+\frac{\partial h_j}{\partial r_{jk}}\frac{\partial r_{jk}}{\partial x_i}+\frac{\partial h_j}{\partial\cos\theta_j}\frac{\partial\cos\theta_j}{\partial x_i} \\ &= \frac{\partial h_j}{\partial r_{ij}}\frac{\partial r_{ij}}{\partial x_i}+\frac{\partial h_j}{\partial\cos\theta_j}\frac{\partial\cos\theta_j}{\partial x_i} \end{aligned} \tag{A.14}$$

$$\begin{aligned} \frac{\partial h_k}{\partial x_i} &= \frac{\partial h_k}{\partial r_{ik}}\frac{\partial r_{ik}}{\partial x_i}+\frac{\partial h_k}{\partial r_{jk}}\frac{\partial r_{jk}}{\partial x_i}+\frac{\partial h_k}{\partial\cos\theta_k}\frac{\partial\cos\theta_k}{\partial x_i} \\ &= \frac{\partial h_k}{\partial r_{ik}}\frac{\partial r_{ik}}{\partial x_i}+\frac{\partial h_k}{\partial\cos\theta_k}\frac{\partial\cos\theta_k}{\partial x_i} \end{aligned} \tag{A.15}$$

We derive the partial derivatives of the two terms h_i over r_{ij} and r_{ik}, respectively,

$$\begin{aligned} \frac{\partial h_i}{\partial r_{ij}} &= -8.4\epsilon\exp\left[\left(\frac{\sigma}{r_{ij}-r_{c1}}\right)+\left(\frac{\sigma}{r_{ik}-r_{c1}}\right)\right]\left(\frac{\sigma^2}{r_{ij}r_{ik}}\right)^4\left(\frac{4}{r_{ij}}+\frac{\sigma}{(r_{ij}-r_{c1})^2}\right) \\ &\quad -3(50-25\cos\theta_i^2)\exp\left[3\left(\frac{\sigma}{r_{ij}-r_{c2}}\right)+3\left(\frac{\sigma}{r_{ik}-r_{c2}}\right)\right]\frac{\sigma}{(r_{ij}-r_{c2})^2} \end{aligned} \tag{A.16}$$

$$\begin{aligned} \frac{\partial h_i}{\partial r_{ik}} &= -8.4\epsilon\exp\left[\left(\frac{\sigma}{r_{ij}-r_{c1}}\right)+\left(\frac{\sigma}{r_{ik}-r_{c1}}\right)\right]\left(\frac{\sigma^2}{r_{ij}r_{ik}}\right)^4\left(\frac{4}{r_{ik}}+\frac{\sigma}{(r_{ik}-r_{c1})^2}\right) \\ &\quad -3(50-25\cos\theta_i^2)\exp\left[3\left(\frac{\sigma}{r_{ij}-r_{c2}}\right)+3\left(\frac{\sigma}{r_{ik}-r_{c2}}\right)\right]\frac{\sigma}{(r_{ik}-r_{c2})^2} \end{aligned} \tag{A.17}$$

Similar expressions for the other partial derivatives of the two terms h_j and the two terms h_k are

$$\begin{aligned}
\frac{\partial h_j}{\partial r_{ij}} &= -8.4\epsilon \exp\left[\left(\frac{\sigma}{-r_{ij}-r_{c1}}\right)+\left(\frac{\sigma}{r_{jk}-r_{c1}}\right)\right]\left(\frac{\sigma^2}{-r_{ij}r_{jk}}\right)^4\left(\frac{4}{-r_{ij}}-\frac{\sigma}{(-r_{ij}-r_{c1})^2}\right) \\
&\quad +3(50-25\cos\theta_j^2)\exp\left[3\left(\frac{\sigma}{-r_{ij}-r_{c2}}\right)+3\left(\frac{\sigma}{r_{jk}-r_{c2}}\right)\right]\frac{\sigma}{(-r_{ij}-r_{c2})^2} \qquad \text{(A.18)} \\
\frac{\partial h_j}{\partial r_{jk}} &= -8.4\epsilon \exp\left[\left(\frac{\sigma}{-r_{ij}-r_{c1}}\right)+\left(\frac{\sigma}{r_{jk}-r_{c1}}\right)\right]\left(\frac{\sigma^2}{-r_{ij}r_{jk}}\right)^4\left(\frac{4}{r_{jk}}+\frac{\sigma}{(r_{jk}-r_{c1})^2}\right) \\
&\quad -3(50-25\cos\theta_j^2)\exp\left[3\left(\frac{\sigma}{-r_{ij}-r_{c2}}\right)+3\left(\frac{\sigma}{r_{jk}-r_{c2}}\right)\right]\frac{\sigma}{(r_{jk}-r_{c2})^2} \qquad \text{(A.19)} \\
\frac{\partial h_k}{\partial r_{ik}} &= -8.4\epsilon \exp\left[\left(\frac{\sigma}{-r_{ik}-r_{c1}}\right)+\left(\frac{\sigma}{-r_{jk}-r_{c1}}\right)\right]\left(\frac{\sigma^2}{r_{ik}r_{jk}}\right)^4\left(\frac{4}{-r_{ik}}-\frac{\sigma}{(-r_{ik}-r_{c1})^2}\right) \\
&\quad +3(50-25\cos\theta_k^2)\exp\left[3\left(\frac{\sigma}{-r_{ik}-r_{c2}}\right)+3\left(\frac{\sigma}{-r_{jk}-r_{c2}}\right)\right]\frac{\sigma}{(-r_{ik}-r_{c2})^2} \qquad \text{(A.20)} \\
\frac{\partial h_k}{\partial r_{jk}} &= -8.4\epsilon \exp\left[\left(\frac{\sigma}{-r_{ik}-r_{c1}}\right)+\left(\frac{\sigma}{-r_{jk}-r_{c1}}\right)\right]\left(\frac{\sigma^2}{r_{ik}r_{jk}}\right)^4\left(\frac{4}{-r_{jk}}-\frac{\sigma}{(-r_{jk}-r_{c1})^2}\right) \\
&\quad +3(50-25\cos\theta_k^2)\exp\left[3\left(\frac{\sigma}{-r_{ik}-r_{c2}}\right)+3\left(\frac{\sigma}{-r_{jk}-r_{c2}}\right)\right]\frac{\sigma}{(-r_{jk}-r_{c2})^2} \qquad \text{(A.21)}
\end{aligned}$$

The partial derivertives of the two terms $h-$functions over the corresponding angles are

$$\begin{aligned}
\frac{\partial h_i}{\partial \cos\theta_i} &= -50\exp\left[3\left(\frac{\sigma}{r_{ij}-r_{c2}}\right)+3\left(\frac{\sigma}{r_{ik}-r_{c2}}\right)\right]\cos\theta_i \\
\frac{\partial h_j}{\partial \cos\theta_j} &= -50\exp\left[3\left(\frac{\sigma}{-r_{ij}-r_{c2}}\right)+3\left(\frac{\sigma}{r_{jk}-r_{c2}}\right)\right]\cos\theta_j \\
\frac{\partial h_k}{\partial \cos\theta_k} &= -50\exp\left[3\left(\frac{\sigma}{-r_{ik}-r_{c2}}\right)+3\left(\frac{\sigma}{-r_{jk}-r_{c2}}\right)\right]\cos\theta_k
\end{aligned}$$

With the cosin law,

$$\begin{aligned}
\cos\theta_i &= \frac{r_{ij}+r_{ik}-r_{jk}}{2r_{ij}r_{ik}} \\
\cos\theta_j &= \frac{r_{ij}+r_{jk}-r_{ik}}{-2r_{ij}r_{jk}} \\
\cos\theta_k &= \frac{r_{ik}+r_{jk}-r_{ij}}{2r_{ik}r_{jk}}
\end{aligned}$$

Then we derive:

$$\frac{\partial \cos\theta_i}{\partial x_i} = \frac{r_{xij} + r_{xik}}{r_{ij} r_{ik}} - \frac{r_{ij} + r_{ik} - r_{jk}}{2(r_{ij} r_{ik})^3} (r_{ik} r_{xij} + r_{ij} r_{xik}) \quad \text{(A.22)}$$

$$\frac{\partial \cos\theta_j}{\partial x_i} = \frac{r_{xij} - r_{xjk}}{-r_{ij} r_{jk}} + \frac{r_{ij} + r_{jk} - r_{ik}}{2(r_{ij} r_{jk})^3} r_{jk} r_{xij} \quad \text{(A.23)}$$

$$\frac{\partial \cos\theta_k}{\partial x_i} = \frac{r_{xik} - r_{xij}}{r_{ik} r_{jk}} - \frac{r_{ik} + r_{jk} - r_{ij}}{2(r_{ik} r_{jk})^3} r_{jk} r_{xik} \quad \text{(A.24)}$$

With the one term $h-$function in Eq. A.4, we have simple expressions:

$$\frac{\partial h_i}{\partial x_i} = \frac{\partial h_i}{\partial r_{ij}} \frac{\partial r_{ij}}{\partial x_i} + \frac{\partial h_i}{\partial r_{ik}} \frac{\partial r_{ik}}{\partial x_i} \quad \text{(A.25)}$$

$$\frac{\partial h_j}{\partial x_i} = \frac{\partial h_j}{\partial r_{ij}} \frac{\partial r_{ij}}{\partial x_i} + \frac{\partial h_j}{\partial r_{jk}} \frac{\partial r_{jk}}{\partial x_i} = \frac{\partial h_j}{\partial r_{ij}} \frac{\partial r_{ij}}{\partial x_i} \quad \text{(A.26)}$$

$$\frac{\partial h_k}{\partial x_i} = \frac{\partial h_k}{\partial r_{ik}} \frac{\partial r_{ik}}{\partial x_i} + \frac{\partial h_k}{\partial r_{jk}} \frac{\partial r_{jk}}{\partial x_i} = \frac{\partial h_k}{\partial r_{ik}} \frac{\partial r_{ik}}{\partial x_i} \quad \text{(A.27)}$$

The partial deriverties of the one term $h-$functions can be easily get by taking the first term in equations A.16-A.21. Substituting proper equations for the partial derivatives into Eq. A.12, we can find the 3-body force acting on atom i as a function of the coordinates. In the same way, we can find the 3-body force (due to atom i and k) acting on atom j, $f3_{xj}$, and the 3-body force (due to atom i and j) acting on atom k, $f3_{xk}$. The algorithm for implementing these equations into the reaction NEMD program is reported in the following section.

A.3 Algorithm

To compute energy, forces and pressure tensor, we shall optimize 'loops' over the number of all accepted pairs and triplets of atoms in a n body system. In the force routine of our NEMD program, neighborhood lists for inner loops j and k are used to avoid expensive simulations. Below are the pseudo codes for the force routine.

```
% before the triple loop, some variables are initialized.
total energy ← 0
do loop i = 1, n
  total acceleration x(i)← 0
  total acceleration y(i)← 0
  total acceleration z(i)← 0
end loop i
```

% outer loop over $n$atoms
do loop $i = 1, n-1$

% inner loop for j starts
% loop over all possible pairs between atom i and its neighborhood atom j
do loop j = first neighborhood of atom i, last neighborhood of atom i

% use minimum image conversion to calculate the distance square r_{ij}^2
$r_{ij}^2 \leftarrow$ formula for r_{ij}^2
if $r_{ij}^2 <$ first cut off distance square (3.6^2) then
2-body energy ← formula for $u2$
total energy ← total energy + 2-body energy
% calculate 2-body force for atom i and j in x, y and z directions
total acceleration x(i)← total acceleration x(i)+$f2_{xi}$/mass (i)
total acceleration y(i)← total acceleration y(i)+$f2_{yi}$/mass (i)
total acceleration z(i)← total acceleration z(i)+$f2_{zi}$/mass (i)
total acceleration x(j)← total acceleration x(j)+$f2_{xj}$/mass (j)
total acceleration y(j)← total acceleration y(j)+$f2_{yj}$/mass (j)
total acceleration z(j)← total acceleration z(j)+$f2_{zj}$/mass (j)
end if
if j < the last neighborhood atom then
% inner loop for k starts
% loop over all possible triples among atom i and its neighborhood atoms
% j and k ($k > j$)
do loop k = j+1, last neighborhood of atom i
% use minimum image conversion to calculate the distance squares
% r_{ik}^2 and r_{jk}^2
$r_{ik}^2 \leftarrow$ formula for r_{ik}^2
$r_{jk}^2 \leftarrow$ formula for r_{jk}^2
if $r_{ij}^2 <$ second cut off distance square (2.8^2) then
if $r_{ik}^2 <$ second cut off distance square (2.8^2) then
$h_i \leftarrow$ two terms h_i function
$-\frac{\partial h_i}{\partial x_i}, -\frac{\partial h_i}{\partial y_i}, -\frac{\partial h_i}{\partial z_i}, -\frac{\partial h_i}{\partial x_j}, -\frac{\partial h_i}{\partial y_j}, -\frac{\partial h_i}{\partial z_j}, -\frac{\partial h_i}{\partial x_k}, -\frac{\partial h_i}{\partial y_k}, -\frac{\partial h_i}{\partial z_k}$
← formula of partial derivatives of two terms h_i function for atoms i,j and k in 3 directions.
if $r_{jk}^2 <$ second cut off distance square (2.8^2) then
$h_j \leftarrow$ two terms h_j function
$h_k \leftarrow$ two terms h_k function
$-\frac{\partial h_j}{\partial x_i}, -\frac{\partial h_j}{\partial y_i}, -\frac{\partial h_j}{\partial z_i}, -\frac{\partial h_j}{\partial x_j}, -\frac{\partial h_j}{\partial y_j}, -\frac{\partial h_j}{\partial z_j}, -\frac{\partial h_j}{\partial x_k}, -\frac{\partial h_j}{\partial y_k}, -\frac{\partial h_j}{\partial z_k}$
← formula of partial derivatives of two terms h_j function for atoms i,j and k in 3 directions.
$-\frac{\partial h_k}{\partial x_i}, -\frac{\partial h_k}{\partial y_i}, -\frac{\partial h_k}{\partial z_i}, -\frac{\partial h_k}{\partial x_j}, -\frac{\partial h_k}{\partial y_j}, -\frac{\partial h_k}{\partial z_j}, -\frac{\partial h_k}{\partial x_k}, -\frac{\partial h_k}{\partial y_k}, -\frac{\partial h_k}{\partial z_k}$
← formula of partial derivatives of two terms h_k function for atoms i,j and k in 3 directions.

elseif $r_{jk}^2 <$ first cut off distance square (3.6^2) then
$h_j \leftarrow$ one term h_j function
$h_k \leftarrow$ one term h_k function
$-\frac{\partial h_j}{\partial x_i}, -\frac{\partial h_j}{\partial y_i}, -\frac{\partial h_j}{\partial z_i}, -\frac{\partial h_j}{\partial x_j}, -\frac{\partial h_j}{\partial y_j}, -\frac{\partial h_j}{\partial z_j}, -\frac{\partial h_j}{\partial x_k}, -\frac{\partial h_j}{\partial y_k}, -\frac{\partial h_j}{\partial z_k}$
$\leftarrow$ formula of partial derivatives of one term h_j function for atoms i,j and k in 3 directions.
$-\frac{\partial h_k}{\partial x_i}, -\frac{\partial h_k}{\partial y_i}, -\frac{\partial h_k}{\partial z_i}, -\frac{\partial h_k}{\partial x_j}, -\frac{\partial h_k}{\partial y_j}, -\frac{\partial h_k}{\partial z_j}, -\frac{\partial h_k}{\partial x_k}, -\frac{\partial h_k}{\partial y_k}, -\frac{\partial h_k}{\partial z_k}$
$\leftarrow$ formula of partial derivatives of one term h_k function for atoms i,j and k in 3 directions.
else
$h_j \leftarrow 0$
$h_k \leftarrow 0$
$-\frac{\partial h_i}{\partial x_i}, -\frac{\partial h_i}{\partial y_i}, -\frac{\partial h_i}{\partial z_i}, -\frac{\partial h_i}{\partial x_j}, -\frac{\partial h_i}{\partial y_j}, -\frac{\partial h_i}{\partial z_j}, -\frac{\partial h_i}{\partial x_k}, -\frac{\partial h_i}{\partial y_k}, -\frac{\partial h_i}{\partial z_k} \leftarrow 0$
$-\frac{\partial h_k}{\partial x_i}, -\frac{\partial h_k}{\partial y_i}, -\frac{\partial h_k}{\partial z_i}, -\frac{\partial h_k}{\partial x_j}, -\frac{\partial h_k}{\partial y_j}, -\frac{\partial h_k}{\partial z_j}, -\frac{\partial h_k}{\partial x_k}, -\frac{\partial h_k}{\partial y_k}, -\frac{\partial h_k}{\partial z_k} \leftarrow 0$
endif
elseif $r_{ik}^2 <$ first cut off distance square (3.6^2) then
$h_i \leftarrow$ one term h_i function
$-\frac{\partial h_i}{\partial x_i}, -\frac{\partial h_i}{\partial y_i}, -\frac{\partial h_i}{\partial z_i}, -\frac{\partial h_i}{\partial x_j}, -\frac{\partial h_i}{\partial y_j}, -\frac{\partial h_i}{\partial z_j}, -\frac{\partial h_i}{\partial x_k}, -\frac{\partial h_i}{\partial y_k}, -\frac{\partial h_i}{\partial z_k}$
$\leftarrow$ formula of partial derivatives of one term h_i function for atoms i,j and k in 3 directions.
if $r_{jk}^2 <$ second cut off distance square (2.8^2) then
$h_j \leftarrow$ two terms h_j function
$h_k \leftarrow$ one term h_k function
$-\frac{\partial h_j}{\partial x_i}, -\frac{\partial h_j}{\partial y_i}, -\frac{\partial h_j}{\partial z_i}, -\frac{\partial h_j}{\partial x_j}, -\frac{\partial h_j}{\partial y_j}, -\frac{\partial h_j}{\partial z_j}, -\frac{\partial h_j}{\partial x_k}, -\frac{\partial h_j}{\partial y_k}, -\frac{\partial h_j}{\partial z_k}$
$\leftarrow$ formula of partial derivatives of two terms h_j function for atoms i,j and k in 3 directions.
$-\frac{\partial h_k}{\partial x_i}, -\frac{\partial h_k}{\partial y_i}, -\frac{\partial h_k}{\partial z_i}, -\frac{\partial h_k}{\partial x_j}, -\frac{\partial h_k}{\partial y_j}, -\frac{\partial h_k}{\partial z_j}, -\frac{\partial h_k}{\partial x_k}, -\frac{\partial h_k}{\partial y_k}, -\frac{\partial h_k}{\partial z_k}$
$\leftarrow$ formula of partial derivatives of one term h_k function for atoms i,j and k in 3 directions.
elseif $r_{jk}^2 <$ first cut off distance square (3.6^2) then
$h_j \leftarrow$ one term h_j function
$h_k \leftarrow$ one term h_k function
$-\frac{\partial h_j}{\partial x_i}, -\frac{\partial h_j}{\partial y_i}, -\frac{\partial h_j}{\partial z_i}, -\frac{\partial h_j}{\partial x_j}, -\frac{\partial h_j}{\partial y_j}, -\frac{\partial h_j}{\partial z_j}, -\frac{\partial h_j}{\partial x_k}, -\frac{\partial h_j}{\partial y_k}, -\frac{\partial h_j}{\partial z_k}$
$\leftarrow$ formula of partial derivatives of one term h_j function for atoms i,j and k in 3 directions.
$-\frac{\partial h_k}{\partial x_i}, -\frac{\partial h_k}{\partial y_i}, -\frac{\partial h_k}{\partial z_i}, -\frac{\partial h_k}{\partial x_j}, -\frac{\partial h_k}{\partial y_j}, -\frac{\partial h_k}{\partial z_j}, -\frac{\partial h_k}{\partial x_k}, -\frac{\partial h_k}{\partial y_k}, -\frac{\partial h_k}{\partial z_k}$
$\leftarrow$ formula of partial derivatives of one term h_k function for atoms i,j and k in 3 directions.
else
$h_j \leftarrow 0$
$h_k \leftarrow 0$
$-\frac{\partial h_j}{\partial x_i}, -\frac{\partial h_j}{\partial y_i}, -\frac{\partial h_j}{\partial z_i}, -\frac{\partial h_j}{\partial x_j}, -\frac{\partial h_j}{\partial y_j}, -\frac{\partial h_j}{\partial z_j}, -\frac{\partial h_j}{\partial x_k}, -\frac{\partial h_j}{\partial y_k}, -\frac{\partial h_j}{\partial z_k} \leftarrow 0$
$-\frac{\partial h_k}{\partial x_i}, -\frac{\partial h_k}{\partial y_i}, -\frac{\partial h_k}{\partial z_i}, -\frac{\partial h_k}{\partial x_j}, -\frac{\partial h_k}{\partial y_j}, -\frac{\partial h_k}{\partial z_j}, -\frac{\partial h_k}{\partial x_k}, -\frac{\partial h_k}{\partial y_k}, -\frac{\partial h_k}{\partial z_k} \leftarrow 0$
endif
else

$h_i \leftarrow 0$
$h_j \leftarrow 0$
$-\frac{\partial h_i}{\partial x_i}, -\frac{\partial h_i}{\partial y_i}, -\frac{\partial h_i}{\partial z_i}, -\frac{\partial h_i}{\partial x_j}, -\frac{\partial h_i}{\partial y_j}, -\frac{\partial h_i}{\partial z_j}, -\frac{\partial h_i}{\partial x_k}, -\frac{\partial h_i}{\partial y_k}, -\frac{\partial h_i}{\partial z_k} \leftarrow 0$
$-\frac{\partial h_j}{\partial x_i}, -\frac{\partial h_j}{\partial y_i}, -\frac{\partial h_j}{\partial z_i}, -\frac{\partial h_j}{\partial x_j}, -\frac{\partial h_j}{\partial y_j}, -\frac{\partial h_j}{\partial z_j}, -\frac{\partial h_j}{\partial x_k}, -\frac{\partial h_j}{\partial y_k}, -\frac{\partial h_j}{\partial z_k} \leftarrow 0$
if $r_{jk}^2 <$ second cut off distance square (2.8^2) then
$h_j \leftarrow$ one term h_j function
$-\frac{\partial h_j}{\partial x_i}, -\frac{\partial h_j}{\partial y_i}, -\frac{\partial h_j}{\partial z_i}, -\frac{\partial h_j}{\partial x_j}, -\frac{\partial h_j}{\partial y_j}, -\frac{\partial h_j}{\partial z_j}, -\frac{\partial h_j}{\partial x_k}, -\frac{\partial h_j}{\partial y_k}, -\frac{\partial h_j}{\partial z_k}$
$\leftarrow$ formula of partial derivatives of two terms h_j function for atoms i,j and k in 3 directions.
elseif $r_{jk}^2 <$ first cut off distance square (3.6^2) then
$h_j \leftarrow$ one term h_j function
$-\frac{\partial h_j}{\partial x_i}, -\frac{\partial h_j}{\partial y_i}, -\frac{\partial h_j}{\partial z_i}, -\frac{\partial h_j}{\partial x_j}, -\frac{\partial h_j}{\partial y_j}, -\frac{\partial h_j}{\partial z_j}, -\frac{\partial h_j}{\partial x_k}, -\frac{\partial h_j}{\partial y_k}, -\frac{\partial h_j}{\partial z_k}$
$\leftarrow$ formula of partial derivatives of one term h_j function for atoms i,j and k in 3 directions.
else
$h_j \leftarrow 0$

$-\frac{\partial h_j}{\partial x_i}, -\frac{\partial h_j}{\partial y_i}, -\frac{\partial h_j}{\partial z_i}, -\frac{\partial h_j}{\partial x_j}, -\frac{\partial h_j}{\partial y_j}, -\frac{\partial h_j}{\partial z_j}, -\frac{\partial h_j}{\partial x_k}, -\frac{\partial h_j}{\partial y_k}, -\frac{\partial h_j}{\partial z_k} \leftarrow 0$
endif
endif
elseif $r_{ij}^1 <$ first cut off distance square (3.6^2) then
if $r_{ik}^2 <$ second cut off distance square (2.8^2) then
$h_i \leftarrow$ one term h_i function
$-\frac{h_i}{x_i}, -\frac{h_i}{y_i}, -\frac{h_i}{z_i}, -\frac{h_i}{x_j}, -\frac{h_i}{y_j}, -\frac{h_i}{z_j}, -\frac{h_i}{x_k}, -\frac{h_i}{y_k}, -\frac{h_i}{z_k}$
$\leftarrow$ formula of partial derivatives of one term h_i function for atoms i,j and k in 3 directions.
if $r_{jk}^2 <$ second cut off distance square (2.8^2) then
$h_j \leftarrow$ one term h_j function
$h_k \leftarrow$ two terms h_k function
$-\frac{\partial h_j}{\partial x_i}, -\frac{\partial h_j}{\partial y_i}, -\frac{\partial h_j}{\partial z_i}, -\frac{\partial h_j}{\partial x_j}, -\frac{\partial h_j}{\partial y_j}, -\frac{\partial h_j}{\partial z_j}, -\frac{\partial h_j}{\partial x_k}, -\frac{\partial h_j}{\partial y_k}, -\frac{\partial h_j}{\partial z_k}$
$\leftarrow$ formula of partial derivatives of one term h_j function for atoms i,j and k in 3 directions.

$-\frac{\partial h_k}{\partial x_i}, -\frac{\partial h_k}{\partial y_i}, -\frac{\partial h_k}{\partial z_i}, -\frac{\partial h_k}{\partial x_j}, -\frac{\partial h_k}{\partial y_j}, -\frac{\partial h_k}{\partial z_j}, -\frac{\partial h_k}{\partial x_k}, -\frac{\partial h_k}{\partial y_k}, -\frac{\partial h_k}{\partial z_k}$
$\leftarrow$ formula of partial derivatives of two terms h_k function for atoms i,j and k in 3 directions.
elseif $r_{jk}^2 <$ first cut off distance square (3.6^2) then
$h_j \leftarrow$ one term h_j function
$h_k \leftarrow$ one term h_k function
$-\frac{\partial h_j}{\partial x_i}, -\frac{\partial h_j}{\partial y_i}, -\frac{\partial h_j}{\partial z_i}, -\frac{\partial h_j}{\partial x_j}, -\frac{\partial h_j}{\partial y_j}, -\frac{\partial h_j}{\partial z_j}, -\frac{\partial h_j}{\partial x_k}, -\frac{\partial h_j}{\partial y_k}, -\frac{\partial h_j}{\partial z_k}$
$\leftarrow$ formula of partial derivatives of one term h_j function for atoms i,j and k in 3 directions.
$-\frac{\partial h_k}{\partial x_i}, -\frac{\partial h_k}{\partial y_i}, -\frac{\partial h_k}{\partial z_i}, -\frac{\partial h_k}{\partial x_j}, -\frac{\partial h_k}{\partial y_j}, -\frac{\partial h_k}{\partial z_j}, -\frac{\partial h_k}{\partial x_k}, -\frac{\partial h_k}{\partial y_k}, -\frac{\partial h_k}{\partial z_k}$
$\leftarrow$ formula of partial derivatives of one term h_k function for atoms

i,j and k in 3 directions.

else

$h_j \leftarrow 0$

$h_k \leftarrow 0$

$-\frac{\partial h_j}{\partial x_i}, -\frac{\partial h_j}{\partial y_i}, -\frac{\partial h_j}{\partial z_i}, -\frac{\partial h_j}{\partial x_j}, -\frac{\partial h_j}{\partial y_j}, -\frac{\partial h_j}{\partial z_j}, -\frac{\partial h_j}{\partial x_k}, -\frac{\partial h_j}{\partial y_k}, -\frac{\partial h_j}{\partial z_k} \leftarrow 0$

$-\frac{\partial h_k}{\partial x_i}, -\frac{\partial h_k}{\partial y_i}, -\frac{\partial h_k}{\partial z_i}, -\frac{\partial h_k}{\partial x_j}, -\frac{\partial h_k}{\partial y_j}, -\frac{\partial h_k}{\partial z_j}, -\frac{\partial h_k}{\partial x_k}, -\frac{\partial h_k}{\partial y_k}, -\frac{\partial h_k}{\partial z_k} \leftarrow 0$

endif

elseif $r_{ik}^2 <$ first cut off distance square (3.6^2) then

$h_i \leftarrow$ one term h_i function

$-\frac{\partial h_i}{\partial x_i}, -\frac{\partial h_i}{\partial y_i}, -\frac{\partial h_i}{\partial z_i}, -\frac{\partial h_i}{\partial x_j}, -\frac{\partial h_i}{\partial y_j}, -\frac{\partial h_i}{\partial z_j}, -\frac{\partial h_i}{\partial x_k}, -\frac{\partial h_i}{\partial y_k}, -\frac{\partial h_i}{\partial z_k}$

$\leftarrow$ formula of partial derivatives of one term h_i function for atoms i,j and k in 3 directions.

if $r_{jk}^2 <$ second cut off distance square (2.8^2) then

$h_j \leftarrow$ one term h_j function

$h_k \leftarrow$ one term h_k function

$-\frac{\partial h_j}{\partial x_i}, -\frac{\partial h_j}{\partial y_i}, -\frac{\partial h_j}{\partial z_i}, -\frac{\partial h_j}{\partial x_j}, -\frac{\partial h_j}{\partial y_j}, -\frac{\partial h_j}{\partial z_j}, -\frac{\partial h_j}{\partial x_k}, -\frac{\partial h_j}{\partial y_k}, -\frac{\partial h_j}{\partial z_k}$

$\leftarrow$ formula of partial derivatives of one term h_j function for atoms i,j and k in 3 directions.

$-\frac{\partial h_k}{\partial x_i}, -\frac{\partial h_k}{\partial y_i}, -\frac{\partial h_k}{\partial z_i}, -\frac{\partial h_k}{\partial x_j}, -\frac{\partial h_k}{\partial y_j}, -\frac{\partial h_k}{\partial z_j}, -\frac{\partial h_k}{\partial x_k}, -\frac{\partial h_k}{\partial y_k}, -\frac{\partial h_k}{\partial z_k}$

$\leftarrow$ formula of partial derivatives of one term h_k function for atoms i,j and k in 3 directions.

else

$-\frac{\partial h_j}{\partial x_i}, -\frac{\partial h_j}{\partial y_i}, -\frac{\partial h_j}{\partial z_i}, -\frac{\partial h_j}{\partial x_j}, -\frac{\partial h_j}{\partial y_j}, -\frac{\partial h_j}{\partial z_j}, -\frac{\partial h_j}{\partial x_k}, -\frac{\partial h_j}{\partial y_k}, -\frac{\partial h_j}{\partial z_k} \leftarrow 0$

$-\frac{\partial h_k}{\partial x_i}, -\frac{\partial h_k}{\partial y_i}, -\frac{\partial h_k}{\partial z_i}, -\frac{\partial h_k}{\partial x_j}, -\frac{\partial h_k}{\partial y_j}, -\frac{\partial h_k}{\partial z_j}, -\frac{\partial h_k}{\partial x_k}, -\frac{\partial h_k}{\partial y_k}, -\frac{\partial h_k}{\partial z_k} \leftarrow 0$

endif

else

$h_i \leftarrow 0$

$h_k \leftarrow 0$

$-\frac{\partial h_i}{\partial x_i}, -\frac{\partial h_i}{\partial y_i}, -\frac{\partial h_i}{\partial z_i}, -\frac{\partial h_i}{\partial x_j}, -\frac{\partial h_i}{\partial y_j}, -\frac{\partial h_i}{\partial z_j}, -\frac{\partial h_i}{\partial x_k}, -\frac{\partial h_i}{\partial y_k}, -\frac{\partial h_i}{\partial z_k} \leftarrow 0$

$-\frac{\partial h_k}{\partial x_i}, -\frac{\partial h_k}{\partial y_i}, -\frac{\partial h_k}{\partial z_i}, -\frac{\partial h_k}{\partial x_j}, -\frac{\partial h_k}{\partial y_j}, -\frac{\partial h_k}{\partial z_j}, -\frac{\partial h_k}{\partial x_k}, -\frac{\partial h_k}{\partial y_k}, -\frac{\partial h_k}{\partial z_k} \leftarrow 0$

if $r_{jk}^2 <$ first cut off distance square (3.6^2) then

$h_j \leftarrow$ one term h_j function

$-\frac{\partial h_j}{\partial x_i}, -\frac{\partial h_j}{\partial y_i}, -\frac{\partial h_j}{\partial z_i}, -\frac{\partial h_j}{\partial x_j}, -\frac{\partial h_j}{\partial y_j}, -\frac{\partial h_j}{\partial z_j}, -\frac{\partial h_j}{\partial x_k}, -\frac{\partial h_j}{\partial y_k}, -\frac{\partial h_j}{\partial z_k}$

$\leftarrow$ formula of partial derivatives of one term h_j function for atoms i,j and k in 3 directions.

else

$h_j \leftarrow 0$

$-\frac{\partial h_j}{\partial x_i}, -\frac{\partial h_j}{\partial y_i}, -\frac{\partial h_j}{\partial z_i}, -\frac{\partial h_j}{\partial x_j}, -\frac{\partial h_j}{\partial y_j}, -\frac{\partial h_j}{\partial z_j}, -\frac{\partial h_j}{\partial x_k}, -\frac{\partial h_j}{\partial y_k}, -\frac{\partial h_j}{\partial z_k} \leftarrow 0$

endif

endif i

else

$h_i \leftarrow 0$

$h_j \leftarrow 0$

$-\frac{\partial h_i}{\partial x_i}, -\frac{\partial h_i}{\partial y_i}, -\frac{\partial h_i}{\partial z_i}, -\frac{\partial h_i}{\partial x_j}, -\frac{\partial h_i}{\partial y_j}, -\frac{\partial h_i}{\partial z_j}, -\frac{\partial h_i}{\partial x_k}, -\frac{\partial h_i}{\partial y_k}, -\frac{\partial h_i}{\partial z_k} \leftarrow 0$
$-\frac{\partial h_j}{\partial x_i}, -\frac{\partial h_j}{\partial y_i}, -\frac{\partial h_j}{\partial z_i}, -\frac{\partial h_j}{\partial x_j}, -\frac{\partial h_j}{\partial y_j}, -\frac{\partial h_j}{\partial z_j}, -\frac{\partial h_j}{\partial x_k}, -\frac{\partial h_j}{\partial y_k}, -\frac{\partial h_j}{\partial z_k} \leftarrow 0$
if $r_{ik}^2 <$ second cut off distance square (2.8^2) then
if $r_{jk}^2 <$ second cut off distance square (2.8^2) then
$h_k \leftarrow$ two terms h_k function
$-\frac{\partial h_k}{\partial x_i}, -\frac{\partial h_k}{\partial y_i}, -\frac{\partial h_k}{\partial z_i}, -\frac{\partial h_k}{\partial x_j}, -\frac{\partial h_k}{\partial y_j}, -\frac{\partial h_k}{\partial z_j}, -\frac{\partial h_k}{\partial x_k}, -\frac{\partial h_k}{\partial y_k}, -\frac{\partial h_k}{\partial z_k}$
$\leftarrow$ formula of partial derivatives of two terms h_k function for atoms i,j and k in 3 directions.
elseif $r_{jk}^2 <$ first cut off distance square (3.6^2) then
$h_k \leftarrow$ one term h_k function
$-\frac{\partial h_k}{\partial x_i}, -\frac{\partial h_k}{\partial y_i}, -\frac{\partial h_k}{\partial z_i}, -\frac{\partial h_k}{\partial x_j}, -\frac{\partial h_k}{\partial y_j}, -\frac{\partial h_k}{\partial z_j}, -\frac{\partial h_k}{\partial x_k}, -\frac{\partial h_k}{\partial y_k}, -\frac{\partial h_k}{\partial z_k}$
$\leftarrow$ formula of partial derivatives of one term h_k function for atoms i,j and k in 3 directions.
else
$h_k \leftarrow 0$
$-\frac{\partial h_k}{\partial x_i}, -\frac{\partial h_k}{\partial y_i}, -\frac{\partial h_k}{\partial z_i}, -\frac{\partial h_k}{\partial x_j}, -\frac{\partial h_k}{\partial y_j}, -\frac{\partial h_k}{\partial z_j}, -\frac{\partial h_k}{\partial x_k}, -\frac{\partial h_k}{\partial y_k}, -\frac{\partial h_k}{\partial z_k} \leftarrow 0$
endif
elseif $r_{ik}^2 <$ first cut off distance square (3.6^2) then
if $r_{jk}^2 <$ first cut off distance square (3.6^2) then
$h_k \leftarrow$ one term h_k function
$-\frac{\partial h_k}{\partial x_i}, -\frac{\partial h_k}{\partial y_i}, -\frac{\partial h_k}{\partial z_i}, -\frac{\partial h_k}{\partial x_j}, -\frac{\partial h_k}{\partial y_j}, -\frac{\partial h_k}{\partial z_j}, -\frac{\partial h_k}{\partial x_k}, -\frac{\partial h_k}{\partial y_k}, -\frac{\partial h_k}{\partial z_k}$
$\leftarrow$ formula of partial derivatives of one term h_k function for atoms i,j and k in 3 directions.
else
$h_k \leftarrow 0$
$-\frac{\partial h_k}{\partial x_i}, -\frac{\partial h_k}{\partial y_i}, -\frac{\partial h_k}{\partial z_i}, -\frac{\partial h_k}{\partial x_j}, -\frac{\partial h_k}{\partial y_j}, -\frac{\partial h_k}{\partial z_j}, -\frac{\partial h_k}{\partial x_k}, -\frac{\partial h_k}{\partial y_k}, -\frac{\partial h_k}{\partial z_k} \leftarrow 0$
endif
else
$h_k \leftarrow 0$
$-\frac{\partial h_k}{\partial x_i}, -\frac{\partial h_k}{\partial y_i}, -\frac{\partial h_k}{\partial z_i}, -\frac{\partial h_k}{\partial x_j}, -\frac{\partial h_k}{\partial y_j}, -\frac{\partial h_k}{\partial z_j}, -\frac{\partial h_k}{\partial x_k}, -\frac{\partial h_k}{\partial y_k}, -\frac{\partial h_k}{\partial z_k} \leftarrow 0$
endif
endif

3-body potential $\leftarrow h_i + h_j + h_k$
total energy $\leftarrow$ total energy + 3-body energy

% calculate 3-body force for triplets in x, y and z directions
total acceleration x(i)$\leftarrow$ total acceleration x(i)$+f3_{xi}$/mass (i)
total acceleration y(i)$\leftarrow$ total acceleration y(i)$+f3_{yi}$/mass (i)
total acceleration z(i)$\leftarrow$ total acceleration z(i)$+f3_{zi}$/mass (i)
total acceleration x(j)$\leftarrow$ total acceleration x(j)$+f3_{xj}$/mass (j)
total acceleration y(j)$\leftarrow$ total acceleration y(j)$+f3_{yj}$/mass (j)
total acceleration z(j)$\leftarrow$ total acceleration z(j)$+f3_{zj}$/mass (j)
total acceleration x(k)$\leftarrow$ total acceleration x(k)$+f3_{xk}$/mass (k)
total acceleration y(k)$\leftarrow$ total acceleration y(k)$+f3_{yk}$/mass (k)

total acceleration z(k)← total acceleration z(k)+$f3_{zk}$/mass (k)

% end inner loop for k
enddo loop k
endif

% end inner loop for j
enddo loop j

% end outer loop for i
enddo loop i

A.3.1 Neighborhood lists: NEIGHBOUR3

This subroutine NEIGHBOUR3 constructs a list of triplets by combining pairs from the pair list, which had one particle in common. To save CPU time a list of pairs was made with a distance from each other smaller than a limited cut off distance, r^*_{list}=4. Pair interactions were calculated when r^* was equal to or smaller than this value. Within a limited time interval, the lists for 2-body and 3-body neighborhoods are required to update.

```
subroutine construct(update)
  use constants  % define constants
  use posvel
  implicit none
  integer(long) i,np,j,ipf,ipl,k
  integer neibj,neibk
  real (8) rxij,ryij,rzij,rijsq
  logical update


  open(88,file='nblist.dat',status='unknown') % The file stores neighborhoods for possible pairs
  open(888,file='ntlist.dat',status='unknown')% The file stores neighborhoods for possible triplets

  do 2100 i=1,n
     pntr(i)=0
     nlist(i)=0
     qx(i)=0.00
     qy(i)=0.00
     qz(i)=0.00
2100 continue

     do 2200 i=1,nbmax
        nblist(i)=0
2200  continue

      np=1
      do 2400 i=1,n-1
         do 2300 j=i+1,n

            rxij=rx(i)-rx(j)
            if (rxij.gt.0.5d0) then
               rxij=rxij-1.0d0
            else if (rxij.lt.-0.5d0) then
               rxij=rxij+1.0d0
```

```
            endif
            if (dabs(rxij).gt.rls) go to 2300
            ryij=ry(i)-ry(j)
            if (ryij.gt.yxrat2) then
               ryij=ryij-yxrat
            else if (ryij.lt.-yxrat2) then
               ryij=ryij+yxrat
            endif
            rijsq=rxij**2+ryij**2
            if (rijsq.gt.rls2) go to 2300
            rzij=rz(i)-rz(j)
            if (rzij.gt.yxrat2) then
               rzij=rzij-yxrat
            else if (rzij.lt.-yxrat2) then
               rzij=rzij+yxrat
            endif
            rijsq=rijsq+rzij**2
            if (rijsq.gt.rls2) go to 2300 % rls2 is the square of the rlist
            nlist(i)=nlist(i)+1
            nlist(j)=nlist(j)+1
            ntlist(i,nlist(i))=j
            ntlist(j,nlist(j))=i

            nblist(np)=j
            np=np+1

            if (np.gt.nbmax) then
               write (*,*) '  Not enough room in nblist'
               stop
            endif

2300        continue
            pntr(i)=np-1

2400        continue

            update=.false.
            ipf=1
            do i=1,n-1
               ipl=pntr(i)
               if(ipf.le.ipl) then
                  do neibj=ipf,ipl
                     j=nblist(neibj)
                     write(88,'(2i5)') i,j
                  enddo
               endif
               ipf=ipl+1
            enddo
            do i=1,n
               do neibj=1,nlist(i)-1
                  j=ntlist(i,neibj)
                  do neibk=neibj+1,nlist(i)
                     k=ntlist(i,neibk)
                     write(888,'(3i5)') i,j,k
                  enddo
               enddo
            enddo

            close(88)
            close(888)
            return
      end
```